EV Fleet as Distributed Energy Resource in Community Microgrid

Qiyun Dang

Department of Electrical & Computer Engineering

McGill University

Montréal, Québec, Canada

February, 2022

A thesis submitted to McGill University in partial fulfillment of the requirements of the degree of

Master of Engineering

Abstract

The penetration of electric vehicles (EVs) has been increasing very quickly in the last few years. EVs can help reduce the dependency on the fossil energy, greenhouse gas emission, and improve energy efficiency. Besides the aforementioned benefits, EVs could also provide extra benefits for neighborhood-level networks. This thesis presents a few case studies to analyze the potential benefits of using an EV fleet as energy storage in order to cut off and save extra battery packs investments on energy storage. Particularly, the thesis provides a Continuous Time Markov Chain (CTMC) based EV fleet total available battery capacity estimation framework to deal with cost savings oriented community energy storage sizing problems. The local fast charging station (FCS) queuing situation and queuing theory are also considered. Simulation results show that the adoption of EVs could significantly reduce the investment in battery storage which could bring significant economic and social benefits.

This thesis also proposes a method to manage electric vehicle charging behavior in order to reduce its effect on the grid. We first summarize the charging patterns of electric vehicle users, based on charging profile observations from the advanced metering system. The method distinguishes supervision-free user patterns and establishes a novel schedule strategy to reduce grid peak power demand. The strategy is based on the "valley filling" concept while also considering cutting down the total interference time of users' charging process. The general grid impact of vehicle charging before and after the adoption of the proposed strategy is simulated and compared. The results show that the proposed method is able to relieve grid impact and thereby increase the EVs service capability of distribution grids.

This thesis also introduces an improved Q-learning algorithm-based dynamic charging scheduling framework for electric vehicles. The scheduling problem involved, which considers the fast charging station (FCS) congestion situation, focuses on the bidirectional power exchange between the vehicle and the distribution grid. Particularly, the technique transforms the scheduling problem into the establishment of a suitable reward table for EV charging. The simulation models it as a Q-learning grid world problem in 3-Dimensional-space, where the optimal path implies the best series of actions to take at each time slot. The advancement of the current Q-learning framework refers specifically to the extra consideration of the limited service capability of the FCS. The queuing theory (M/M/1/N/∞ queue) is brought in to address the EV charging congestion phenomenon. A brief literature review on the impacts of EV charging, time-of-use (TOU) pricing is presented. The Q-learning framework provides a practical solution to mitigate EV load impacts in grids, including altering charging time due to TOU and grid support by adopting a vehicle-to-grid (V2G) plan.

Abrégé

La pénétration des véhicules électriques (VÉ) a augmenté très rapidement ces dernières années. Les véhicules électriques peuvent aider à réduire la dépendance à l'énergie fossile, aux émissions de gaz à effet de serre et à améliorer l'efficacité énergétique. Outre les avantages susmentionnés, les véhicules électriques pourraient également fournir des avantages supplémentaires pour le réseau électrique de quartier. Cette thèse présente quelques études de cas pour analyser l'avantage potentiel de l'utilisation d'une flotte de véhicules électriques comme stockage d'énergie afin de réduire les coût de batteries supplémentaires sur le stockage d'énergie. En particulier, la thèse propose une chaîne de Markov à Temps Continu (CMTC) base sur le flotte VÉ pour estimation de la capacité de la batterie disponible afin de calculer des économies de coûts dans le problème de dimensionnement de la capacité de la batterie stationnaire. La situation de mise en file d'attente de la station de recharge rapide locale (SRR) et la théorie des files d'attente sont également prises en compte. Les résultats de la simulation montrent que l'adoption de véhicules électriques pourrait contribuer de manière significative à réduire l'investissement sur le stockage de la batterie, ce qui pourrait apporter des avantages économiques et sociaux importants.

Cette thèse propose également une méthode permettant de gérer les comportements de recharge des véhicules électriques afin de réduire leurs effets dans le réseau. Nous résumons les habitudes de charge des utilisateurs de véhicules électriques, sur la base d'observations de profils de facturation provenant du système de mesure avancé. La méthode distingue des modèles d'utilisateurs sans surveillance et établit une nouvelle stratégie de planification pour réduire la demande de puissance de pointe du réseau. La stratégie est basée sur le concept de Valley Filling tout en envisagant également de réduire la durée totale des interférences du processus de charge des utilisateurs. Les impacts généraux sur le réseau de la charge des véhicules avant et après l'adoption de la stratégie proposée sont simulés et comparés. Les résultats montrent que la méthode proposée est capable de soulager l'impact sur le réseau et d'augmenter ainsi la capacité de service des véhicules électriques des réseaux de distribution.

Cette thèse introduit également un cadre de planification de chargement dynamique basé sur des algorithmes à base de Q-learning amélioré pour les véhicules électriques. Le problème d'ordonnancement, qui considére la situation de congestion de la station de recharge rapide (SRR), se concentre sur l'échange d'énergie bidirectionnel entre le véhicule et le réseau de distribution. En particulier, la thèse transforme le problème de planification dans l'établissement de la table de récompense appropriée pour la recharge de véhicule électrique. La simulation du modèle en tant que problème de grille Q-learning dans l'espace à 3 dimensions, où le chemin optimal implique la meilleure série d'actions à prendre à chaque moment. L'avancement du cadre actuel de l'apprentissage Q-learning se réfère spécifiquement à la considération supplémentaire de la capacité de service limitée de SRR. La théorie des files d'attente (file d'attente M/ M/ 1/ N/ ∞) est introduite pour remédier au phénomène de congestion de la recharge des véhicules électriques. Une brève revue de la littérature sur les impacts de la recharge des véhicules électriques, et de la tarification selon l'heure d'utilisation (TOU) est présentée. Le cadre Q-apprentissage fournit une solution pratique pour atténuer les impacts de recharge des véhicules électriques dans les réseaux, y compris l'altération temps de recharge en raison du TOU et de support du réseau en adoptant un plan de véhicule à réseau (V2G).

Acknowledgements

I would like to thank my supervisor, professor Benoit Boulet, for giving me the privilege to be a part of his research group. It is his trust, guidance, and his continuous support that has shaped this thesis in its desired form.

Furthermore, I extend my thanks to the Natural Sciences and Engineering Research Council of Canada (NSERC) for the financial support.

I would like to thank Dr. Di Wu for his help introducing me to the energy management project, and his facilitating my understanding of time series forecasting.

I would like to express my appreciation to all my friends and colleagues in the McGill Intelligent Automation Lab. I would also like to thank my friends from the Centre for Intelligent Machines and Power Lab for their resources and encouragement throughout my research.

Finally, I wish to express my sincerest appreciation and love to my parents for backing me up during my graduate studies.

Contents

List of Figures

List of Tables

List of Acronyms

AC Alternating Current.

BEV Battery Electric Vehicles.

CES Community Energy Storage.

CS Charging Station.

CTMC Continuous Time Markov Chain.

DC Direct Current.

DER Distributed Energy Resource.

DOD Depth of Discharge.

DSM Demand Side Management.

ESS Energy Storage System.

EV Electric Vehicles.

EVCL Electric Vehicle Charging Loads.

FCFS First Come First Served.

FCS Fast Charging Station.

G2V	Grid-to-Vehicle.
GHG	Greenhouse Gases.
HEV	Hybrid Electric Vehicles.
HVAC	Heating Ventilation and Air Conditioning.
ICEV	Internal Combustion Engine Vehicles.
PV	Photovoltaic.
SOC	State of Charge.
TOU	Time-of-Use.
V2G	Vehicle-to-Grid.

Chapter 1

Introduction

1.1 Motivation

The mismatch between renewable power supply and demand is the main problem in community microgrids [5]. For instance, solar power from rooftop PV panels or wind power from local turbines come from unpredictable and weather-dependent sources, which results in overproduction or lack of energy production that does not satisfy the demand in residential load [2, 6, 7]. To balance the supply and demand of these distributed energy resources, one of the solutions is community energy storage (CES). The CES is connected directly to the utility distribution grid at the distribution feeder, and operated by the utility for the purpose of backup power, to mitigate flicker, and to integrate more renewable capacity while maintaining community grid stability. At the broader grid-scale, CES can provide voltage regulation, peak demand shaving, power factor correction, and other important ancillary services [8]. Some utility-driven CES business projects have been successfully implemented, see reports from Chicago-based utility ComEd in 2017 [9] and Quebec-based utility Hydro-Quebec's "EVLO" project report in 2020 [10].

In this thesis, we consider the CES's major function as an energy bank to collect the excess solar power from the PV panels. Moreover, we consider EV fleet batteries in the community as virtual CES resources, for two reasons. First, according to [11–13], although

EVs still represent a small fraction of the overall vehicle market, their annual sales growth rate will be around 30% over the next decade. Thus the resources of the ”EV as CES” idea will be abundant. On the other hand, new Lithium-Ion (Li-Ion) battery technology allows batteries to retain 95% of their life after 1,000 cycles [14]. Thus, coordinating the V2G discharge of fleets to backup the grid will be a more acceptable concept for EV owners. If the vehicle batteries could work as virtual storage, then the strategy that involves them as supplemental CES would reduce capacity requirements during system planning. Thus, this strategy may eventually save money and reduce system design complexity.

The literature digest in Table 1.1 reviews recent research on EV interactions with CES. Most of the papers adopt the EV fleet as an important microgrid sector but only see EV batteries as immobile storage resources. Papers [15, 16] use retired EV batteries as supplemental CES. The papers [17, 18] look into the live, dynamic behavior of EV charging. They use EVs with vehicle-to-grid (V2G) capability as a frequency-controlled normal operation reserve (FNR) provider in the future renewable-based power system.

Rather than a fast frequency reserve, the role of the EV fleet suggested in this thesis is to provide a long-term effect in CES planning and make a difference in capital cost reduction.

1.2 Contributions and Publications

The first objective of this work is to develop a practical scheduling and dispatching scheme for EV fleet interacting with power grids. To achieve this goal, we study and develop the EV charging load (EVCL) model and its load impacts model based on meter side charging power data. We also use Q-learning to help EV fleets make automatic decisions to get the energy in or out of their batteries. The second objective is to build a platform for the EV fleet to be used as a virtual battery resource to back up the community grids. The research contributions of this work are highlighted as follows.

In Chapter 2, we show that a charging model should be built on charging data and avoid generalized vehicle behavior assumptions. As further illustrated in Sections 2.1 and 2.2, the start charging time of EV is largely personalized. There is a large portion of EV users who fix their start charging time in a specific hour to fulfill their needs for the daily commute. Thus, rather than a general Gaussian distribution, a more appropriate choice is to use a piece-wise defined function to describe their start charging time in a day. Also, we show that a bi-modal or log-normal distribution is more suitable to describe the initial state of charge of EVs' batteries in a fleet before charging.

In Chapter 3, we introduce a Q-learning algorithm-based dynamic charging scheduling scheme that intends to optimize the operation benefit for electric vehicles. Particularly, the chapter transforms the scheduling problem into the establishment of a suitable reward table for EV charging. The simulation models it as a Q-learning grid world problem in 3-Dimensional-space, where the optimal path implies the best series of actions to take at each time slot.

The major contributions of Chapter 4 are twofold. First, it describes the stochastic queue nature of individual EVs. Basic charging stations topologies are modeled and studied together with other uncertainties in a community microgrid setting. Second, it shares detailed comparisons between G2V and V2G-based virtual battery strategies and makes a recommendation on future FCS topologies for better deployment of the virtual battery concept. Also, the dynamic electricity pricing (TOU) is considered so that the arrival rate of EVs in the microgrid is affected. Introducing TOU reflects the practical utility environment so that the fleet battery result is more reasonable.

Finally, Chapter 5 concludes this thesis.

The contributions mentioned above are included in the following published peer-reviewed papers. The research presented in this thesis also benefits from the collaborations with other scholars, especially from the co-authors of each paper.

- Qiyun Dang, Di Wu, and Benoit Boulet. ”EV Fleet as Virtual Battery Resource for Community Microgrid Energy Storage Planning Le parc de véhicules électriques comme ressource de batterie virtuelle pour la planification du stockage d'énergie des micro-réseaux communautaires.” IEEE Canadian Journal of Electrical and Computer Engineering (2021).

- Qiyun Dang, Di Wu, and Benoit Boulet. ”EV Fleet Batteries as Distributed Energy Resources Considering Dynamic Electricity Pricing.” 2021 IEEE 12th International Symposium on Power Electronics for Distributed Generation Systems (PEDG). IEEE, 2021.

- Qiyun Dang, Di Wu, and Benoit Boulet. ”Electric Vehicle Battery as Energy Storage Unit Consider Renewable Power Uncertainty.” 2021 IEEE Energy Conversion Congress and Exposition (ECCE). IEEE, 2021.

- Qiyun Dang, Di Wu, and Benoit Boulet. ”Community Microgrid Energy Storage Sizing Considering EV Fleet Batteries as Supplemental Resource.” 2020 IEEE Electric Power and Energy Conference (EPEC). IEEE, 2020.
- Qiyun Dang, Di Wu, and Benoit Boulet. ”EV charging management with ann-based electricity price forecasting.” 2020 IEEE Transportation Electrification Conference & Expo (ITEC). IEEE, 2020.
- Qiyun Dang, Di Wu, and Benoit Boulet. ”An Advanced Framework for Electric Vehicles Interaction with Distribution Grids Based on Q-Learning.” 2019 IEEE Energy Conversion Congress and Exposition (ECCE). IEEE, 2019.
- Qiyun Dang, Di Wu, and Benoit Boulet. ”A Q-learning based charging scheduling scheme for electric vehicles.” 2019 IEEE Transportation Electrification Conference and Expo (ITEC). IEEE, 2019.

During the project, some related work has also been conducted, these work can be treated as complementary work for this thesis, and the publications are listed as follows:

- Qiyun Dang, and Yuchong Huo. ”Flexibility scheduling for microgrids with electric vehicle (ev) penetration.” 2018 IEEE Energy Conversion Congress and Exposition (ECCE). IEEE, 2018.
- Qiyun Dang, Yuchong Huo, and Chu Sun. ”Privacy preservation needed for smart meter system: A methodology to recognize electric vehicle (EV) models.” 2018 IEEE Innovative Smart Grid Technologies-Asia (ISGT Asia). IEEE, 2018.
- Qiyun Dang. ”Electric vehicle (EV) charging management and relieve impacts in grids.” 2018 9th IEEE International Symposium on Power Electronics for Distributed Generation Systems (PEDG). IEEE, 2018.
- Qiyun Dang, and Yuchong Huo. ”Modeling EV fleet load in distribution grids: a data-driven approach.” 2018 IEEE Transportation Electrification Conference and Expo (ITEC). IEEE, 2018.

Reference	Objectives	Digest of cases
[19] [20]	Algorithm aims at maximally enhancing the customer satisfaction while reducing the potential uncertainties. The battery storage and EV fleets are individually operated in both papers.	The maximum output power of PV system is assigned to be 153 kW. 18 chargers are assumed to be installed in the charging station, and less than 18 PEVs can be connected and charging at the same time [19], and in [20], the systems are tested in managing the grid peak load in a real power-distribution network, located in Australia
[21] [22]	Strategies use local battery storage in households with vehicle battery and PV generation to shave the peak loading. Also consider profit criteria based on Electricity Day Ahead Market.	In [21], among the 15 houses, four houses have an electric vehicle, five houses have solar panels, and one house has both EV and solar panel. In [22], the charging of EVs is in the hours of high PV production. The discharging of vehicles is in the evening, when the load demand increases.
[15] [16]	By utilizing second-life EV batteries, the first goal is to minimize yearly operation cost of a battery-PV system. The second goal is to optimize the size of the PV-panel in the system.	Residential load demand data in one year is obtained from a utility company. The cost of the retired battery pack per kWh, and the cost of the power electronics circuit per kW are assumed to be \$100/kWh and \$260/kW, respectively. The maximum size of the PV system PV_{max} is set as 10 kW
[23] [2]	Studies on the impacts of stationary and mobile battery integration to substation. The target is either for a commercial building or community microgrid with stationary [23] and mobile [23] [2] battery storage.	The problem in [23] is formulated into a two-stage stochastic programming problem. In the problem BESS max/min charging power is set as 40 kW/20 kW, EV max charging power 6.6 kW, discharging power 2.0 kW. Paper [2] shows a continuous time markov chain queueing problem with 12 houses and 12 EVs.

*In our research, we are specifically trying to optimize the capacity of the storage system, not on PV panels as the papers above. And the battery is dynamic rather than stationary.

Table 1.1: REVIEW OF EV AND COMMUNITY ENERGY STORAGE

Chapter 2

EV Fleet Behavior Modeling[1]

2.1 Modeling Charging Loads of EV Fleet

This section proposes a modeling method for electric vehicle (EV) charging loads in the distribution grids. Different from previous work that uses modeling under general car travel distance based statistics, we advocate using real world power consumption data, which are collected from the charging port meters. The essential charging behavior characteristics were retrieved from such high-resolution data. The vehicle behavior indicates that the distribution of the initial SOC when an EV is charged is not necessarily log-normal type. Possible causes for such distribution are discussed. The new model proposed here can incorporate the stochastic nature of EV charging to improve researchers' analysis. An explicit description of the model along with its operating dynamics and a practice to analyze the total power load of a mid-sized EV fleet is provided. We demonstrate that the proposed model can more correctly reflect the total power need of a fleet and can be adopted as a load-forecasting tool of EV fleet charging load.

2.1.1 Backgrounds

The load model is essential to the distribution system simulation. The objective of load modeling is to represent dynamic profiles of a variety of loads, ranging from appliance level to grid level, into simple mathematical models in order to reduce the complexity of

[1]Parts of this chapter have been presented in [24, 25]

computation [26]. According to appliance level models, previous research has been focused on studying heating, ventilation, and air conditioning (HVAC) loads. In recent years, as a larger population of electric vehicles are integrated into the power grid, there has been a lot of interest in modeling the electric vehicle charging loads (EVCL). There are mainly three types of electric vehicles, classified by their energy source for electrification. The Hybrid Electric Vehicles (HEVs) and Plug-in Hybrid Electric Vehicles (PHEVs) are powered by both petroleum and electricity. The Plug-in Electric Vehicles (PEVs) are fully electric and do not have a petrol engine. The HEVs battery is recharged by its own braking system thus grid operator does not need to consider its interaction with the distribution system. However, the PHEVs and PEVs are recharged by plugging-in to an external electrical charging point, which charging process can be measured, observed from grids, and generalized into load models. The types of electric vehicles connecting simultaneously into the power grid may vary, which drives complexity in modeling load of an EV fleet. However, the energy storage technologies they adopted are the same. The energy storage units in vehicles currently used widely are packages of lithium-ion batteries, due to their energy density and power density advantages [27]. Therefore, different EVs has essentially identical charging profile, the modeling of either PHEVs or PEVs charging can be reduced to one modeling problem. The remaining differences between charging profile of a PHEV and a PEV are (1) the instantaneous peak charging power (kW) and (2) charging cycle duration (min). Compared to PHEVs, the PEVs have relatively higher battery capacity. Thus, the average charging cycle of PEVs is longer. Modeling EV fleet charging load is a concept analogous to the residential total load modeling. Assume the load profiles of appliances are linearly independent, the aggregated residential load $\mathrm{P_L}$ can be represented as a linear combination of home appliance load $\mathrm{P_{L,i}}$ on the site. Similarly, in a given fleet of EVs, assume the charging event of car$i$ does not interfere with the charging process of another car$j(i \neq j)$, then the fleet total load profile at time t can be represented as $\mathrm{P_L(t)} = \Sigma\left[p_{\mathrm{L,i}}(\mathrm{t})\right]$. In a real situation, the available charging facilities at a given charging station could be limited. When the station experience a full load operation, the arriving vehicles car n in the fleet may have to wait or choose a nearby station, thus their charging cycles could be delayed, the time denoted as T n . In this chapter we assume adequate EV charging resources are available for the fleet, however if there is a congestion, the fleet total load at time t can be simply modified as, $\mathrm{P_L(t)} = \Sigma\left[p_{\mathrm{L,i}}(\mathrm{t}), p_{\mathrm{L,n}}\left(\mathrm{t}-\mathrm{T_n}\right)\right]$. The EV charging model in this chapter is developed on direct observation on the EV charging profile through charging port smart meters. Smart meters are designed to offer high-resolution load readings to utilities and users, down to the minute level. Before large-scale deployment of EV charging smart meters, there has been some literature on the EV load modeling, based on general travel statistics of traditional vehicles. In [28], a specified operation model for EVs under domestic and public charging situation is proposed. The model assumed a log-normal type probability density function of battery state of charge (SOC), according to the distribution of vehicle daily travel distance from the national travel survey by U.K. in 2009. The model also assumed a Gaussian distribution of start time of EV charging, with a center around 1:00 am. In [29], a similar EVCL model based on U.K.'s vehicle travel survey is demonstrated, the model sees the single lithium-ion EV battery charging process as a right-angled trapezoid figure, and the model is further employed to optimize power system demand. The work in [30] employed bivariate normal distribution model in a theoretical analysis, and described the total power demand of EVs in a station in a Weibull distribution. Reference [31] monitored charging of a fleet of 15 Mitsubishi EVs in Ireland for 9 months, resulting in a model adopting conditional probabilities of variables including state of charge (SOC), and trip number. Except for [31] , most previous works made estimations of EV behavior using travel surveys. This holds identical views with [31] that a charging model should be built on charging data and avoid generalized vehicle behavior assumptions. For instance, as further illustrated in the section below, the start charging time of EV is largely personalized. There is a large portion of EV users who fix their start charging time in a specific hour, e.g. 4:30 am, to fulfill their needs in the daytime, which cannot be described as a general Gaussian distribution over 24 hours in a day.

2.1.2 Data Collection

The meter data adopted in this study are collected from the Mueller community in Austin, Texas. It is envisioned as a sustainable community that deployed smart meters at device-level, including EV charging port, to continuously monitor the power use and feedback to residents. Under community's consent, the datasets intended for research purposes is available on Dataport. The total number of EVs in Muller community is around 120, the type of EVs vary from HEV, PHEV, and PEV.

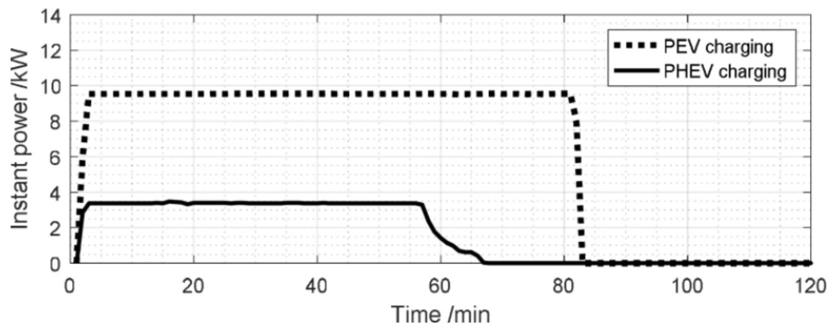

Figure 2.1: Comparison of charging profile of a PHEV and a PEV

A. Electrical Vehicle Charging Process

The charging process of EVs from meter data is visualized in Fig.2.1. As shown in the figure, two different kinds of EV, PHEV and PEV have similar charging profile. The PEV here is referred to a Tesla Model S and PHEV referred to a Ford Fusion Hybrid in database. The charging profiles are based on their meter data on 2016-Mar-10th. According to their charging process, the EV charging power p(t) reaches its on-board charging rate $max[p(t)]$, or $\bar{p}$ rapidly in just a few minutes. The power maintains a constant value in the course of charging and it rapidly decreased to zero towards the end of the charging. The process can be mathematically expressed as equation (2.1). Where t in [0,t_1] represents the rising edge of charging and [t_2,t_3] represents the down edge. The $\bar{p}$, peak-charging power for the given EVs is 10kW and 3.33kW respectively from the figure 2.1.

$$p(t) = \begin{cases} \bar{p} \cdot \left(\frac{t}{t_1}\right), & 0 < t \leq t_1 \\ \bar{p}, & t_1 < t \leq t_2 \\ \bar{p} \cdot \left(\frac{t_3 - t}{t_3 - t_2}\right), & t_2 < t \leq t_3 \end{cases} \tag{2.1}$$

As the minutes level transient process in $[0, t_1]$ or $[t_2, t_3]$ is trivial compared to the steady charging stage $[t_1, t_2]$. The equation (2.1) can be further simplified in equation (2.2).

$$p(t) = \begin{cases} \bar{p}, & t_1 < t \leq t_2 \\ 0, & \text{others} \end{cases} \tag{2.2}$$

The equation (2.2) in nature represents a train of square waves in the time domain.

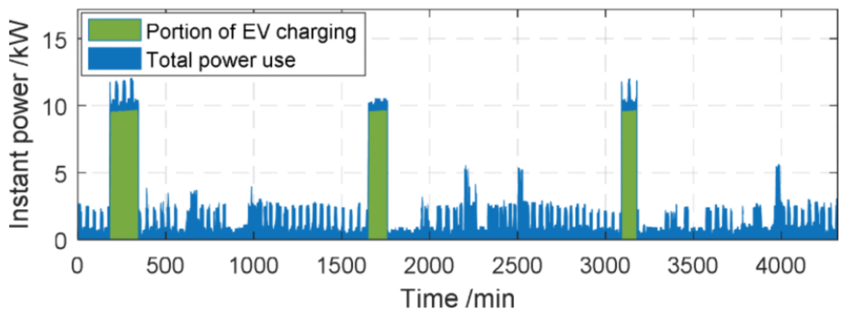

Figure 2.2: EV charging load component in total residential load (kW) in 3 days

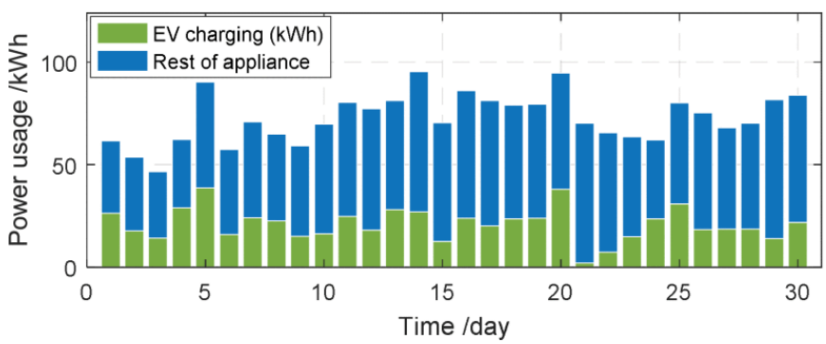

Figure 2.3: Compare EV charging load energy consumption to the total residential load (kWh) in 30 days

From meter side data, shown in Fig.2.2, the EV profile component in total residential load is square wave type, although the intervals of each square may vary. The benefit of modeling EV charging profile in pure square pulse in equation (2.2), besides a reduction of computation cost, is to help us become more aware of the impacts when EVs terminate their charging. As the system is always seeking a balance between generations and demand, when the demand of EVs decreases concurrently on the shape of the negative edge of the square pulse, the power mismatch may happen and result in a quick increase in system frequency.

B. EV Charging Loads Component in Residential Loads

To understand the EVs future influences in grids, we compared the EVCL of an EV user's house to its total home load in Fig.2.2 and Fig.2.3. Unlike adding traditional appliances, the emerging EV loads will remarkably increase the peak house power. As shown in Fig.2.2, the residential peak power was lower than 5 kW before an EV is integrated. The peak power nearly tripled to 14 kW when a vehicle is under recharge. Moreover, the periodical minute level minor spikes on Fig.2.2 results from start-stop of refrigerator compressor. Also as shown in Fig.2.3, the emerging EV loads in residential side will take up around 30% of total power need in each day. The percentage data at day n is derived from,

$$\text{ratio}\ _n = \frac{\int p(t)dt}{\int P_1(t)dt} \cdot 100\% \tag{2.3}$$

where P1(t) represents total appliance power. In addition, for residents that have more EVs, the EVCL may take up 50% in total load. This situation calls for a more redundant design in distribution system protection. It also prompts economic and environmental analysis on EVs charging aspects in distribution grids. An accurate EV fleet charging model will support in solving both problems.

2.1.3 Parameters for EV Charging

The EV fleet charging load contains superimposed layer of single EV charging loads. The feature analysis of single EV charging load requires a group of data handling methods. Note that the meter data needs cleansing before it is loaded, a basic pre-processing method is shown in [16]. As illustrated in expression equation (2.1) and equation (2.2), the profile of single EV charging can be expressed as pure square wave with fixed amplitude $\bar{p}$, the on board charging rate. The EV charging features to be modeled here is the start of charging time in a day, t_1 , and the length of charging cycle t_c= [t_2-t_1]. The value of variable t_1 and t_c are determined by their probability distribution function.

A. Probability Distribution of Start Charging Time

Assume the meter data loaded is m(t), the first step is to convert m(t) into binary code [0 0 0 1 1 1..] under expression (2.4).

$$\mathrm{M(t)} = \begin{cases} 1, & \text{if } : \mathrm{m(t)} > \frac{\bar{p}}{2} \\ 0, & \text{others} \end{cases} \tag{2.4}$$

the length of m(t) chosen is 525,600 which is $365day \times 1440min/day$. The start of charging time t_1 can be derive from rising edge of binary strings M(t).

Two types of the accumulated t_1's distribution of single EV are shown in Fig.2.4. The first type is fixed-time charging type shown in Fig.2.4(a) The other one is random charging, shown in Fig.2.4(b). Empirically if the probability value of a certain hour is higher than 0.3, this EV owner can be regarded as a fixed-time charging user. The random charging user's t_1 distribution is seen as a Gaussian distribution, however, for the user who schedules their charging at certain times, the distribution lacks randomness. A synthesized model should consider both situations. Randomly pick 30 EV users' one year start of charging time data from database, around 35% users are fixed-time charging type. Together with the 65% random charging users, the overall distribution is shown in Fig.2.5. The total distribution in the figure can be described as,

$$f\left(t_1 \mid \mu_1, \mu_2, \sigma_1, \sigma_2, k\right) = \frac{1}{\sigma_1\sqrt{2\pi}} e^{\frac{-(t_1-\mu_1)^2}{2\sigma_1^2}} + \frac{k}{\sigma_2\sqrt{2\pi}} e^{\frac{-(t_1-\mu_2)^2}{2\sigma_2^2}} \tag{2.5}$$

The (2.5) describes the bi-modal feature of distribution of t1. Such distribution is a continuous probability distribution with two different modes, appearing as two distinct peaks in the probability density function, as shown in Fig.2.5 The k is the mathematical bi-modal ratio of the left and right peaks. The μ and σ are the mean and standard deviation of first and second Gaussian distributed peaks. In profile of Fig.2.5, the parameters $[\mu_1, \mu_2, \sigma_1, \sigma_2]$ are [3.22, 19.18, 0.83, 4.61] respectively.

B. Probability Distribution of Charging time Duration

The total charging duration each time an EV is put under charge is stochastic. However as the energy storage capability of the EVs battery, E_{bat} is limited, then the distribution range of t_c will be bounded by, $(\mathrm{E_{bat}}/\bar{p})$

The value of t_c is computed by,

$$t_c = \left[\int_{t_1}^{t_2} p(t)dt\right] / \bar{p} \tag{2.6}$$

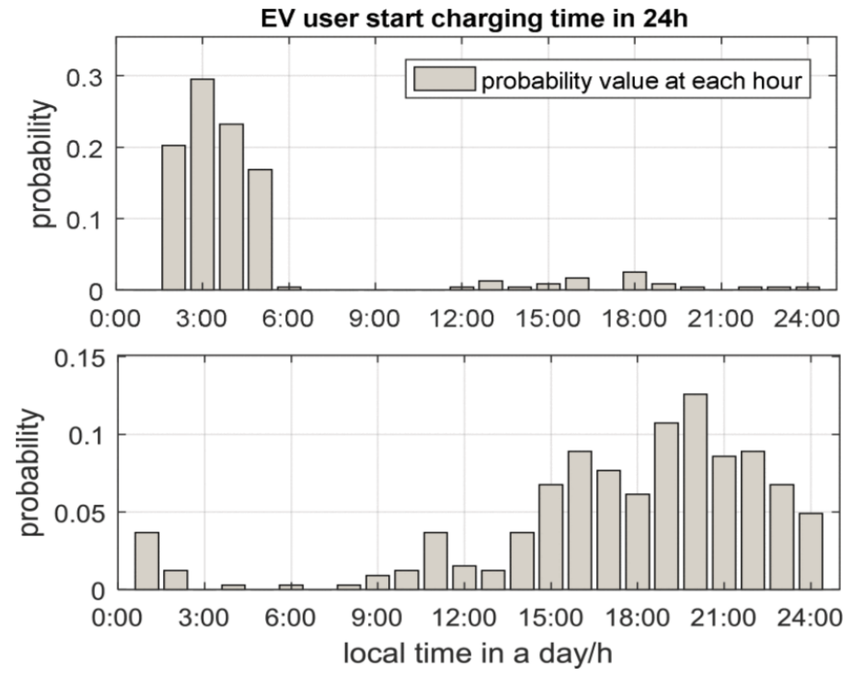

Figure 2.4: Comparison of start charging time distribution of different types EV user. (a) shows fixed-time charging type (b) random time charging type

The duration t_c reflects the initial Depth-of-Discharge (DoD) of the vehicle when it put under charge, the longer the t_c the deeper DoD the EV battery has. To ensure more generalized results, first pick 50 different types of EV's one year charging data from database. According to the data, vehicles are averagely charged 342 times per year. To see the distribution of the t_c (or the DoD), randomly take 10% of the t_c data as a subset, do it 6 times and see each of subset's probability distribution. Result is displayed in Fig.2.6. As shown in Fig.2.6 the charging probability at each percent DoD is different. The general shape of each distribution all follows bi-modal type, as two distinct peaks can be seen from each figure. A combination of Fig.2.6 is shown in Fig.2.7. A turning point at DoD = 80 % can be seen from the figure. The figure's left segment (DoD <80%) part is similar to a left-centered normal distribution (or lognormal distribution), the right segment can be viewed as a normal distribution which centered at 90% DoD. Previous literatures describe the distribution of DoD of EV put under charge as Normal or Weibull distribution. However, as Fig.2.7 shows, from the observations of meter side data, neither fitting curves

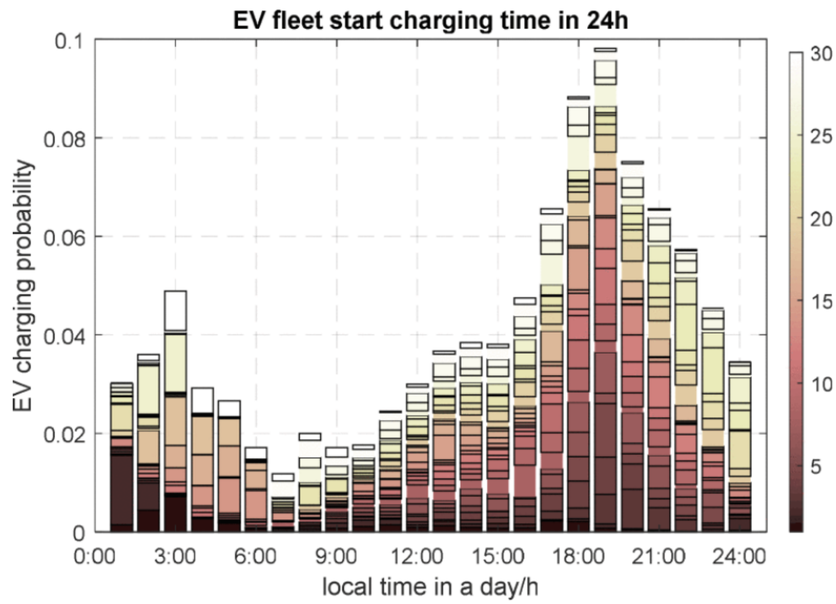

Figure 2.5: Start charging time distribution of vehicles in the sample EV fleet. The fleet size is 30 and each color represents one vehicle

is good enough to represent the DoD distribution. As the distribution has a 2nd peak begins at 80% DoD, the mismatch of the such fitting curves will be very high when DoD is in range 80% 100%. The reason for such second peak at high DoD may result from battery energy loss between two trips. A stand-by mode EV is still consuming energy, thus at the time when an EV battery is put into recharge, the DoD is deeper than its DoD at the end of last trip. The longer the EV is not put into use, the more the energy loss (including battery self-discharge). When EV has a long enough stand-by time, the DoD would be close to 100%. In addition, from Fig.2.7, most of charging events seemed only refilled 15% 20% of battery capacity, this may result from people tends to not wait DoD to be 100% (battery used up) to charge their vehicle, and intend to fully charge the vehicle again even if the distance of last trip is short. The bi-modal distribution of the t_c (or the DoD) can then be generalized in the expression similar to equation (2.6).

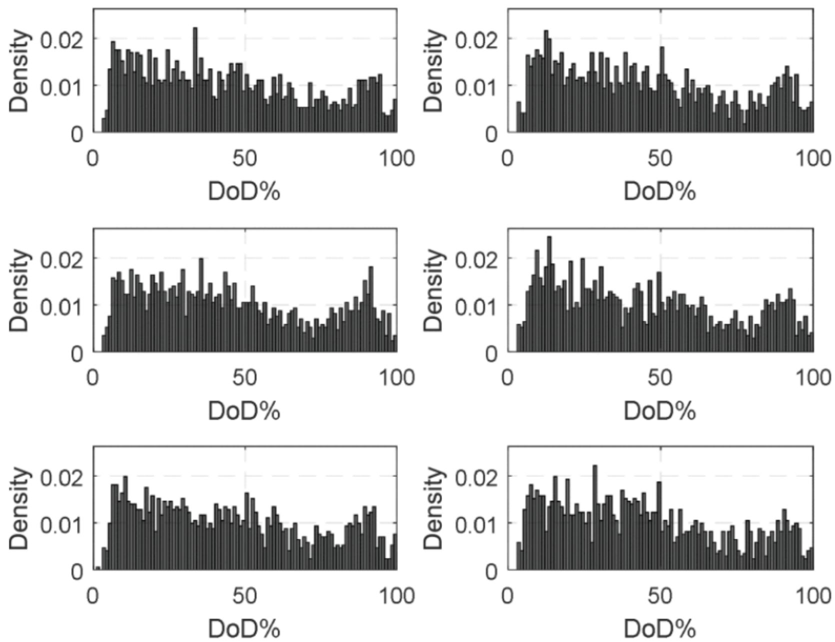

Figure 2.6: Distribution of Depth of Discharge (DoD) in each sample, each sample represents 10% of total charging data

2.1.4 Modeling EV Fleet Charging

A. Simulation Setup

The EV fleet power load is established on single EV charging loads. For modeling single EV charging, since the two key parameters, variable t_1 and t_c are determined by their probability distribution function, the rest of input to consider is only E_bat and $\bar{p}$. Both of them are constant value which can be read from manufacture data sheet. In addition, the proposed constitution of local EV fleet load profile should consider car manufacture's market share.

B. Simulation Results

Fig.2.8 shows the simulated EV fleet load profile using model described in Sec.III. The fleet in Fig.2.8 is chosen to have 55% of vehicle to be Chevrolet Volt, 25% Nissan Leaf, 15% Tesla model S and 5% Fusion Hybrid. Which reflects the EV market of Canada. When the fleet size is set as 100 EV (Case 1), the maximum load in 3 days is around 70kW. When fleet size

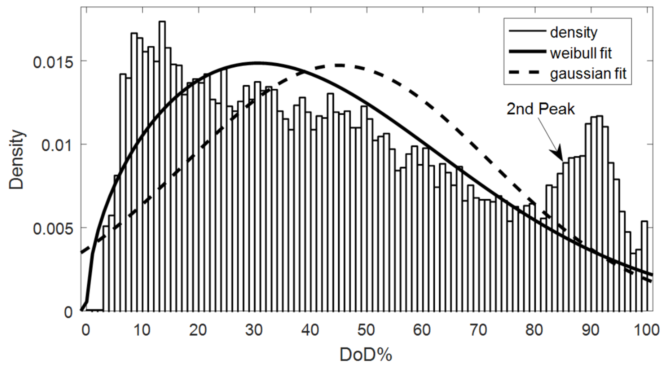

Figure 2.7: Aggregated initial DoD distribution profiles of 50 EVs in one year. Use of ideal Gaussian or Weibull fitting curves is not suitable here because there is a second peak in distribution

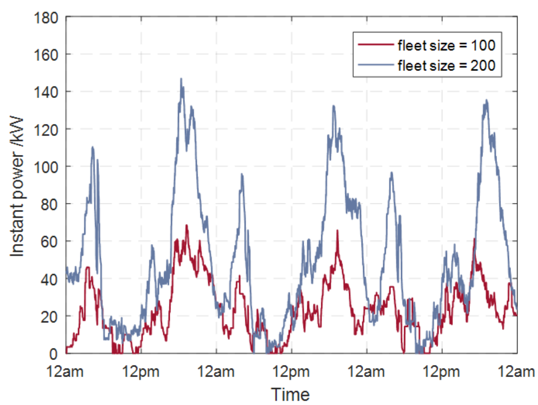

Figure 2.8: Fleet power load simulation in 3 days. Case 1 and 2 's size are 100 and 200

doubled to 200 EV (Case 2), the maximum load is 150kW, which also doubled. On each day different fleet size of EVs has similar bi-modal type load profile, the first peak is around 3am and the second peak at 9pm. The load profile is periodical and has a period of 24 hour.

2.2 Modeling EV Charging Impacts in Grids

This section proposed a method to manage electric vehicles charging behaviors in order to reduce its effects in grids. The chapter summarizes the charging patterns of electric vehicle users, based on charging profile observations from advanced metering system at first. The method distinguishes supervision-free user patterns and establishes a novel schedule strategy to reduce grid peak power demand. The strategy is based on the ”valley filling” concept while also considering cutting down the total interference time of users’ charging process. The general grid impacts of vehicle charging before and after the adoption of the proposed strategy is simulated and compared. The results show that the proposed method is able to relieve grid impact and thereby increase the EVs service capability of distribution grids.

2.2.1 Backgrounds

Compared to traditional power loads, the EV charging load tends to be more random in nature [32]. The charging station selection of EV user is spatially stochastic, and can appear anywhere on the topology of the distribution network. The arrival time of vehicle is also largely user-personalized, some user tends to refill their EV battery at a fixed time in the early morning, and some charge their vehicles at a random afternoon time. If EV charging events are left unscheduled, the utility grid can be affected negatively. Besides, the EVs are usually recharged either at a public charging station or at home, thus it affects the distribution grids more directly. Moreover, the effect of charging load will be more severe when the EV charging process coincides with the grid peak loading hours [33].

According to the survey [34], vehicle charging loads effect can be analyzed in several aspects including voltage drop, power unbalance, and harmonic distortion. To simplify, in this section the impacts are mainly explained in voltage drop on a distribution grids system.

However, by the end of this section we employ a simple and feasible load shifting strategy that helps ease EV charging impacts on grids.

2.2.2 Simulation Setup

The grid impact is simulated in Matpower [35] and the test bench adopted is an updated IEEE-33 bus distribution system.

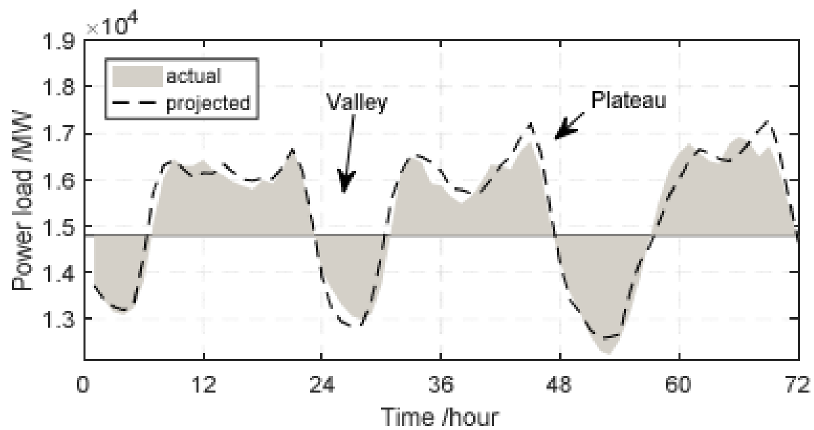

Figure 2.9: Base power load profile adopted from IESO

One can conclude from Fig.2.9 that the system load is periodical and has certain peaks and valleys. The load is low at mid-nights and plateaued at daytime from 9am to 9pm.

The average load in Ontario province is close to 15 GW, serving 15 million people. The distribution grid assumed here serves a 1.5 thousand people community. The base load chosen in test bench is scaled down to 1.5 MW, with load profile referred to Fig.2.9. To simplify, the EV loads are connected to bus 6 only, which represents a public charging station in distribution grids. The static var compensator (SVC) installed at bus 30 is for voltage regulation and power factor correction purpose, and will be further illustrated in Section 2.2.4.B. The simulation horizon is 24 hours.

2.2.3 EV Load Patterns

As described in previous Section 2.1, the profile can be regarded as pure square waves with positive amplitude. The amplitude is numerically equivalent to vehicle on-board charging rate, mostly 3.33/6.67 kW. What makes a charging profile different from others is its start charging time selection distribution.

A. Types of Charging Pattern

The accumulated distribution of such start charging time has different shapes with each shape indicates a specific charging pattern of EV user [36].

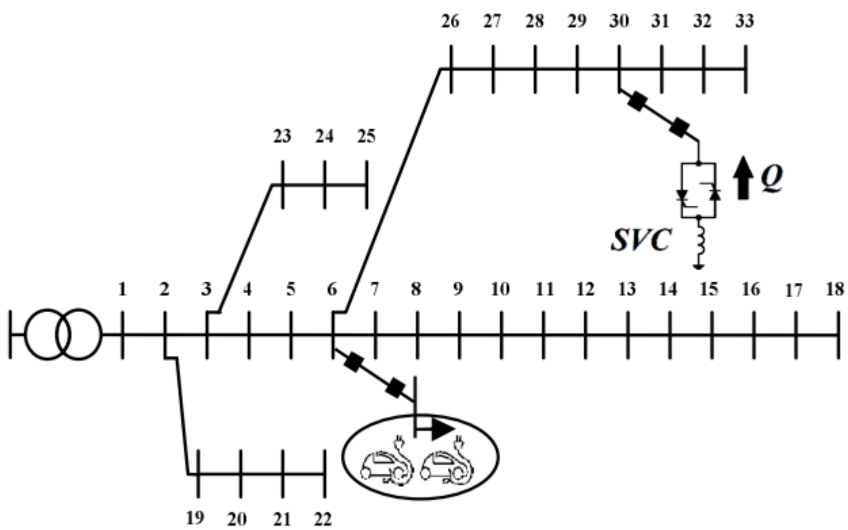

Figure 2.10: IEEE-33 bus distribution system test bench with Bus 6 connected to EV charging station. Static Var Compensators (SVCs) will be installed on several buses to regulate the voltage

Three particular kinds of charging patterns are summarized in Fig.2.11, each type proposed two examples (a), (b). Type 1 refers to users who fix their charging event in early morning. The accumulated probability for them to charge from 1:00 am to 6:00 am is greater than 70%. Type 2 refers to users who randomly charge their vehicles from mid-day to afternoon. This pattern has some obvious overlap with system peak load profile in Fig.2.9. It may further burden the system and has a potential to be re-channeled to non-peak hours. The type 3 pattern refers to users who arrive to charging ports mid-night. From 9:00 pm to 1:00 am its integrated charging probability is over 50%.

The type 1 or 3 users have the least effect in grids, however they appear relatively infrequently in the community. Most of users charging behavior follows a type 2 pattern.

B. EV Fleet Total Load

Assume the penetration level of EVs in the proposed distribution grid is high. Up to 500 vehicles are fully electric and acquire the energy they need from the grid. Randomly pick and aggregate 500 charging events in database to emulate the one-day EV fleet power demand in the community. The fleet total load profile is influenced by the charging patterns of all

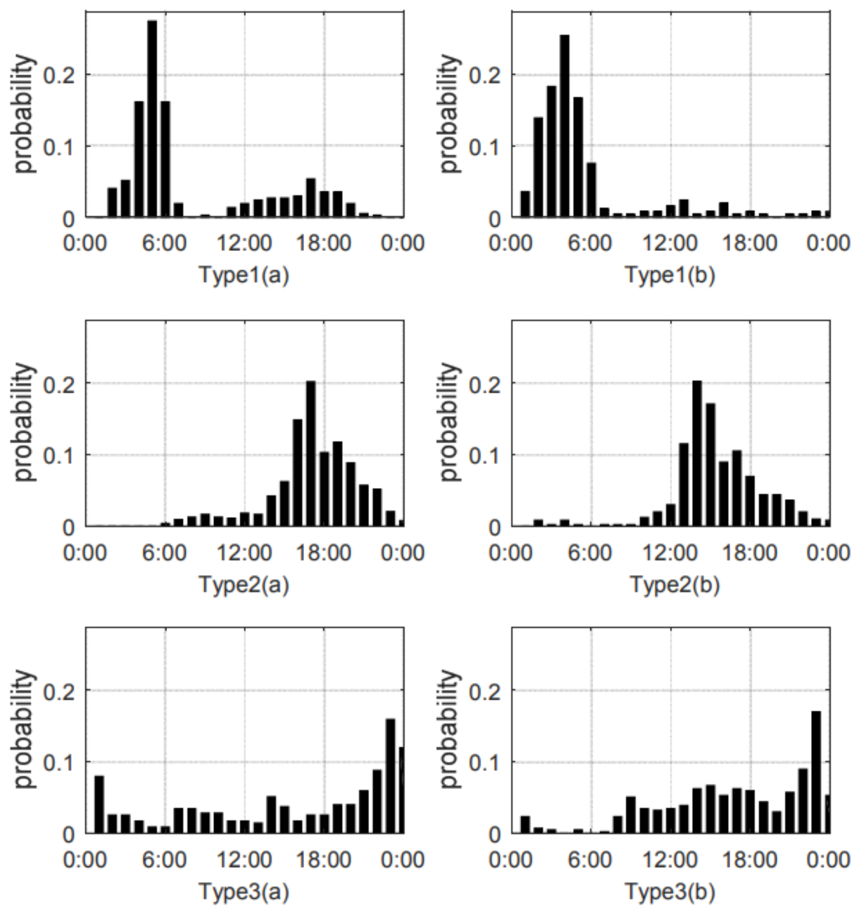

Figure 2.11: Basic behavioral patterns of EV user. Derived from start charging time distribution of vehicle in one year. Two examples (a) and (b) are given for each type of users

three kinds of charging pattern. The EVs power demand at late afternoon is particular high, which reflects the charging behaviors of type 2 user. A second peak can be seen at around 4am, reflecting the power need for fixed time charging users. The type 3 user has lower population that has little influence on the aggregated load profile.

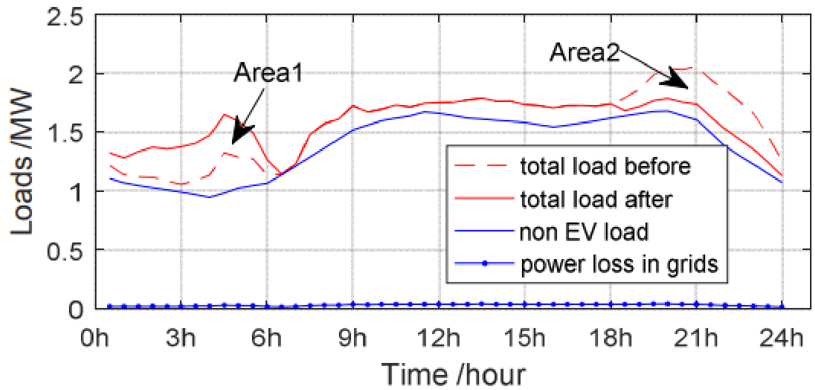

Figure 2.12: Grid total load with non-EV load part indicated. The power loss during grid operation is sketched, total load before and after EV charging reschedule is shown. Areas 1 and 2 contains equivalent amount of energy

2.2.4 Load Management and Performance

A. The Principal Demand Shifting Strategy

When the peak EVs charging load coincides with non-EV residential load, the total grid power demand will reach its peak, shown in Fig.2.12. The upstream transformer in distribution grid has to withstand great pressure at that moment. The core EV load management strategy adopted here is shifting the charging events from high load time to off-peak time. To avoid affecting all EV users, the demand shifting strategy here distinguishes pattern 1 and pattern 3 users at first and then focuses on adjustments to pattern 2 users only. The price of electricity at charging port will be lower in 1am-6am for this user group and higher in 6pm-11pm. The user's pattern category will be dynamically updated according to vehicle's recent charging history. The anticipated grid total load after adoption of demand shifting strategy is shown in Fig.2.12. The strategy expects minimal impact on EV users. Although the EVs aggregated charging profile is changed in Fig.2.12, the area (shifted energy/kWh) of Area1 and Area2 is equivalent. The battery power demand is still fulfilled under proposed demand shifting strategy as the total energy consumption is the same. In addition, as shown in the dotted line in Fig.2.12, the grid power loss is proportional to the grid total load. As the pattern-change method proposed here does not make EV users cut down the total battery charging power they need, to solve

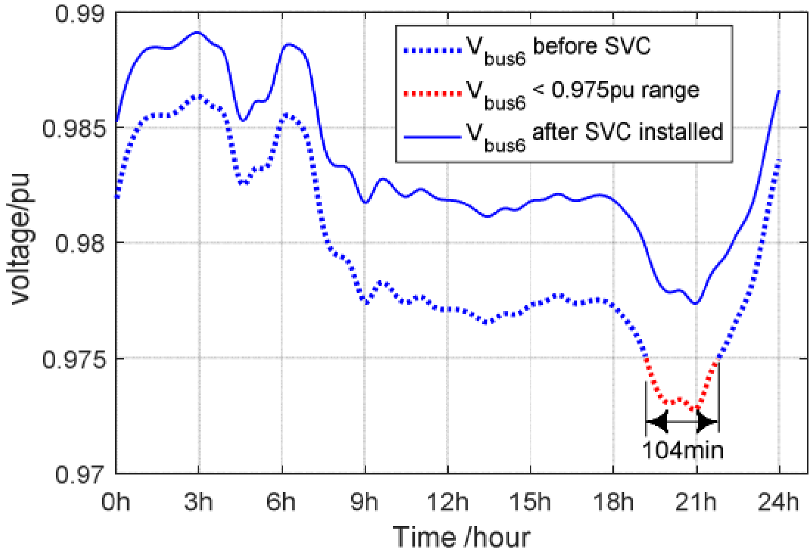

Figure 2.13: Bus 6 voltage profile over 24 hours. The Bus 6 refers to the charging station and received the most interests here

the power loss issue ask for user to save energy in their daily life.

B. A Complementary Method

The power quality issue focused on here is the bus voltage drop. The higher the peak load value, the more severe the voltage dips. The method in Section 2.2.4.A will alleviate the peak load thus relieves its voltage impacts. If the voltage after demand shifting adoption is still low, a complementary method that installs static var compensators (SVC) at buses is recommended. Principles of SVC to regulate the voltage are illustrated in [37]. Assume the voltage level requirement for EV charging station is 0.975 p.u., if the charging of EVs is unscheduled, according to Fig.2.13 the total affected operation time of charging station (bus 6) is going to be 104 minutes. Under the same grid load profile, if SVCs are installed to compensate the low power factor bus in distribution grids (bus 4, 11, 14, 30 is chosen), the bus 6 voltage over 24hr will be markedly improved and ensure a 24hr uninterrupted operation. The SVC compensation is a backup approach to relieving EVs charging loads impacts in grids. In addition, the power loss in grids is lower when the reactive power is locally compensated.

C. Strategy Performance

The performance of the strategy is evaluated by bus voltage profile before and after the strategy adoption in 24 hours. The results are displayed in Fig.2.14. Assume a voltage higher than 0.96 p.u. ensures the proper operation of power loads on non-EV charging buses. According to Fig.2.14(a), when the EV charging loads are not integrated into the grids, the worst voltage profile will be occurring at bus 18 or bus 33 at 10pm. According to IEEE-33 bus system topology, those buses are the terminal bus at each branch. As the color is getting darker from bus 6 to 7, 8 ... 18 and bus 26 to 27, 28 ... 33, one can conclude that the closer the bus to the terminal bus, the more the voltage will drop. Fig.2.14(b) shows the voltage contour of buses when EV loads are integrated in grids. Compared to (a), the overall profile is even darker as the load at each hour is higher. A ribbon can be seen from 4 am to 6 am, which is resulting from type 1 users charging events. Two etch areas can be seen also. Etch represents voltage lower than 0.96 p.u. in certain range of time. Either etch 1 or 2 has 4hr wide and 5 buses long in the contour map. Define the service availability of distribution grids as expression below,

$$\text{Availability } = \left(1 - \frac{N_{in} \cdot T_{in}}{N \cdot T}\right) \times 100\% \tag{2.7}$$

where N_in refers to the number of influenced buses, T_in refers to total influenced hours, N for total quantity of buses, T for total observation time. Then the availability of the buses is 94.95% in a day. Although the value is over 90%, in certain hours (7pm to 9pm) the availability for buses is lower than 70%, which remains a problem to be solved. The chosen solution here is the load reschedule strategy. The strategy shifts the power demand from dark blue region (Etch 1 and 2) to the non-peak regions, result is shown in Fig.2.14(c). According to Fig.2.14(c), although the resulted voltage profile in region 1 am to 4 am is a little bit lower than (b), the maximum voltage dip in that region is around 0.02p.u. which have little influence on residents.

The etch area shrinkage from (b) to (c) reveals the method's positive effects on grid, as the subsequent bus voltages all maintain a higher 0.96 p.u. level operation in the next 24 hours.

2.3 Chapter Summary

In Section 2.1, we developed an EV fleet load modeling method based on load features observed from meter side data. We conclude the two key features of charging are (1) start-of-charging time and the (2) duration of charging time. Distribution of these two parameters is concluded in expressions. The distributions are all bi-modal types and are different from previous literature assuming pure Log-normal or Normal type. The reason lies in rather than charging randomly, there are lots of users fixing their charging time in early morning. Moreover, as the existence of stand-by energy loss, the distribution of trip travel distances of traditional vehicles cannot be directly mapped into battery initial SOC distribution in EV. The case study showed that the proposed approach can reflect the stochastic nature of EV charging and can predict the peak power of EVCL in a given period. Besides, in the proposed method, the fleet size and fleet constitution can be adjusted to reflect the local EV market and to fulfill simulation needs.

The Section 2.2 has discussed three main charging patterns of EV users from observations on meter data. Although a portion of users schedule their charging ahead of grid peak load hours in the early morning, most users still recharge the vehicle at afternoon peak load time. Possible EV loads influences in grids' power quality under unscheduled charging are summarized. The method picks the bus voltage as a power quality indicator and introduced a load management strategy to reduce the voltage dip via load shifting and backed it up with a reactive power injection scheme. The case study in Section 2.2.4.C shows even without static var compensator activated, the loads reschedule strategy proposed is sufficient to ensure grids safe operation. The strategy is compact and easy to deploy.

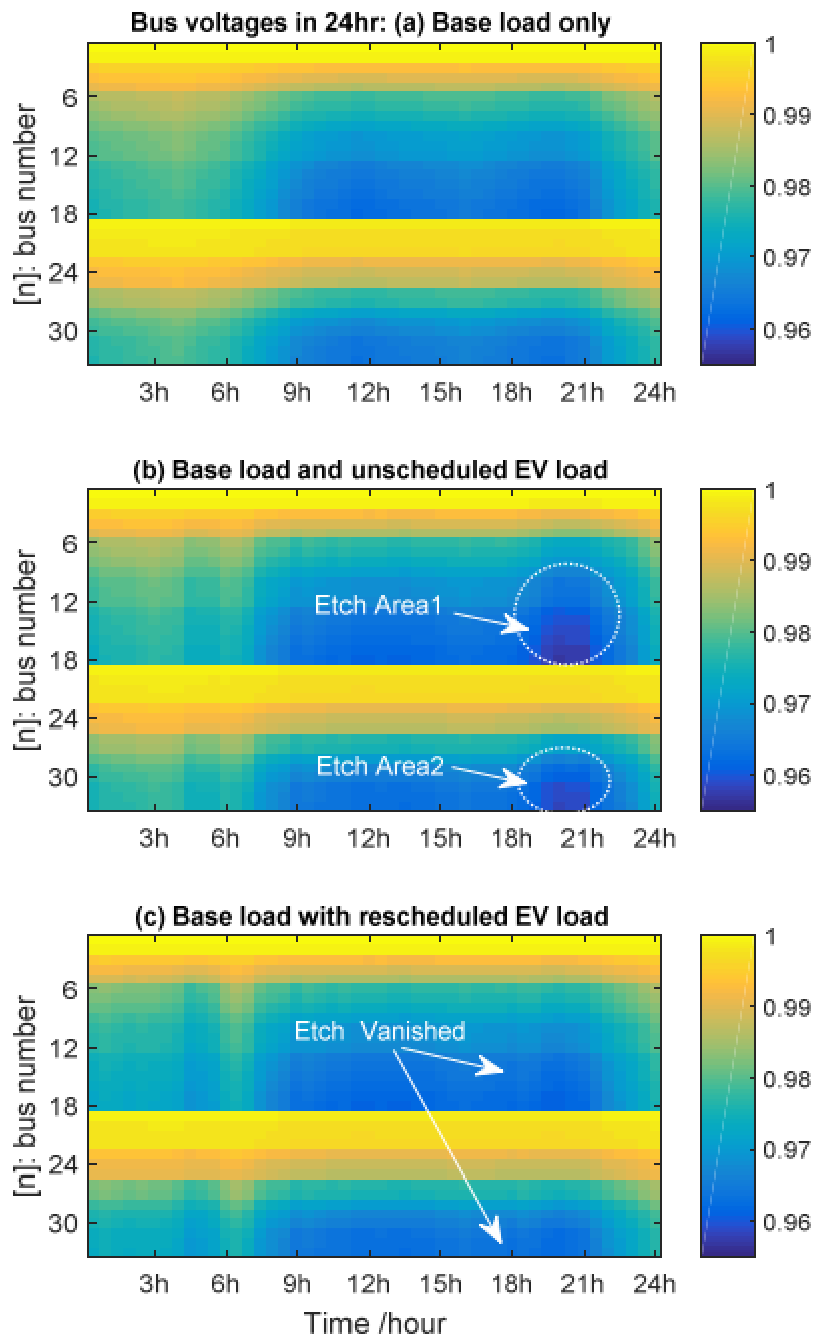

Figure 2.14: Bus voltage contour map of proposed IEEE-33 bus system over 24 hours. (a) The non-EV loads impacts in grids. (b) The impacts of addition EV loads in grids. (c) The performance of EV load management methods

Chapter 3

Reinforcement Learning Based Decision Making Strategies for Fleet[1]

3.1 A Q-Learning Based Charging Scheduling Scheme for Electric Vehicles

This Section 3.1 presents a Q-learning algorithm based dynamic charging scheduling scheme which intends to optimize the operation benefit for electric vehicles. The method imitates the charging station operator's decision procedure which is similar to solving a reinforcement learning problem. The scheduling problem involved is focused on the bidirectional interaction between the vehicle and the grid, including the grid-to-vehicle charging and the vehicle-to-grid (V2G) electricity returning. Regarding the dynamic characteristics of the electricity market, the scheme has included the time-of-use electricity rates as a core parameter to establish the reward tables which is necessary for learning. Furthermore, several simulations were conducted which demonstrates the day-long optimum vehicle charging decisions under the proposed scheme. Favorable expansibility and maintainability can be achieved in this Q-learning framework.

[1]Parts of this chapter have been presented in [13, 38]

3.1.1 Background

Most previous research studies have not considered (1) the dynamic nature of electricity price, TOU and (2) the V2G potential of vehicles. The problem scale of EV charging scheduling is growing and several decisions are expected to be made at one time. The machine learning method has proved to be an option to solve power system energy management problems [39, 40]. The work in [39]has used supervised learning to recognize EV power load in distribution system. In [40], a customer selection model for decision making in a demand response program is established. By modeling demand response as a reinforcement learning problem it allows the retailer to make fast and informed decisions on doing V2G actions or G2V actions.

Reinforcement learning algorithms push up the probabilities of taking good actions to achieve desired goals. Q-learning is a model-free reinforcement learning algorithm. The goal of Q-learning is to learn a policy, which tells an agent what action to take under certain circumstances [41]. In this section, we will solve the charging scheduling problem using Q-learning technique. This section suggests a method based on single EV charging scheduling. However, for multi-EV charging, paper [42] has introduced a method to ensure EV demands to be aggregated and operated as an ensemble.

3.1.2 Model for Charging Scheduling

A. Q-learning Parameters

The Q learning algorithm has a function that calculates the quality of a state-action (S, A) combination:

$$\mathrm{Q} : \mathrm{S} \times \mathrm{A} \rightarrow \mathbb{R} \tag{3.1}$$

Before learning begins, Q is initialized to an arbitrary fixed value. Then at each time t the agent selects an action a_t, observes a reward r_t, enters a new state $s_{(t+1)}$that depend on both the previous state s_t and the selected action and Q is updated. The value iteration update is shown below:

$$\mathrm{Q}\left(\mathrm{s_t}, \mathrm{a_t}\right) \leftarrow (1-\alpha) \cdot \mathrm{Q} + \alpha \cdot \left(\mathrm{r_t} + \gamma \cdot \max_{\mathrm{a}} \mathrm{Q}\left(\mathrm{s_{t+1}}, \mathrm{a}\right)\right) \tag{3.2}$$

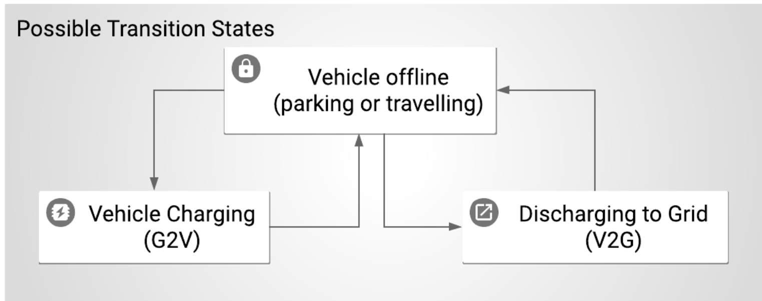

Figure 3.1: Possible transition states for vehicle scheduling

Where α stands for the learning rate and γ for discount factor. The term $\max_a Q(s_{t+1}, a)$ represents the estimation of optimal future value.

In this research, we suggest choosing discount factor $\gamma = 0.9$ and learning rate, $\alpha = 0.2$. Influence of these parameters is explained in [41].

B. The Reward Table

The specification of reward table is shown in Table 3.1. The reward values are based on the action taken at each current state. The proposed states for EV charging scheduling are illustrated in Fig.3.1. For V2G actions, that is, selling power back to grids from EV batteries discharging, the reward is proportional to the TOU price. For charging actions, the reward is set inversely proportional to power retail price, correlated to 1/TOU. The reward for offline is suggested to be set with a very small number ε, greater than zero. In Fig.3.2 the time on the vertical axis exemplarily stand for several consecutive proposed scheduling hours of a day. On the horizontal axis, one can see different states, which are labeled charging, offline through V2G. The slots are marked with “x” represent the service is unavailable for a period of time. Including scheduled maintenance on charging station, or predicted charging queue congestion.

The reward on blocked actions is set with negative infinity-$-\infty$. The consecutive unmarked slots represent the windows for actions. A charging window from 9 a.m. to 11 a.m. indicates no vehicle that is currently checking in and requests charging at that time.

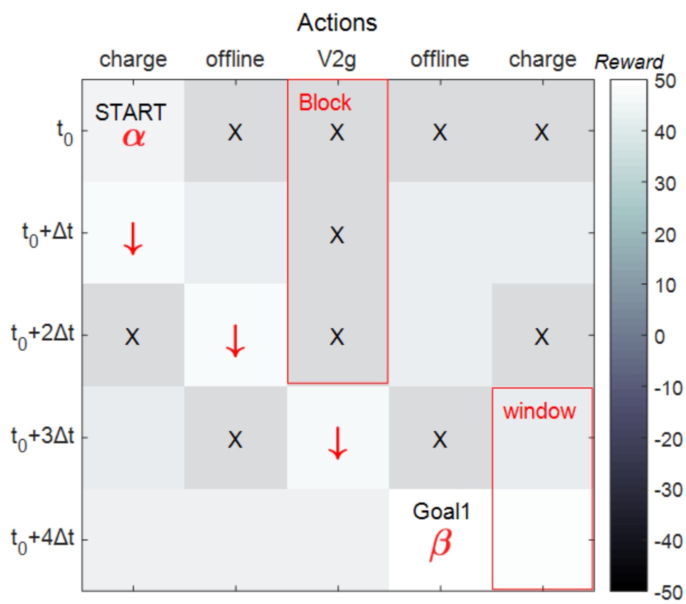

Figure 3.2: Reward table setup with optimum schedule solution

3.1.3 The 2 Dimensional Action Space

Consider now that an EV is charging at t_0. Request by EV user, the vehicle is going to be on duty at $t_0 + 4\delta t$, and would not be online for V2G or charging action at that time. The EV is asked to collect the most benefit given it has several options when making the decisions at each time slot.

The algorithm above will return the optimal charging sequence of states from the initial state to the goal state. The result is plotted as red arrows (route from α to β) in Fig.3.2. Consider that the vehicle has received new information about the charging environments at $t_0+4\delta t$. For a scheduling request at $t_0+4\delta t$, we first reset the time to t_0 in our algorithm (see Fig.3.3) then successively scan rewards (see Table.3.1) to established new reward table. In the new task the objective is noted as γ, represents vehicle is request to be on road (offline) in $t_0 + 3\delta t$. Although the amount of decisions to be made increases exponentially as the table grows, by implementing same procedure stated above, the algorithm has successfully returned the optimal charging path from the intermediate state to the goal state (from β to γ). The route is plotted as red arrows in Fig.3.3. From result updates from Fig.3.2 to Fig.3.3 one can see that proposed algorithm is adaptive to new configurations of the charging

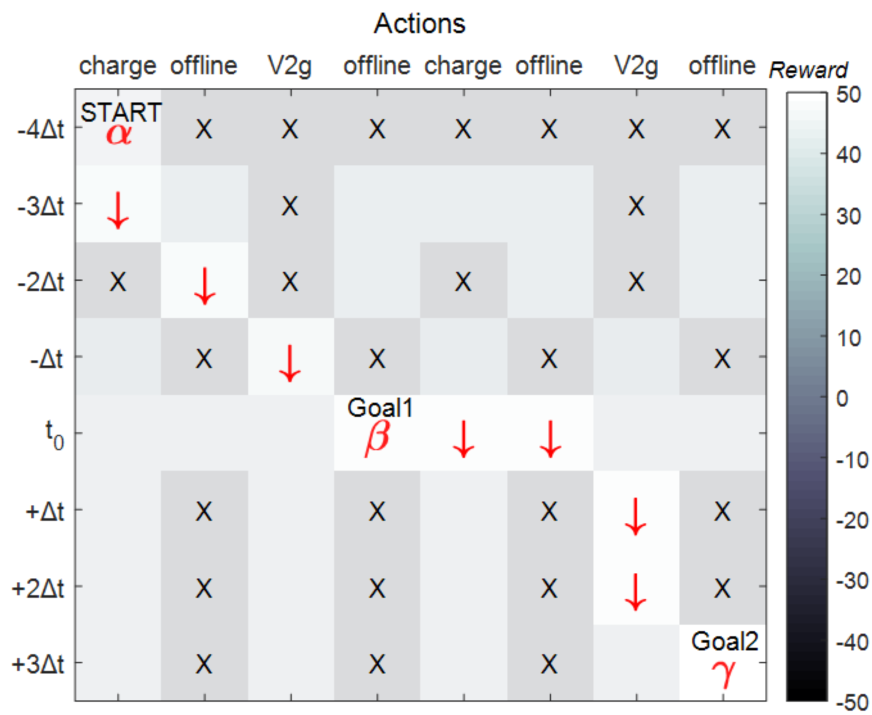

Figure 3.3: Example of reward table Updating from after $t_0 + 4\delta t$, the optimum schedule route from start state α to intermediate state β to goal state γ is solved and plotted

environment. Every time the schedule method is invoked it selects the route that gets the most returns. Obviously, for block α, going left exceeds the border of the table. But for other blocks, the next step can be arbitrarily allocated throughout the 8 directions. If we assume time is not reversible, we have 5 directions left i.e., down, left, right, diagonally lower right and diagonally lower left. Besides these 5 directions, reward is negative infinity. Thus any other action other than above action will not occur. The resulted initial Q-table for a 5×5 reward table (i.e. Fig.3.2) is 25×25. By updating Q table using equation (3.2) in Section 3.1.2.A, we will receive a trained Q table with an implied optimal schedule route. To utilize our trained Q matrix: 1. Set current state = initial state. 2. From current state, find the action with the highest Q value. 3. Set current state = next state. 4. Repeat Steps 2 and 3 until current state = goal state. The decision starts with block "α". The time interval in which the user wants to be offline is indicated by the mark "β", or, his Goal 1. The reward at block β is then set to a large value, r_β=50. From block α the vehicle has 3

symbol	Description	Reward value [a]
α	starting state	$-\infty$
β	intermediate state	r_β
γ	objective state	$r_\gamma = 2 \cdot r_\beta$
a	vehicle on traveling	–
b	offline	ε, greater than zero
c	charging	f$(1/p)$
d	parking	–
e	discharging (V2G)	f(p)
p	time-of-use price (TOU)	–

[a]Function appeared as f$(\cdot)$ is linear by default. Actions that travel to start state are prohibited in reward table with reward=$-\infty$.

Table 3.1: VALUES FOR REWARD TABLE ESTABLISHMENT

options: switch from charging state to offline at t_0, keep charging status from t_0 to $t_0 + \delta t$ or switch charging status to offline from t_0 to $t_0 + \delta t$. Simply choosing the highest reward block around block α does not guarantee global optimum, as some route (from α to β) with higher long term reward may be missed after such decision. Each of the 3 options is associated with a reward value stored in Q table. For setup convenience, other than those 3 options, the action rewards from block α to all other blocks in Fig.3.1 are also stored in Q table.

3.1.4 The 3 Dimensional Action Space

The method introduced in previous section adopts a 2-Dimensional schedule table which give 2 degrees of freedom of charging schedule. In the case study, we will apply the algorithm into a charging space with more degree of freedom. That is, the EV agent is going to have more options other than G2V and V2G.

A. The New Reward Table and New Actions

The new reward table is established on specifications in Table.3.2. The scheduling problem under 2-Dimensional space can be treated as a special case for a 3-Dimensional problem.

There are 5 types of actions (or directions, see Table.3.2) to be taken in a 3-D scheduling

action	Description	Reward value
1	stay on current state	$r_{\mathrm{aa}}, r_{\mathrm{bb}}, r_{\mathrm{cc}}, r_{\mathrm{dd}}, r_{\mathrm{ee}}$
2	to left state	$r_{\mathrm{ab}}, r_{\mathrm{bd}}, r_{\mathrm{db}} \cdots$
3	to lower state	$r_{\mathrm{ab}}, r_{\mathrm{bd}}, r_{\mathrm{db}} \cdots$
4	to right state	$r_{\mathrm{ab}}, r_{\mathrm{bd}}, r_{\mathrm{db}} \cdots$
5	to upper state	$r_{\mathrm{ab}}, r_{\mathrm{bd}}, r_{\mathrm{db}} \cdots$
6*	time reversal	$-\infty$

*Time reversal action that travel from $\mathrm{t_0}$ to $(\mathrm{t_0} - \Delta \mathrm{t})$ is prohibited with reward set to $= -\infty$.

Table 3.2: SEARCH DIRECTIONS AND ASSOCIATED REWARD

problem. Time reversal action that travels from t_0 to $t_0 - \delta t$ is prohibited. Such blocked action is shown in Fig.3.4, illustrated as the blue transparent block. The grey blocks represent the possible searching blocks for current red block. As shown in Fig.3.5, if the scheduling problems starting with the corner block, the possible directions are restricted to direction 1, 4&5. The Fig.3.6 represents a scheduling route under 3-Dimensional case. The route "b-c-c" in Fig.3.6 can be interpreted as "starting by offline at t_0, switch to charging into grid at t_0, and keep charging in $t_0 + \delta t$. The horizontally stacked red blocks in Fig.3.7 represents the solved optimal schedule is to stay on previous action. Term "b-b" represents stay offline, and "a-a" stands for vehicle stay on traveling during t_0 to $t_0 + \delta t$ period.

B. The 3 Dimensional Case Solution

a	*b*	*d*	*b*	*a*	*b*	...
b	*c*	*b*	*e*	*b*	*c*	*b*
d	*b*	*a*	*b*	*d*	*b*	*a*
b	*e*	*b*	*c*	*b*	*e*	*b*
a	*b*	*d*	*b*	*a*	*b*	*d*
b	*c*	*b*	*e*	*b*	*c*	*b*
	b	*a*	*b*	*d*	*b*	*a*

Table 3.3: THE TRAJECTORY OF OPTIMAL SCHEDULE

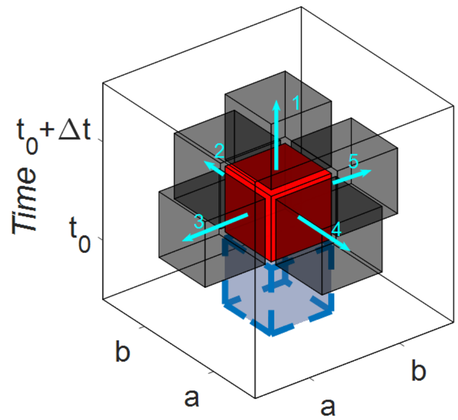

Figure 3.4: The 3-Dimensional action space for EV charging. Symbol a,b are illustrated in Tab.3.1 and Tab.3.2

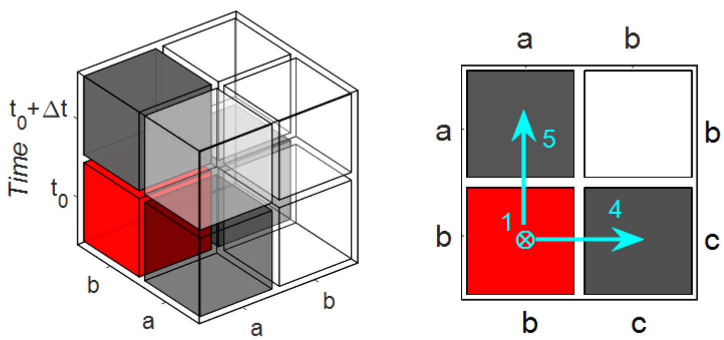

Figure 3.5: The searching directions for the corner block

In this case study, we suppose an EV is scheduled to V2G at $t_0 + 3\delta t$, and doing another discharging at $t_0 + 5\delta t$. The stating action is charging at t_0. Then in the proposed algorithm the intermediate goal and the final goal from β to γ are settled as coordinates (β, $+3\Delta t$) and (γ, $+5\Delta t$). The resulting initial 2-Dimensional Q-table for such 3-Dimensional 63 reward table has a scale of 216×216, that is, more than 45,000 transition states. By updating Q table using equation (3.2) in Section 3.1.2.A, we will receive a trained Q table with optimal schedule route. We can then solve the optimal schedule by method described in Section 3.1.3. The TOU price to establish reward table has referred to Ontario time of use price. And the resulting optimal schedule is shown in Fig.3.8. Results show that the best schedule

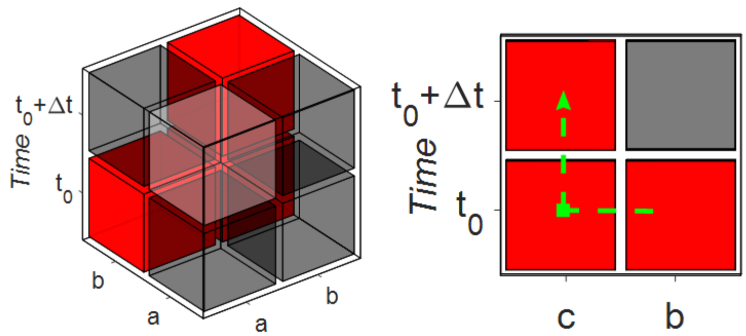

Figure 3.6: Example of a scheduling path (b-c-c)

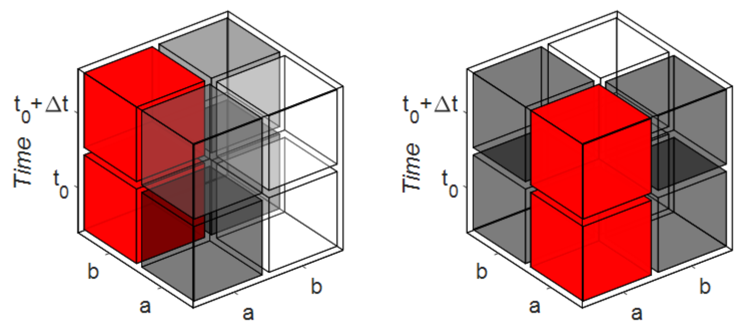

Figure 3.7: Examples of stay-on actions(a-a, b-b)

is to "keep V2G process from t_0 to $t_0+3\delta t$ period, turn offline vehicle before charging another δt period. Stay offline for consecutive δt period and do the V2G again until $t_0 + 5\delta t$. For easy understanding, the trajectory projection on the 2-Dimensional plane is shown in Table 3.3.

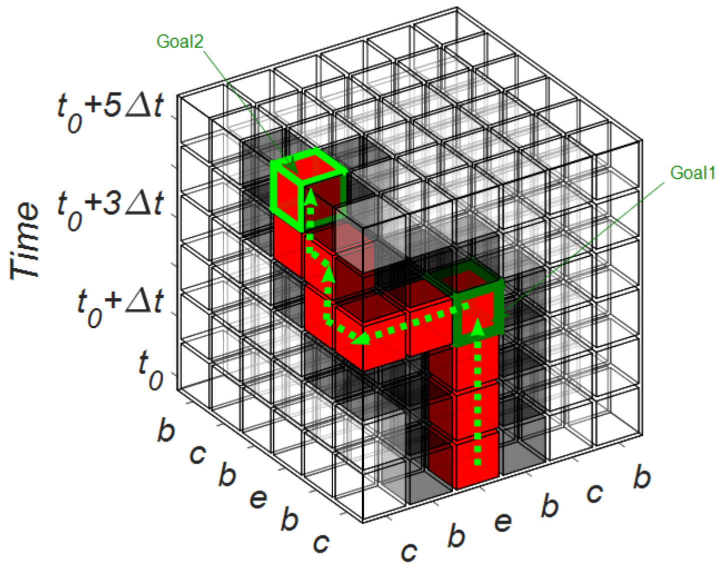

Figure 3.8: Solution of the Path in 3-Dimensional scheduling

3.2 EV Charging Scheduling Considering FCS Congestion

The Section 3.2 aims to provide an improved Q-learning algorithm based dynamic charging scheduling framework for electric vehicles. The scheduling problem involved, which considers the fast charging station (FCS) congestion situation, is focusing on the bidirectional power exchange between the vehicle and the distribution grid. Particularly, the section transforms the scheduling problem into the establishment of the suitable reward table for EV charging. The simulation models it as a Q-learning grid world problem in 3-Dimensional-space, where the optimal path implies the best series of actions to take at each time slot. The advancement of current Q-learning framework refers specifically to the extra consideration of limited service capability of FCS. The queuing theory (M/M/1/N/∞ queue) is brought in to address the EV charging congestion phenomenon. The Q-learning framework provides a practical solution to mitigate EV load impacts in grids, including altering charging time due to TOU and support grids by adopting vehicle-to-grid (V2G) plan.

3.2.1 Background

The space for improvement of previous section lies in its adaptability, the charging congestion and conflicts of multi-EV charging events will inevitably influence the reward table of single EV charging. In this section, an advanced reward table based on previous section with adjusted reward values for EV charging scheduling Q-learning problem is presented.

A. M/M/1/N/∞ queue of vehicles

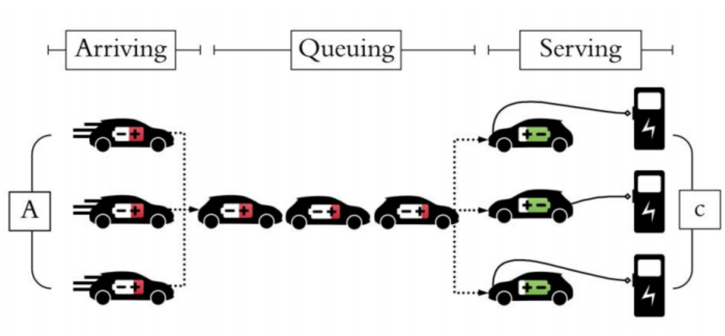

Figure 3.9: The model of EV charging with finite queue size (N=3)

Queuing theory here is a method of analyzing the EVs congestion or delays of waiting in queue. Here an M/M/1/∞ queue (a stochastic process whose state space is the set 0,1,2,3,...) is adopted where the elements of set corresponds to the number of EVs in the queuing system, including EVs currently in charging service. Arrivals occur at rate λ (averagely=λ car is visiting the FCS per hour) according to a Poisson process, shown in expression (2) and move the process from state i to i + 1.

$$P(X = N) = \frac{e^{-\lambda}\lambda^{N}}{N!} \tag{3.3}$$

Service times have an exponential distribution with rate parameter noted as μ in the M/M/1/N/∞ queue, where $1/\mu$ is the mean service time. In a fast charging station (FCS) we assume the average serving time for one EV is 30 minutes, that is, in each hour the FCS is able to serve and fulfill two EVs' battery power demand. For single FCS this research has set average serving rate μ to be 2 EV/hour. The vehicles serving time depends on the state of charge (SOC) of EVs, usually a log-normal distribution. To simplify we assume serving time follows the negative exponential distribution, shown in expression.

$$P(X = N) = \frac{e^{-\mu}\mu^N}{N!} \mid \mu = \mu_0 \tag{3.4}$$

A single FCS serves EV one at a time from the front of the queue, according to a first-come first-served (FCFS) discipline. When the service is complete the EV leaves the queue and the total number of EVs in the system reduces by one. The queue is of finite size N, so there is a limit on the number of EVs it can contain. In this simulation we set N to be 3, this assumes the EV owner is expecting a queue no longer than the assigned value N=3. When the EV is searching for a FCS to charge, if the vehicle observes a queue already with a queue length of 3 EVs, the EV will decide to pass through the FCS before join in the waiting queue, and search for next FCS nearby.

3.2.2 Models for Multi-EV Scheduling

A. Proof of Congestion

Consider vehicle arriving rate = 2 car/hour in average (Poisson distribution) and FCS processing rate = 2 car/hour in average, both under Poisson distribution. This means the processing rate of FCS equals the rate of arriving EVs. The risk of FCS congestion is relatively low.

However, according to simulation results in Fig.3.11, although the first 5 vehicles arriving at the FCS have encountered no queuing time and start charging their battery at once, the rest of vehicles (number 6 to 34) in FCS 24 hours of operation have waited on average 1.2 hours before having a charge. According to Fig.3.11, even if the average electric vehicle arrival rate has now been set to 1 car/hour (Poisson distribution), and we keep the FCS serving rate = 2 car/hour, the congestion still occurs. The first 4 vehicles arriving at the FCS have suffered no queuing time, while the rest have an average 0.6 hour waiting time in the queue. The simulations in Fig.3.10 and Fig.3.11 represents that in real charging situation, the congestion of FCS is possibly inevitable. In the suggested Q-learning based 3-D scheduling problem, the congestion is illustrated as the common block of 2 or more different scheduling routes. According to Fig.3.12, the individual optimum path (from stating point α to end state γ, calculated by Q-learning algorithm) may conflict with others. Note that as

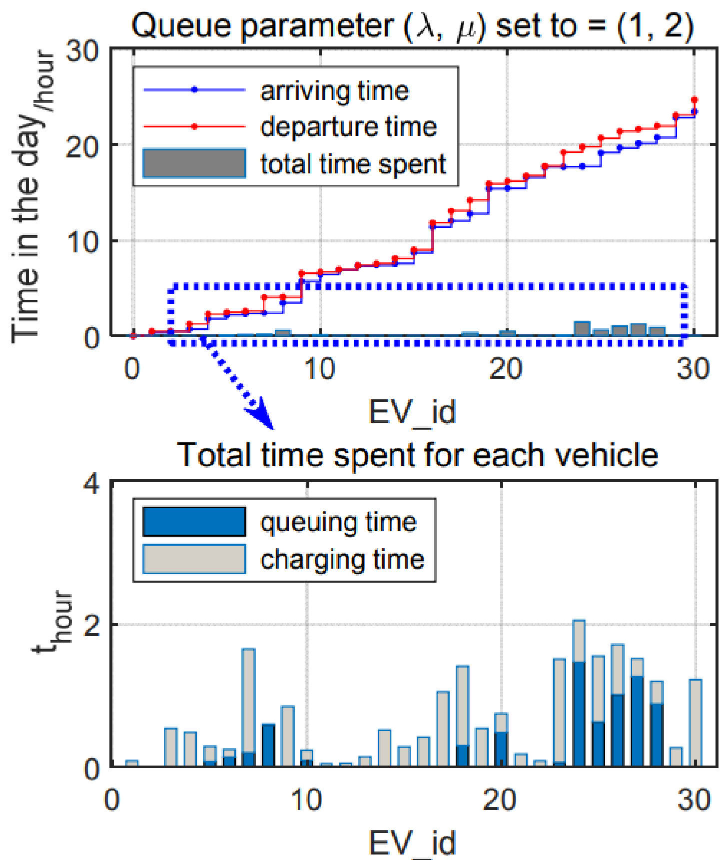

Figure 3.10: EV time spent on single FCS, consider arriving rate = 1 car/hour average and FCS processing rate = 2 car/hour average, Poisson distribution

shown in Fig.3.9, the conflicts blocks under notation 'a', 'b' or 'd' are not considered conflicts as they represents non grid connected state, namely 'vehicle on travelling', 'offline mode', 'parking mode' respectively. The trajectory showed in Tab.3.4 represents the only congested block goes to coordinates (c, c, t+3δt). The rest of routes have no conflicts.

B. Solution for Congestion

This chapter assumes the communication protocol between EVs exists and the coordination is provided by FCS. Furthermore, here we suggest adjusting the reward value for EV scheduling at congested block (the congested state in Q-learning) to some lower values iteratively for both EVs until the congestion does not occur. In addition, a lower reward value refers to

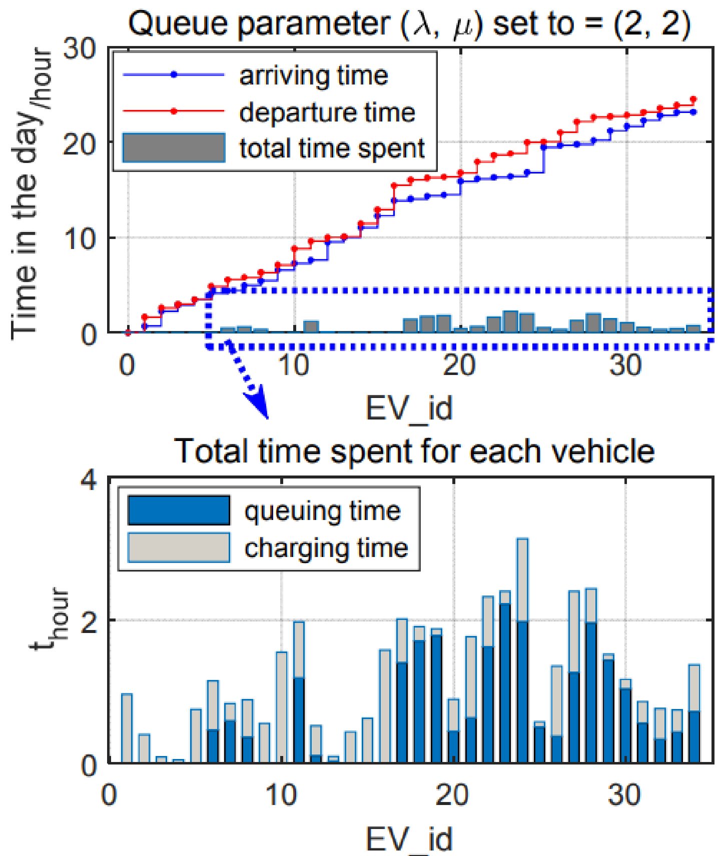

Figure 3.11: EV time spent on single FCS, consider vehicle arriving rate = 2 car/hour average and FCS processing rate = 2 car/hour average, both under Poisson distribution

(1) higher power price (which is higher than utility TOU price) at FCS when EV tries to charge the vehicle, and (2) lower price (decreased utility TOU price) when EV is trying to sell power back to the grid. The surplus for the FCS exists and equals to:

$$\text{surplus } = \int_0^T \text{TOU}(t)_{FCS} - \text{TOU}(t)\text{d}t \tag{3.5}$$

From the equation above , the more congestion are solved the more surplus remains in FCS.

a	*b*	*d*	*b*	*a*	*b*	...
b	*c*	*b*	*e*	*b*	*c*	*b*
d	*b*	*a*	*b*	*d*	*b*	*a*
b	*e*	*b*	*c*	*b*	*e*	*b*
a	*b*	*d*	*b*	*a*	*b*	*d*
b	*c*	*b*	*e*	*b*	*c*	*b*
	b	*a*	*b*	*d*	*b*	*a*

*Symbol of states (a,b,c,d,e) are illustrated in Tab.II

Table 3.4: THE TRAJECTORY OF OPTIMAL SCHEDULE

3.2.3 Results

The new reward table considering EVs congestion at FCS and fluctuation of EVs penetration level is presented in Tab.3.5. The reward for charging events and discharging events as now not only considered the time-of-use TOU price but also allow the EVs to compete for prices and provide surplus for FCS coordinators.

3.3 Chapter Summary

The Section 3.1 proposes the method to solve multi-dimensional EV charging scheduling problem. The time-of-use pricing TOU, the V2G capability of vehicles and the flexibility of charging are taken into account. This study is established in the context of a bidirectional power exchange between EVs and grids. This research solves the scheduling problem by using the Q-learning algorithm which is regarded as a fundamental reinforcement learning approach. Research pointed out the importance of adaptability in EV scheduling algorithm, in terms of providing more degree of freedom for EV to take actions. The method is convenient to deploy and satisfy both EV users' and grid operators' needs (save power and reduce peak).

In Section 3.2, an improved charging scheduling algorithm for multi EVs at fast charging station FCS based on queuing model and Q-learning reward table is established. The section

symbol	DESCRIPTION	Classic reward value	New reward value[a]
α	starting state	$-\infty$	$-\infty$
γ	objective state	$r_\gamma > 0$	$r_\gamma > 0$
λ	vehicle arriving rate /hour	-	-
μ	FCS processing rate /hour	-	-
a	vehicle on traveling	ε0	ε0
b	offline	ε1	ε1
c	charging	f(1/*p*)	f(1/p, λ) | μ=μ0
d	parking	-	-
e	discharging (V2G)	f(*p*)	f(p, λ) | μ=μ0
p	time-of-use price (TOU)	-	-

[a]Function appeared as f(·) is linear by default. Actions that travel to start state are prohibited in reward table with reward=-∞. $\lambda = r_t \cdot \lambda_0$ $(r > 0)$

Table 3.5: VALUES FOR REWARD TABLE ESTABLISHMENT

proved that the congestion can still happen when the serving rate of FCS is higher than the vehicle arriving rate, thus the reward table must be updated to avoid the charging (or discharging) conflicts. The surplus for FCS coordinator has been considered, and the penetration level is also taken into account.

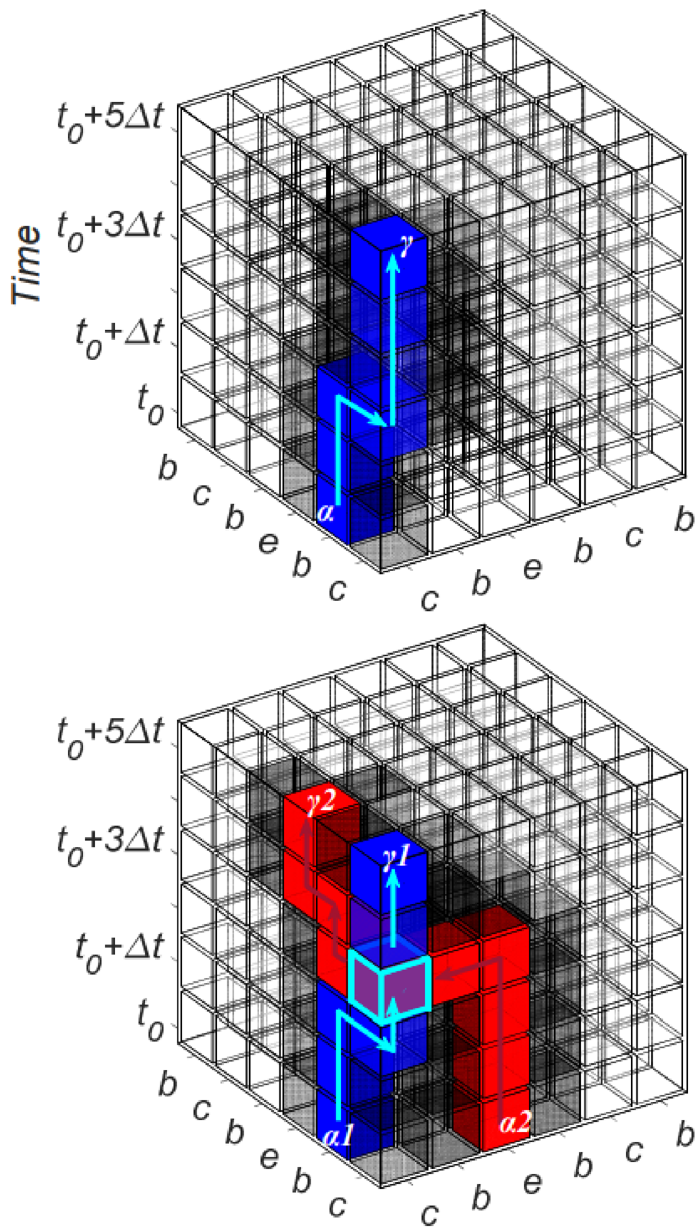

Figure 3.12: The 3-Dimensional action space for EV charging.Blue route: optimal scheduling path for EV1, Red route: optimal scheduling path for EV2, the 2 routes congested at time t+3δt. Symbol α,γ,b,c,e on axis are illustrated in Tab.3.5

Chapter 4

EV Fleet as Virtual Battery Resource for Community Microgrid[1]

This chapter provides a strategy to involve the EV fleet as energy storage to cut and save on extra battery pack investments in community microgrids. Notably, this chapter presents a Continuous Time Markov Chain (CTMC) based Electric Vehicle (EV) fleet total available battery capacity estimation framework to reduce costs in a community energy storage sizing problem. The chapter also considers the local fast-charging station (FCS) queueing situation. The queueing theory (M/M/1/K queue) is brought in to address practical EV charging. The mathematical expectation of the total amount of EV battery capacity in the community over one day, given the queueing scenario in FCS, is calculated. A brief literature review on EVs interacting with PV panels and working as community peak load shedding is presented. Three storage sizing case studies considering Grid-to-Vehicle (G2V) and Vehicle-to-Grid (V2G) scenarios with four different types of charging stations is designed and tested.

4.1 Community Microgrid Framework

4.1.1 Power Loads in Community Microgrid

In the microgrid, we assume that each house on average possesses one EV for use. Besides EV adoption, the environmentally friendly community also contains a photo-voltaic (PV)

[1]Parts of this chapter have been presented in [2, 43–45]

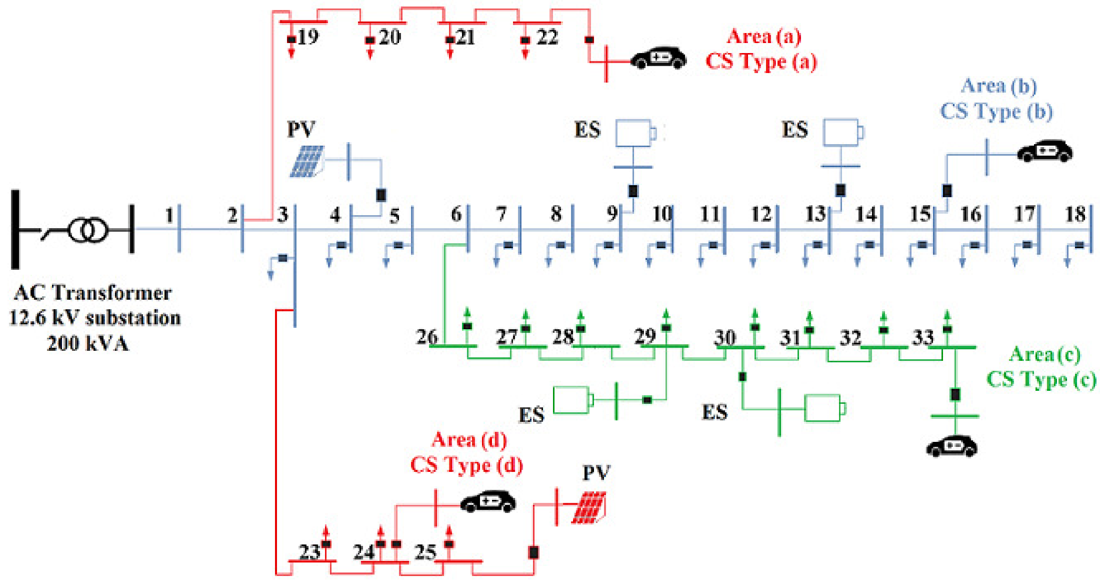

Figure 4.1: Energy storage concept on the modified IEEE 33-bus substation system, based on [1]. Energy storage in a local sense is battery only, but in a broad sense is battery plus EV as storage strategy

system to collect solar power. An overview of the system based on a modified IEEE 33-bus distribution system is shown in Fig.4.1. As illustrated in the figure, the microgrid here serves two types of loads, the EV charging load and the normal residential load.

The residential load behaviours across the community over one day are very much alike. An example of the load in one randomly picked house of the community is shown in Fig.4.2. Note that all load data referred to in this research is acquired from the open source database, Muller Community dataport [46]. As shown in Fig.4.2, in each home solar power generation will exceed the maximum of the power that the house can consume for certain hours of the day. As a consequence, the net load of the system, shown as the blue curve, could be negative during that time. If no energy storage is introduced in the system, when the microgrid works in the islanding mode, then there will be unused energy on the community's renewable energy generation. In addition, the cyclical spike on the red curve in Fig.4.2 refers to the on and off operation of a central air conditioning system. The Fig.4.3 represents PV output uncertainty. In most cases, each home's solar output stays around the solid line, the

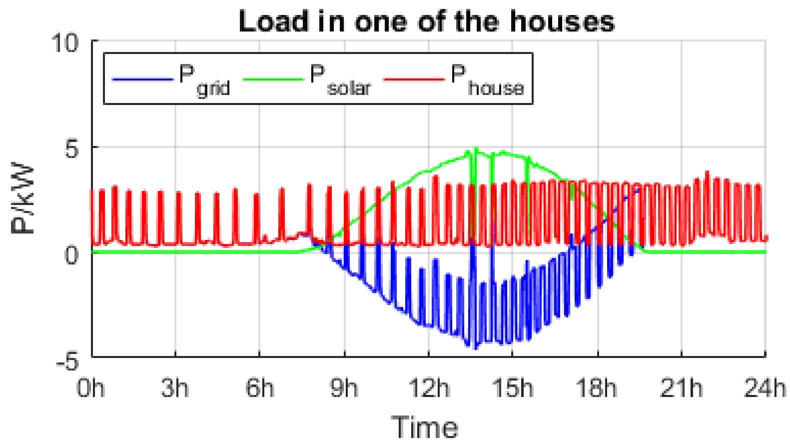

Figure 4.2: Power loads in one randomly picked house of the community. Negative power indicates the surplus PV generation output

mean value in the figure. However under specific weather conditions actual observations may deviate up to ±20%.

In this research, we assume the home level grid has uni-polar power flow only. However, we assume there are centralized and bi-directional power converters at fast charging stations [47]. Centralized surplus-PV-power-collecting focused battery can transfer power to FCS, and then use FCS's converters to feed power back to the grid.

In this community, we have 36 houses. Fig.4.4 presents the cumulative power consumption of these houses. Note that the power load on weekdays is different from weekends. The weekend loads are smoother and have a relatively lower value than weekdays in the early morning and afternoons. However, on any given day the solar panel generates a homogeneous power curve in spite of being a weekday or not. As a result, on weekends the negative net PV power green energy will be a bit more.

A comparison of weekdays and weekends surplus solar power is shown in Fig.4.5. The red curve in kWh is the integration of the blue power curve. The max value of the red curve indicates the maximum excess PV energy in one day. For a regular weekday, the non-collected power could go up to 132.41 kWh. For weekends it could be 165.93 kWh. In total it is around 52,000 kWh per year. The Utility company's report [48] shows that the average electricity use for a home in a plex or multiunit building with air-conditioning in Quebec is 14,000 kWh per year. Compared to this, the unused PV power in this community could

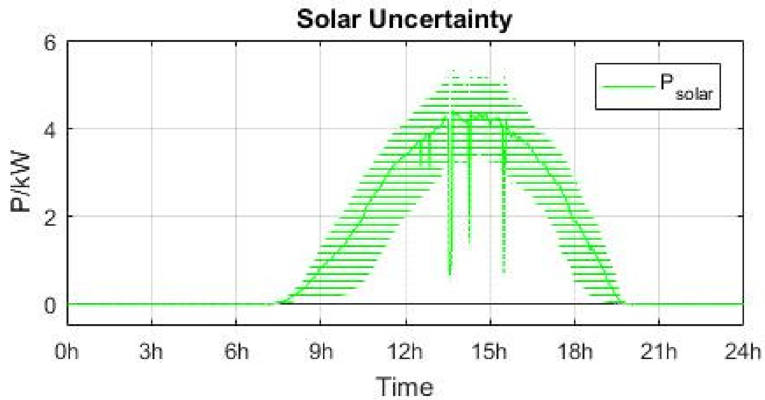

Figure 4.3: Solar generation uncertainty in one home according to historical data. Uncertainty PV output region is around its mean value±20%

have fulfilled the annual energy demand of three homes in Quebec.

4.1.2 The CES Sizing Problem

The purpose of introducing community energy storage (CES) in this system is twofold. First, as we showed in Section II.A, it is essential for surplus solar energy to be collected and reused. Second, when the upstream transformer is overloaded, the battery could shave the peak power demand and ensure the safe operation of the microgrid. The critical question that follows is how much battery capacity is enough for both of these objectives.

A direct answer is to plan the local battery capacity to the maximum PV power generation per day. In the sample 36-home case, the maximum PV energy is around 166 kWh, for which a correspondingly-sized battery system does not seem too costly. However, in practice such a microgrid could serve hundreds of homes [49], and in this case, the battery system investment could be much higher.

A solution to this is shown in Fig.4.1. A narrow sense of energy storage sizing for community microgrids is considering the deployment of fixed batteries only. However, a broad sense of CES sizing for such a highly EV penetrated community would consider EV fleet batteries as a dynamic virtual energy storage resource.

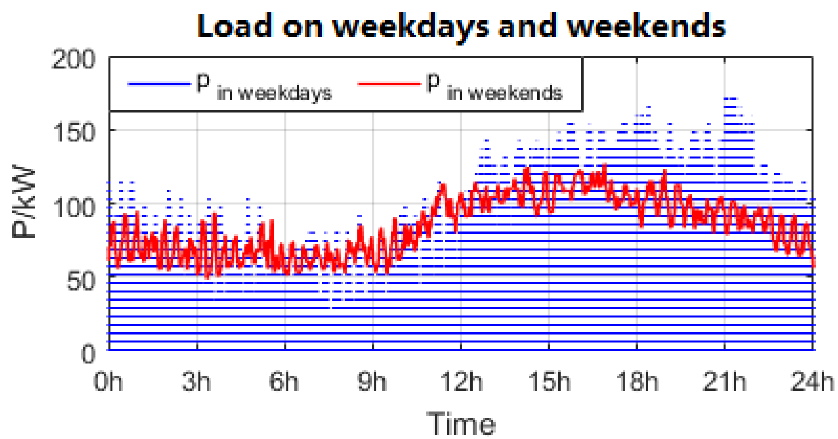

Figure 4.4: Power loads in all the houses of the community. Weekdays load profile compared to weekends profile. Weekdays usually has higher power demand

4.1.3 Continuous-time Markov Chain (CTMC) Queue Model

We use a continuous-time Markov Chain (CTMC) queue model to analyze the dynamic states in the FCS queue. EVs arrive at a charging port in a stochastic process. The incoming rate of a charging port is around one vehicle per day. For the station configuration, the simplest state space of the $M/M/1/K$ queue is the set $\{0, 1, 2, 3, ..., K\}$ where K corresponds to the number of EVs in the FCS, including any currently connected to the grid. For instance, if we set K to 1, this means the EV driver only tolerates a queue no longer than size one, otherwise the EV will leave the FCS instead of joining in and waiting.

The arrival of EVs occurs at the rate λ, that is, on average λ car is visiting the charging port per minute. An EV-arrival event moves the state from i to $(i+1)$. The arrival pattern is assumed to follow a Poisson process. The Poisson distribution providing the probability of arrival of N cars per minute is shown below:

$$P\left(X = N\right) = \frac{e^{-\lambda}\lambda^{N}}{N!} \tag{4.1}$$

The vehicle incoming rate is a time dependent variable. It is described in equation (4.2) below. Consider a base vehicle incoming rate λ_0 of 1/1440 per minute, then the terms in $[\cdot]$ of equation (4.2) are constant, and λ (t) will be fluctuating according to ratio(t) over one day.

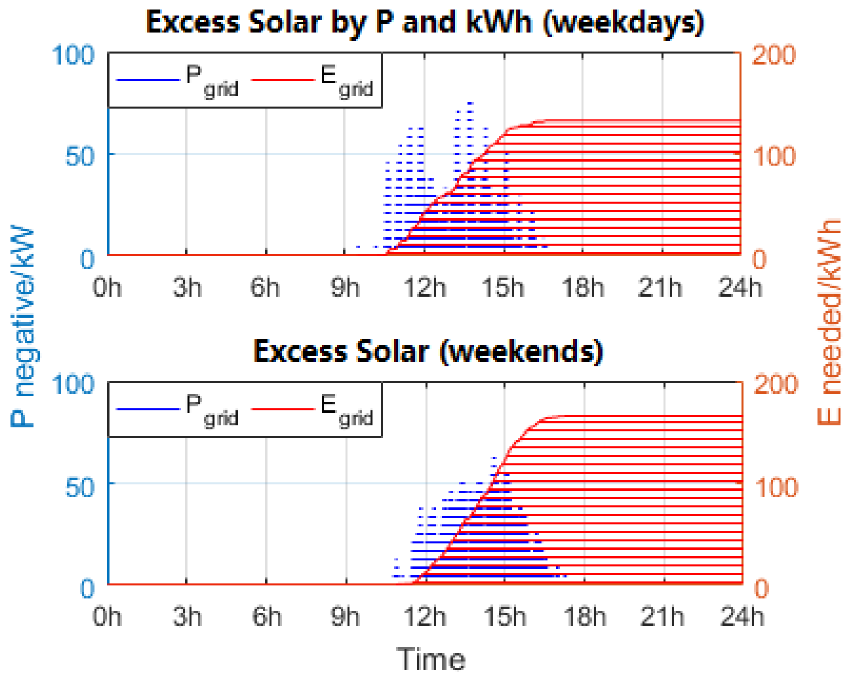

Figure 4.5: The extra PV generation from a small sized community. The red curve E is simply excess solar P integrated with respect to time. Weekdays and weekends have different excess solar profiles

$$\lambda(\mathrm{t})=\text{ ratio }(\mathrm{t})\cdot[\lambda_0\cdot(1+\text{ ratio }_{\text{guest}})] \tag{4.2}$$

The guest population is set to $ratio_{guest}$=10% of the residential population. The time varying coefficient ratio(t) over time is referred to in [24, 28, 50]. According to these works, a Gaussian distribution is employed to depict the probability density function of an EV start-charging time in a day, so it will result in the bell type plot in Fig.4.6. This figure also shows that weekend and weekday EV charging has different charging behaviors.

Another key queueing parameter is the station service rate μ. In the station's CTMC queue, μ reflects the rate of charging of different EVs.

For EVs with bigger battery capacity and lower charging rates, the service time will be longer, thus rate μ will be smaller. The service time should also depend on the initial state-of-charge (SOC) of EVs. Following the setting in [25,51,52], an initial SOC following a

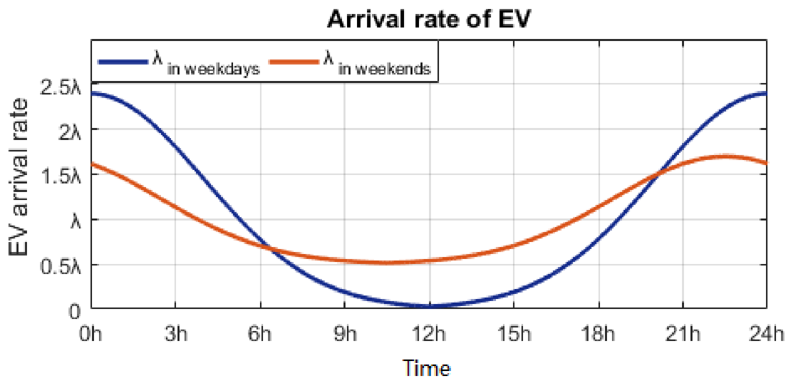

Figure 4.6: Arrival rate of EVs: average number of cars visiting the charging station per minute during weekdays and weekends

normal distribution with mean value around 33% is adopted. To simplify, we set the initial SOC of each EV, despite the EV brand and model, to be 33%. The service time T should then be calculated as follows:

$$\mathrm{T} = \frac{Cap_{kWh}}{Rate_{kW}} \cdot (1 - SOC) \ . \tag{4.3}$$

And service rate μ is calculated by:

$$\mu = 1/\left(60 \cdot T\right) \ . \tag{4.4}$$

The unit in equation (4.4) for service time T is the hour. In the computation we unify the units of μ and λ (min^{-1}) by multiplying T by 60 min/h.

4.1.4 Markov Chain (CTMC) for Single-port FCS

In this subsection, we focus on two charging station topologies, shown in the left most diagrams in Fig.4.7.

The first one represents a single charging port CS, with no extra parking space. If another vehicle spotted this type of CS, and it is being occupied by an EV, it will not queue after the car. The second example allows a second EV to join the CS as it has a parking space for one vehicle to wait. Thus the queue size is not zero, but one. It can serve one EV at a

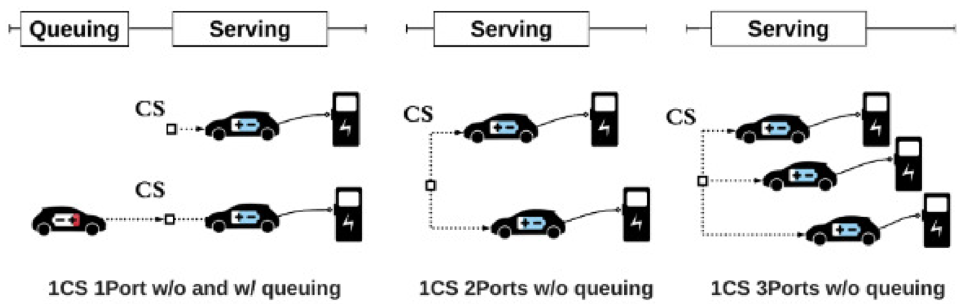

Figure 4.7: Four basic topologies of Charging Station (CS) in this research. 1-CS-1-Port without and with queueing, 1-CS-2-Ports without queueing, 1-CS-3-Ports without queueing

time from the front of the queue, according to a first-come first-served (FCFS) rule.

We assume vehicles arrive at the CS in a Poisson process with a rate of λ(t) vehicles per minute. According to Canada's EV market shares, for the configuration of the community EV fleet, we assume that some of the cars are Chevrolet Bolts (battery capacity $Chevy_{kWh}$) but most are Tesla Model 3s (battery capacity $Tesla_{kWh}$). Assume there is no other type of EV in the microgrid.

The infinitesimal generator matrix Q is an array of numbers describing the instantaneous rate at which a continuous time Markov chain transitions between states. The element q_{ij} denotes the rate of departing from state i and arriving in state j. The diagonal elements q_{ii} are defined by:

$$q_{ii} = -\sum_{j \neq i} q_{ij} \,. \tag{4.5}$$

By observing the three-state Markov chains on Fig.4.8 and computing diagonals by equation (4.5), we find the corresponding transition rate matrix Q for the first CS topology:

$$\mathrm{Q} = \begin{bmatrix} -\lambda & (1-p_{ch})\,\lambda & p_{ch}\lambda \\ \mu_{\mathrm{T}} & -\mu_{\mathrm{T}} & 0 \\ \mu_{\mathrm{c}} & 0 & -\mu_{\mathrm{c}} \end{bmatrix} \tag{4.6}$$

The variable p_{ch} denotes the probability for EV to be a Chevy Bolt, and λ is the arrival rate which can be sampled from Fig.4.6 and equation (4.2). After a certain period, the steady state probability p of each state will be constant. As a result, we can solve for $\vec{\mathbf{p}} =$

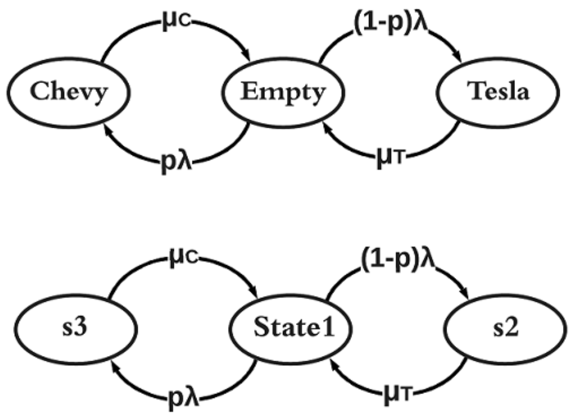

Figure 4.8: The Markov chain for 1-CS-1-Port non-queueing system of three basic states. The numerical order of states is shown in the lower graph

[p1 p2 p3] from:

$$\overrightarrow{\mathbf{p}}\mathrm{Q} = 0 \tag{4.7}$$

Subject to:

$$\sum_{i=1}^{3} p_i = 1 \tag{4.8}$$

Moreover, as shown in Fig.4.8, the states s1 to s3 are respectively: (0), (T), (C). So the average available battery capacity from EV fleet associated with the non-queueing 1-CS-1-Port is:

$$\begin{aligned} N = \overrightarrow{\mathbf{p}} \cdot States = 0 \cdot p_1 + Tesla_{kWh} \cdot p_2 + \\ Chevy_{kWh} \cdot p_3 \end{aligned} \tag{4.9}$$

The second example is built on the basis of the first one. It is described as chains on Fig.4.9. In this example, the Q Matrix can be written as,

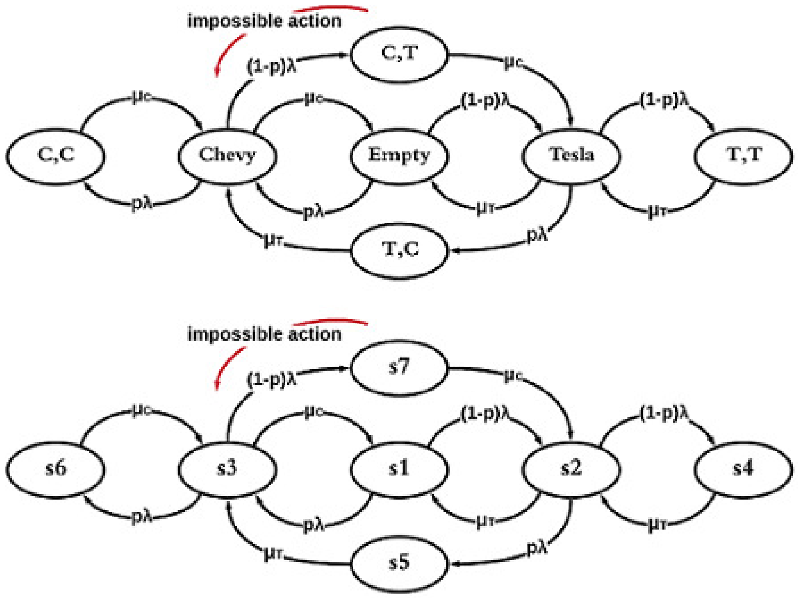

Figure 4.9: The Markov chain for 1-CS-1-Port queueing system of seven basic states. Transition from (C,T) to (C,0) is prohibited as the Tesla in the queue is assumed to wait for the Chevy to finish charging after joining the queue, and similar transitions are likewise prohibited. The numerical order of states is shown in the lower graph

$$
Q = \begin{bmatrix}
-\lambda & (1-p_{ch})\,\lambda & p_{ch}\lambda & 0 & 0 & 0 & 0 \\
\mu_{\mathrm{T}} & -\lambda-\mu_{\mathrm{T}} & 0 & (1-p_{ch})\,\lambda & p_{ch}\lambda & 0 & 0 \\
\mu_{\mathrm{c}} & 0 & -\lambda-\mu_{\mathrm{c}} & 0 & 0 & p_{ch}\lambda & (1-p_{ch})\,\lambda \\
0 & \mu_{\mathrm{T}} & 0 & -\mu_{\mathrm{T}} & 0 & 0 & 0 \\
0 & 0 & \mu_{\mathrm{T}} & 0 & -\mu_{\mathrm{T}} & 0 & 0 \\
0 & 0 & \mu_{\mathrm{c}} & 0 & 0 & -\mu_{\mathrm{c}} & 0 \\
0 & \mu_{\mathrm{c}} & 0 & 0 & 0 & 0 & -\mu_{\mathrm{c}}
\end{bmatrix} \tag{4.10}
$$

As from Fig.4.9, the states s1 to s7 are: (0, 0), (T, 0), (C, 0), (T, T), (T, C), (C, C), (C, T), where the first entry in the pairs corresponds to the charger state and the second entry corresponds to the queue state. After steady-state probability vector p is calculated, the average available battery capacity from EVs can be obtained by:

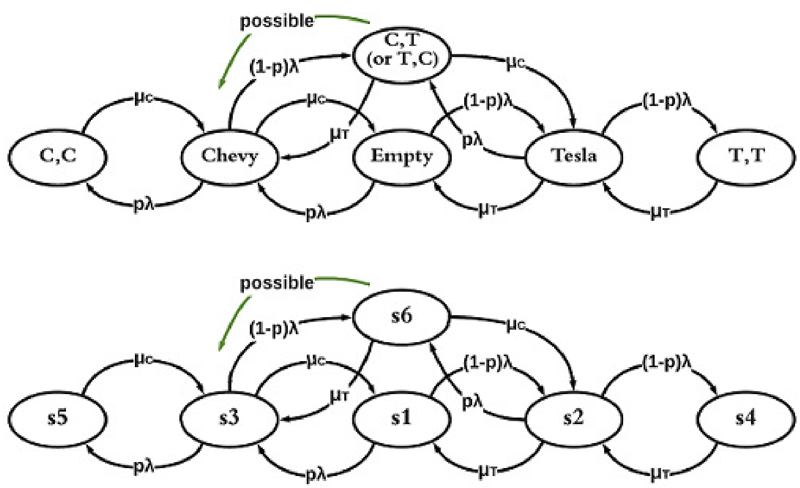

Figure 4.10: The Markov chain for a non-queueing charging station with 2 charging ports. This charging station can serve two vehicles at the same time. Thus the transition from (C,T) to (C,0) is possible and implies one vehicle leaving the station. The numerical order of states is shown in the lower graph

$$N = \overrightarrow{\mathbf{p}} \cdot States = \ 0 \cdot p_1 + Tesla_{kWh} \cdot p_2 + Chev\\ y_{kWh} \cdot p_3 + Tesla_{kWh} \cdot p_4 + Tesla_{kWh} \cdot p_5 + \\ Chevy_{kWh} \cdot p_6 + \ Chevy_{kWh} \cdot p_7 \tag{4.11}$$

As shown in the above equation, s7 only multiplies one vehicle battery. The Tesla battery on state 7 is ignored. This is because the states (C, T) or (C, C) represent a Chevy charging at the port while a Tesla or Chevy is waiting in the queue. So the battery connected to the grid for these states is one Chevy battery only.

4.1.5 Markov Chain (CTMC) for Multi-port FCS

The multi-port FCS examples can be seen in the last two diagrams in Fig.4.7. The multi-port FCS charging case is further developed from the one-port FCS queueing-permitted charging

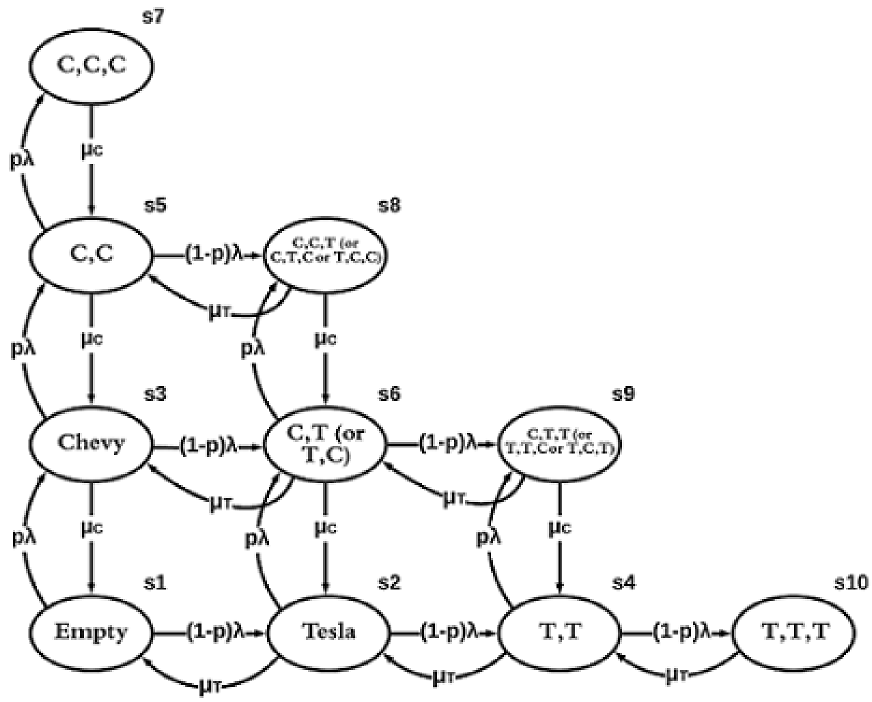

Figure 4.11: The Markov chain for a 1-CS-3-Ports non-queueing system with ten basic states. This charging station has three charging ports, which can serve 3 vehicles at the same time. The numerical order of states to generate the Q matrix is shown in the superscript from s1, s2 to s10

case. In the one-port queueing case shown in Fig.4.8, a transition from state (C,T) to (C,0) is prohibited.

A non-queueing charging station with two charging ports is somehow similar to the one-port with queue case. The difference lies in that a 2-port station can serve two vehicles at the same time. Thus, the transition from (C,T) to (C,0) is possible, see Fig.4.10. The latter state (C,0) implies a Tesla has left the second port of the station. Notice that although we have more charging ports, we now have less states. As we are not considering a queue in the 2-port FCS, we can combine (C,T) and (T,C) from Fig.4.8 into one state, then a Q matrix of size 6 by 6 is generated. The transition matrix of a 2-port FCS non-queueing system is shown below.

$$Q = \begin{bmatrix} -\lambda & (1-p_{ch})\,\lambda & p_{ch}\lambda & 0 & 0 & 0 \\ \mu_{\mathrm{T}} & -\lambda{-}\mu_{\mathrm{T}} & 0 & (1-p_{ch})\,\lambda & 0 & p_{ch}\lambda \\ \mu_{\mathrm{c}} & 0 & -\lambda{-}\mu_{\mathrm{c}} & 0 & p_{ch}\lambda & (1-p_{ch})\,\lambda \\ 0 & \mu_{\mathrm{T}} & 0 & -\mu_{\mathrm{T}} & 0 & 0 \\ 0 & 0 & \mu_{\mathrm{c}} & 0 & -\mu_{\mathrm{c}} & 0 \\ 0 & \mu_{\mathrm{c}} & \mu_{\mathrm{T}} & 0 & 0 & -\mu_{\mathrm{c}}{-}\mu_{\mathrm{T}} \end{bmatrix} \tag{4.12}$$

A non-queueing charging station with 3 charging ports is simply an expansion of the 2-port case. As illustrated in Fig.4.11, we have 10 states for this non-queueing 3-port FCS. Then a corresponding Q matrix with size 10 by 10 is obtained, as shown below.

$$Q = \begin{bmatrix} -\lambda & (1-p_{ch})\,\lambda & p_{ch}\lambda & 0 & 0 & 0 & \cdots & 0 \\ \mu_{\mathrm{T}} & -\lambda{-}\mu_{\mathrm{T}} & 0 & (1-p_{ch})\,\lambda & 0 & p_{ch}\lambda & \cdots & 0 \\ \mu_{\mathrm{c}} & 0 & -\lambda{-}\mu_{\mathrm{c}} & 0 & p_{ch}\lambda & (1-p_{ch})\,\lambda & \cdots & 0 \\ 0 & \mu_{\mathrm{T}} & 0 & -\lambda{-}\mu_{\mathrm{T}} & 0 & 0 & \cdots & (1-p_{ch})\,\lambda \\ 0 & 0 & \mu_{\mathrm{c}} & 0 & -\lambda{-}\mu_{\mathrm{c}} & 0 & \cdots & 0 \\ 0 & \mu_{\mathrm{c}} & \mu_{\mathrm{T}} & 0 & 0 & -\lambda-\mu_{\mathrm{c}}{-}\mu_{\mathrm{T}} & \cdots & 0 \\ \vdots & \vdots & \vdots & \vdots & \vdots & \vdots & \ddots & \vdots \\ 0 & 0 & 0 & \mu_{\mathrm{T}} & 0 & 0 & \cdots & -\mu_{\mathrm{T}} \end{bmatrix} \tag{4.13}$$

The abbreviated elements in the matrix above can be read from corresponding values on the transition chains in Fig.4.11.

Up to now, we have introduced the simple 2-port and 3-port non-queueing charging station transition matrices. However, more complicated cases with N-ports, N>3 allowing queueing situations are simply cases with more states. Thus their transition matrix can be obtained by applying the proposed method.

The probabilities p solved for 1-FCS-1-port queueing situation, 1-FCS-2-port non-queueing situation and 1-FCS-3-port non-queueing situation having, respectively 7 by 7, 6 by 6 and 10 by 10 matrices are shown in Fig.4.12, Fig.4.13 and Fig.4.14. These figures show that as the vehicle arrival rate λ increases, the probability that the fast charging

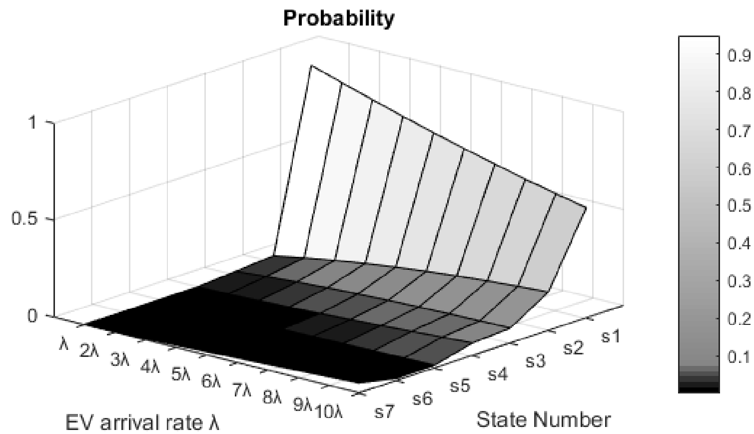

Figure 4.12: The steady-state distribution of each of 7 states of 1-CS-1-Port with queue scenario, solved by using the 7 by 7 transition rate matrix Q. When λ increases, the probability of CS in 1st state (empty EV state) decreases

station stays empty (state1) decreases. The probability of other states also goes up steadily with λ.

4.2 Strategies

Either G2V or V2G strategy uses the same four types of CTMC model from Fig.4.8 to Fig.4.11 in order to compute the steady-state probability of each state p.

4.2.1 Vehicle battery Serving as Solar Storage (G2V)

After the steady-state probability p is computed, the average available battery capacity for G2V purpose can be calculated by:

$$E_{G2V} = \overrightarrow{\mathbf{p}} \cdot States \cdot DOD_{avg} \, , \tag{4.14}$$

where, $DOD_{avg} = 1 - SOC_{avg}$ represents the average EV battery Depth of Discharge (DOD) when connected to the charging port.

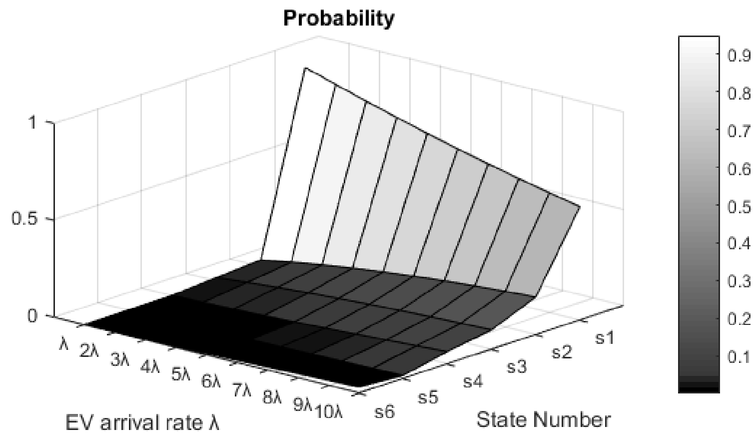

Figure 4.13: The steady-state distribution of each of 6 states of 1-CS-2-Port no queue scenario. Solved by using the 6 by 6 transition rate matrix Q. When λ increases the probability of the 2nd to 6th states increases accordingly

4.2.2 Vehicle Battery Serving Vehicle-to-Grid (V2G)

Similarly, after the steady-state probability is solved, the average battery capacity available for V2G purpose can be obtained by:

$$E_{V2G} = \overrightarrow{\mathbf{p}} \cdot States \cdot SOC_{avg} \,. \tag{4.15}$$

Notice that both E_{V2G} and E_{G2V} are variables that change over time. Although $States$, SOC_{avg} and DOD_{avg} are constant, the state probabilities vector p depends on the time-varying EV arrival rate $\lambda(t)$.

4.2.3 Combination of Two Strategies

The dominant strategy selection function is shown below. The $\overline{E}$ is the net fixed battery capacity needed for the system and will determine the battery capital cost.

$$\overline{E} = \max\left\{\sup_t f\left(t\right), \sup_t g\left(t\right)\right\} \,, \tag{4.16}$$

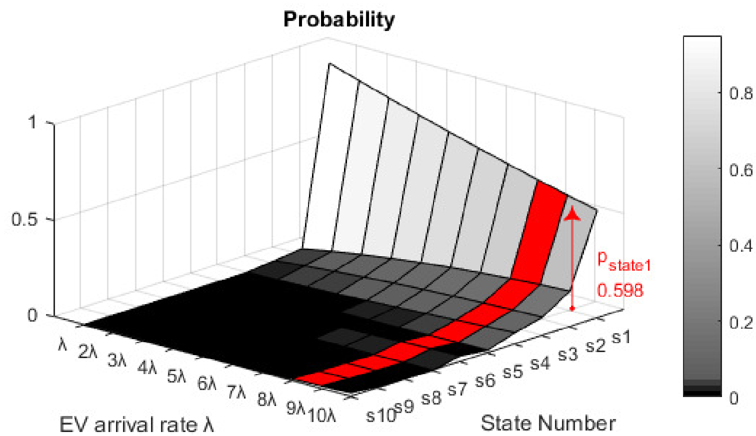

Figure 4.14: The steady-state probability distribution of each of 10 states of 1-CS-3-Port no queue situation. When the EV arrival rate increases, the probability of the 1st state decreases. The red stripe shows that when the car arrival rate set to 9λ, the probability of the charging station to be in empty (1st state) decreases to 0.598

$$\text{where,} \quad \begin{cases} f(t) := \int p_{netPV}(t) \cdot dt - E_{G2V}(t) \\ g(t) := \int p_{exceed}(t) \cdot dt - E_{V2G}(t) \\ t \in [0, 1440] \end{cases}$$

and p_{netPV} represents net surplus PV power generated from the panel, which is not consumed by the local load, as shown in Fig.4.5.

The variable p_{exceed} refers to the power exceeding the up stream transformer limit of the community grid, see the pink curve on Fig.4.15 and Fig.4.16. Assume that in the 36 house community, the transformer is rated at 200KVA and operates at a 0.98 power factor. We suppose overloading only happens on weekdays. When it happens, assume the load is 50% higher than a normal weekday load .

Having explained two available strategies V2G and G2V to reduce costs, we can now look into the capital cost of fixed storage after these strategies are applied. The cost function is shown below.

$$C = C_0 - S_{V2G}\,, \tag{4.17}$$

where the capital battery cost C_0 is,

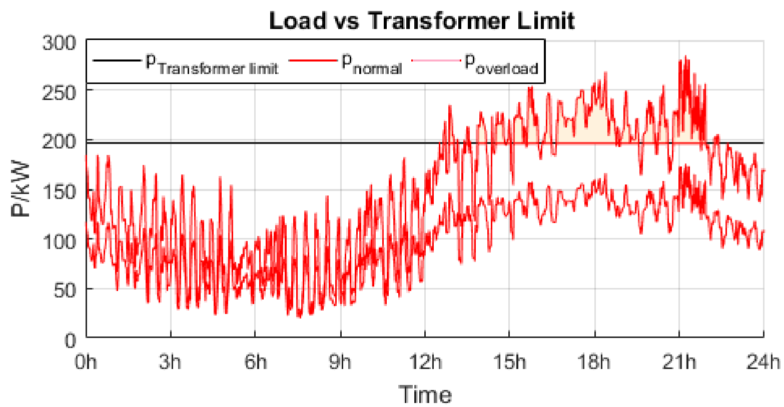

Figure 4.15: Community power load under normal and overloading situation. The transformer capacity limit considers a power factor $pf = 0.98$, and a 50% mean overload ratio is assumed on overloading days

Item	Value
k_0– Inflation coefficient in Canada	1.8%
k_1– Risk-free interest rate Government of Canada marketable bonds Average yield - Over 10 years [53]	3.2%
k = $k_0 + k_1$ Growth ratio for cash flow k_0 refers to consumer price index (CPI)	5.0%

*The values displayed above are assumptions.

Table 4.1: PARAMETERS OF V2G DISCOUNTED CASH FLOW (DCF)

$$C_0 = \overline{E} \cdot c_{bat}/kWh\,, \tag{4.18}$$

and S_{V2G} is the V2G subsidy. It is offered by the utility grids as V2G helps relieve peak loads and protects the health of the transformer. The fixed battery is charged by local solar power instead of grid power. Thus the cost of battery charging is not considered in Eq.(4.17). The S_{V2G} can be calculated from a discounted cash flow (DCF) model, where the cash flow is the revenue from selling power back to the grid. In general,

$$S_{V2G} = \frac{D_0}{k} \cdot \left[1 - \frac{1}{(1+k)^n}\right]\,, \tag{4.19}$$

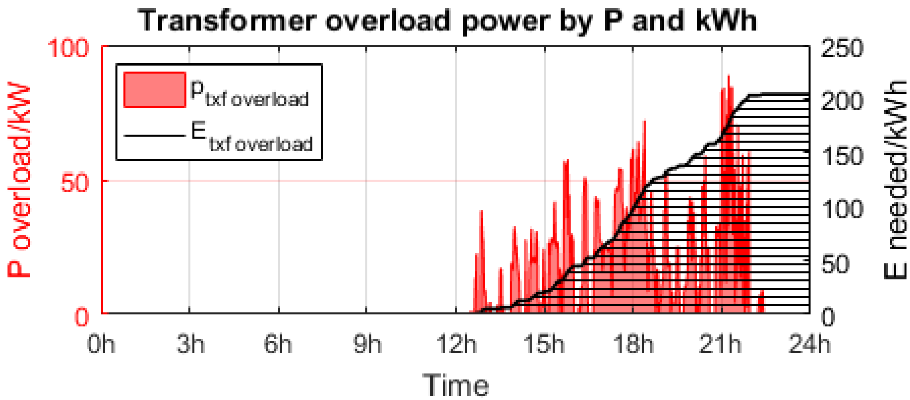

Figure 4.16: The overload power part from previous figure. As p.f.=0.98 the Transformer power limit is set to be 196kW. The black curve is the integration of the red curve over time and implies the battery capacity needed by the system

Battery storage capacity	Battery only	Battery and inverter
3kWh	$ 3,270	$ 6,750
8kWh	$ 7,680	$ 11,760
13kWh	$ 12,350	$ 15,990
18kWh	$ 16,920	$ 24,300

*The table refers to link in [3] and displays average prices from a range of installers. Prices include installation and tax.

Table 4.2: AVERAGE BATTERY INSTALLATION PRICES

where D_0 and k are DCF model parameters. The n represents the investment life cycle in the measure of years.

The main idea of DCF is that, to calculate the value of an investment all future cash flows should be estimated and discounted by using the cost of capital to give their present values [54]. We assume the DCF of V2G strategy is the total subsidy that the community can acquire from the utility grid.

According to [55, 56], microgrid batteries were simulated to perform reliably up to 15 years in a variety of climates and duty cycles. Then, in this section the life expectancy of batteries is set to 15 years. In this case, the Eq.(4.19) can be simplified as,

$$S = \frac{D_0}{(1+k)^1} + \frac{D_0}{(1+k)^2} + \cdots + \frac{D_0}{(1+k)^{15}} \tag{4.20}$$

The D_0, first year cash flow, specifically in V2G case is,

$$D_0^{V2G} = \left(\sup_t g\left(t\right) \cdot c_{electricity}/kWh\right) \cdot days_{overload} \tag{4.21}$$

where, $g\left(t\right) = \int p_{\,exceed}\left(t\right) \cdot dt - E_{V2G}\left(t\right)$.

Note that the yearly cash flow, D_0, in the following case study should consider both dynamic V2G batteries and fixed battery selling power to the grid (B2G). Then the Eq.(4.21) is updated as

$$D_0^{V2G+B2G} = \left(\overline{E} \cdot c_{electricity}/kWh\right) \cdot days_{overload} \tag{4.22}$$

where, $\overline{E}$ is the dominant strategy battery requirement.

In Eq.(4.19) or Eq.(4.20), the growth ratio k considers two parts, the inflation rate k_0 in the country and the federal risk free interest rate k_1. According to Table 4.1, we set k to be 5%. in Eq.(4.20) as the life expectancy of fixed batteries is 15 years, in calculation both the B2G, "fixed battery to grid", and V2G project will perform their end of phase within 15 years. The c_{bat} is the per kWh battery cost from the market. The $c_{electricity}$ is the per kWh electricity cost from the utility, in Eq.(4.21).

The quoted price of battery installation from a company is shown in Table 4.2. From data in the table we are able to find the c_{bat}. By linearly fitting price data and capacity data, see Fig.4.17, we are able to find out the marginal cost for the battery system, which is about 1,137.6 \$/kWh. For the $c_{electricity}$, we know the electricity prices are different across the provinces in Canada. According to the report [57], the average utility rate is 0.175 dollar per kWh. So, the cost parameters are set to $c_{bat/kWh} = 1,137.6$ and $c_{electricity/kWh} = 0.175$ in the calculations.

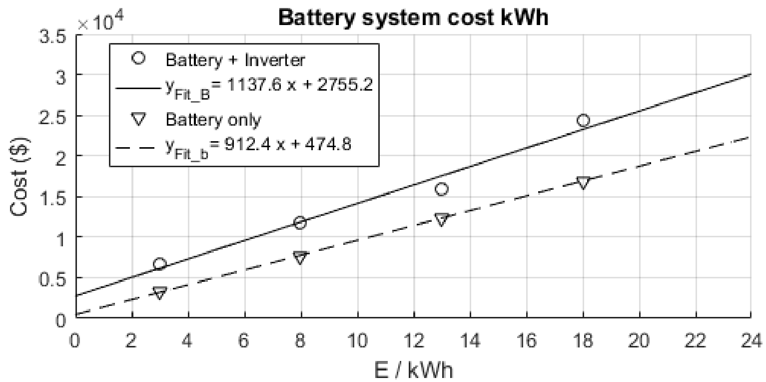

Figure 4.17: Battery system installation cost according to capacity needs [2]. Fitting data from [3]. Results show the unit cost is around 1,000 $/kWh

4.3 Case Study

We are going to present three cases, each with its own focus. Case one is focusing on V2G and G2V based "fleet as battery" strategy comparison, case two on renewable energy uncertainty's effects on "fleet as battery" strategy, case three on TOU's impacts on our strategy.

4.3.1 Case 1 - Base Case with Four Charging Topology

A. Charging System Configuration

In this first case study, we suppose there are four geographically distant areas (a), (b), (c), and (d) in the community. Their locations are indicated in Fig.4.1. Each area has adopted one of the charging station topologies from Fig.4.7. Each area serves 9 houses. The detailed settings are given in Table 4.4. In the load part, we assume the community grid serves 36 houses. Each house has associated surplus solar generation (regrouped in the PV system) and their profile is similar to Fig.4.2.

B. EV Fleet Settings

For the community EV fleet, we assume that most of them are Tesla Model 3s, and the rest are Chevrolet Bolts. This is a realistic situation seen in sales report [58], and the sales of

Bolt is around a quarter of Model 3. Then, p_{ch} in the community is set to be 20%, where p_{ch} denotes the probability for a vehicle showing up to be a Chevy Bolt when an EV arrives at the charging station. The charging rates are assumed to be 19.2kW and 50kW for the Chevy and Tesla, respectively. Their battery capacity are $Chevy_{kWh}$ =60 kWh, $Tesla_{kWh}$ =75 kWh respectively [59]. As the initial SOC is assumed to be 33% for the EVs, the service rates μ_{c} for Chevy and μ_{T} for Tesla per minute can be calculated from equation (4.4) as $\mu_{\mathrm{c}} = 1/125\, min^{-1}$ and $\mu_{\mathrm{T}} = 1/60\, min^{-1}$.

We now find the anticipated energy storage size and the corresponding cost for this community. We then compare the cost before and after the strategies are applied.

C. Battery Reduction Strategies

The case study has four areas and four different CS types. To deal with such a problem, we assume the four areas are operating individually. We solve the problem in a divide-and-conquer manner.

We first assume all areas are equipped with the same type of CS, for example, 1-charging port 1-parking spot type CS. Then the community will have 36 CS, to be specific, 36 charging ports, and 36 parking spots. In another example, all areas are adopting the 3-charging port no-queuing(parking) type station, so the community will have 12 stations, 36 charging ports and 0 parking spots. The assumption is, each house in the community is on average assigned one charging port. There are in total 4 examples as we have 4 types of stations. After the battery planning results are obtained under the same type CS assumption, we can pick 1/4 of the data in each case and combine the results. Under these 4 pure CS type assumptions, we can calculate 12 battery reduction results, shown in Fig.4.18.

Base	Strategy	FCS 1 port (Reduction%)	FCS 1 port 1 queue (Reduction%)	FCS 2 port (Reduction%)	FCS 3 port (Reduction%)
weekdays	G2V	104.3 kWh (21.22%)	104.1 kWh (21.41%)	**103.8** kWh (21.63%)	**103.6** kWh (21.75%)
	V2G	**115.6** kWh (43.41%)	**106.7** kWh (47.78%)	98.5 kWh (51.78%)	86.4 kWh (57.70%)
weekends	G2V	84.3 kWh (49.21%)	80.7 kWh (51.37%)	77.0 kWh (53.62%)	73.5 kWh (55.73%)
	V2G	–	–	–	–

*The Bases for G2V on weekdays, G2V on weekends, and V2G on weekdays before reduction are 132.41 kWh , 165.93 kWh and 204.25kWh. These three values are obtained from Fig.4.5 and Fig.4.18. The V2G on weekends is not considered, as system has low overload risk on those days.

Table 4.3: BATTERY CAPACITY REQUIREMENT AFTER EACH STRATEGY APPLIED

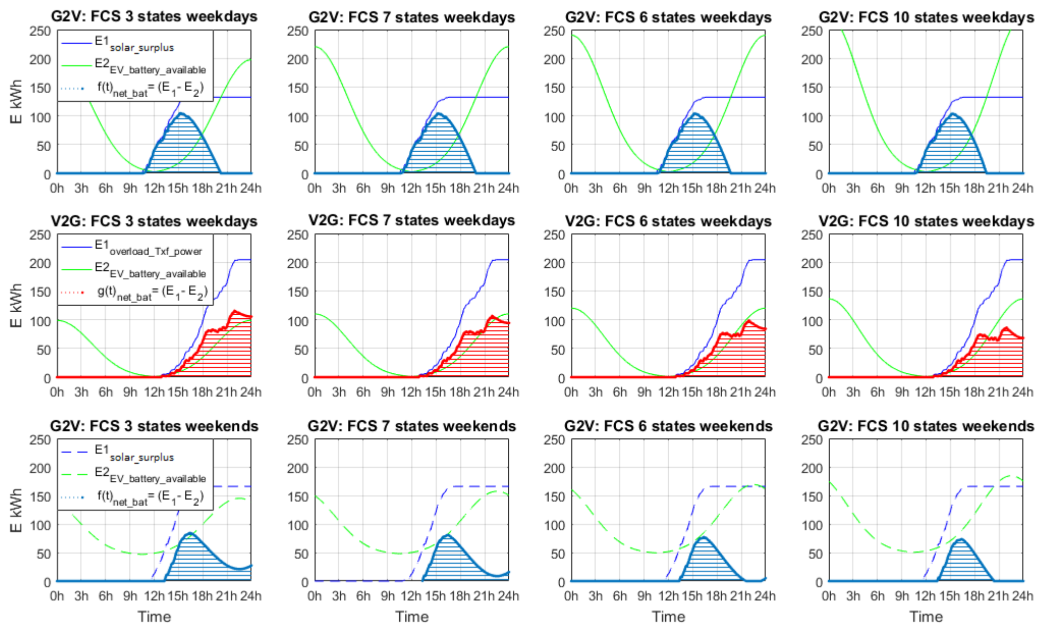

Figure 4.18: Battery capacity requirement after each strategy is applied. Batch G2V and V2G figures under weekdays and weekends situations. If Fast charging station (FCS) has 1 port, then it can be represented by a 3 state Q matrix. If 1 charging port 1 parking-spot, then 7 states. The 2-port no queueing FCS has 6 states, 3-port no queueing FCS has 10 states

The total number of graphs in Fig.4.18 is twelve as each assumption yields three results. They are G2V-weekdays, G2V-weekends, and V2G-weekdays scenarios. The V2G-weekends scenario is not considered as the load at weekends is low and the risk for transformer overloading is much lower.

The graph of Fig.4.18 on V2G strategy using FCS with 7 states on weekdays is shown in Fig.4.19 to illustrate how the reduced battery capacity requirement is determined. There are three lines $E1, E2$ and $E1 - E2$ in this graph. Where $E1$ is the fixed battery capacity needed, to store excess solar generation (G2V) or to prevent transformer overload (V2G), if EV batteries' storage potential is not considered. The green line, $E2$ is the dynamic storage potential for the EV fleet. For G2V purpose $E2$ is the SOC provided by the fleet, calculated by Eq.(4.14). For V2G purpose $E2$ is the battery Depth of Discharge, or DOD, provided by

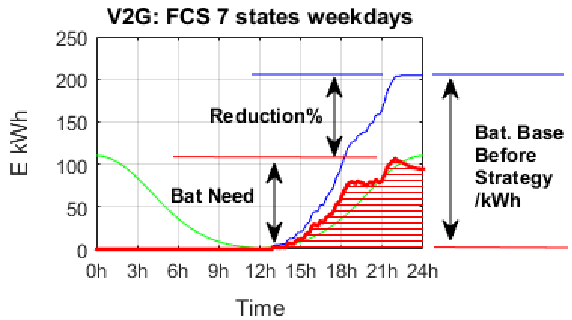

Figure 4.19: Battery capacity needed after "EV as battery" applied. The system saw a 47.78% capacity saving after EV as battery strategy

Base	Strategy	FCS 1 port (↓ %)	FCS 1 port 1 queue (↓ %)	FCS 2 port (↓ %)	FCS 3 port (↓ %)
weekdays	G2V	176.1 kWh (16.97%)	175.8 kWh (17.15%)	175.4 kWh (17.33%)	175.1 kWh (17.46%)
weekends	G2V	162.6 kWh (36.10%)	158.7 kWh (37.61%)	154.2 kWh (39.17%)	150.9 kWh (40.67%)

*The base for G2V on weekdays and weekends consider +20% solar before the reduction should now be 212.12 kWh and 254.4 kWh.The symbol ↓ % means battery reduction from these bases. The battery requirement for G2V on weekdays and weekends consider -20% solar will be around zero kWh, thus not listed on the table.

Table 4.4: BATTERY CAPACITY REQUIREMENT CONSIDER SOLAR UNCERTAINTY

the fleet, calculated by Eq.(4.15). In addition, red curve $E1 - E2$ is the net dynamic battery capacity needed. Its max value, or the $max\,(E1 - E2)$ suggests the fixed battery capacity needed after the "fleet as battery" strategy is considered. Before the strategy it was as high as $max\,(E1)$.

The results in Table 4.3 reveal more details of Fig.4.18. We now explain the results in table column one and row two. The first column of Table 4.3 shows that, if the whole community of 36 households all adopts 1-charging port 0-parking spot type CS, the major strategy that determined the battery capacity is V2G. This is because the overloading of transformers on weekdays is high. V2G allows a 115.6 kWh battery for CES. However, before the "EV fleet as battery" strategy is involved, the required battery capacity is as high as 204.25 kWh. From 204.25 to 115.6 there is a 43.21% battery capacity saving.

The second row of Table 4.3 reveals that if we adopt more complex charging stations, in terms of topology complexity, the performance of battery reduction is better. For Instance, from simple 1-charging port 0-parking spot type CS to complex 3-charging port 0-parking

Area	Strategy Performance							
	CS Topology	main strategy	w/o strategy	w/ strategy	bat. cost C_0	V2G ability	$S_{V2G+B2G}$	Investment
(a)	1port	V2G > G2V	51.1 kWh	28.9 kWh	\$ 32, 876.6	28.9 kWh	\$ 1, 778.9	\$ 31, 097.7
(b)	1port, 1queue	V2G > G2V	51.1 kWh	26.7 kWh	\$ 30, 351.2	26.7 kWh	\$ 1, 778.9	\$ 28, 572.3
(c)	2port	G2V > V2G	41.5 kWh	26.0 kWh	\$ 29, 520.7	24.6 kWh	\$ 1, 444.7	\$ 28, 076.0
(d)	3port	G2V > V2G	41.5 kWh	25.9 kWh	\$ 29, 463.8	21.6 kWh	\$ 1, 444.7	\$ 28, 019.1
Sum	–	–	185.2 kWh	107.5 kWh	**\$ 122, 212.3**	101.8 kWh	**\$ 6, 447.2**	**\$ 115, 765.1**

*Each area has 9 houses. CS: Charging Station. "Bat. w/o Strategy", refers to system battery capacity needed if no EV fleet as Storage Strategy is involved. As in Sec.III.c, investment = C, and $C = C_0 - S_{V2G+B2G}$. Overload days in calculating $S_{V2G+B2G}$ are assumed to be 5% of days in one year. B2G means "Battery-to-Grid", considers fixed batteries transfer power back to the grid.

Table 4.5: CASE STUDY RESULT: INVESTMENT FOR TARGETED COMMUNITY WITH FOUR CS TYPE

port type CS, the net battery required for the system drops gradually. It goes from 115.6 kWh down to 86.4 kWh. In general, the multiport charging station [60], with extensive parking spaces is most suitable for EV as storage purpose.

In addition, some results for redundancy design consider solar output uncertainty is shown in Table 4.5. For extreme sunshine case, the system will observe an averagely 20% more PV output. So the battery requirement is higher. The solar peak time is around 12 pm, it is not the same as EV arrival peak hour 9 pm, the mismatch will cause battery requirement to increase by more than 20%. For instance, the G2V weekdays base was 132.41 kWh, now it will increase to 212.12 kWh due to extra PV output. However, in this case study, we will consider normal weather conditions.

D. Results

The results for this four-area community case study are shown in Table 4.3. The third column in Table 4.3 shows that, if more complicated stations (2-port and 3-port CS) are deployed in the community, on average more EV batteries would appear on the grid, the overloading of the transformer will be significantly relieved, so the dominant strategy to consider by the system is then G2V. If the dominant strategy is G2V>V2G, it means that the battery system will focus on storing surplus PV power and will not resell previously stored power back to the grid (V2G).

From Table 4.3 column 4 result, the battery capacity planned before the "EV as storage" strategy applied is 185.2 kWh. With the EV as storage strategy, the fixed battery to install is only 107.5 kWh. Specifically in the area (d), as it has adopted 3-port parallel charging stations, the battery needed for the area is only 25.9 kWh.

Fig.4.20 shows the total battery investment and the reduced battery cost for the whole community. Before the "EV as virtual battery" strategy, the total investment was planned to be around 211,000 dollars. With the strategy, the capital cost drops to around 121,000 dollars. And finally, if we consider selling battery energy back to the grid, the total cost could be further decreased to around 115,000 dollars.

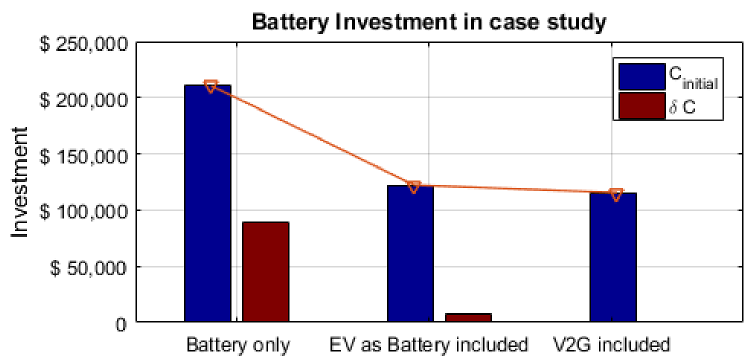

Figure 4.20: Battery system cost reduction after strategies applied to studied case. It used to be over $200k investment and now it is decreased to half the price

4.3.2 Case 2 - Base Case Consider Renewable Energy Uncertainty

A comparative storage sizing case study considering fleet batteries as wind and solar power banks is designed and evaluated in this case study. In this study, both weekdays load and weekends load scenarios with minimum or maximum renewable output situations are considered.

Experimental results show that involving the EV fleet as energy storage units could cut down local battery needs, however, in excess of expectations of renewable generations the strategy's effect is canceled out.

the EVs are assumed centralized charged at FCS and not charged at home.

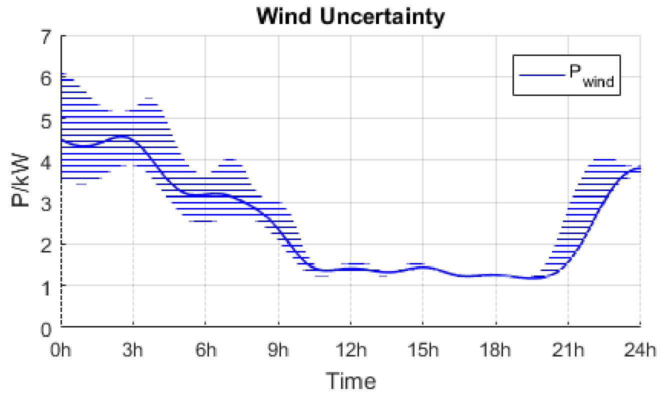

Figure 4.21: Wind generation uncertainty in one home according to historical data. Uncertainty wind output region is around its mean value$\pm$20%

A. Renewable Power Generation and Their Uncertainty

The Fig.4.21 represents wind output uncertainty. In most cases, each home's wind output stays around the solid blue line, which is the mean value in the figure. However, under specific weather conditions, actual observations may deviate up to $\pm$20%. Similar to wind each home's solar output stays around historical mean value. Under extreme weather conditions, actual observations may also deviate up to $\pm$20%. The Fig.4.22 represents combined renewable output. Under some weather conditions, actual observations may occur in the region of its mean value$\pm$30%.

The customer non-EV load behaviors across the community are similar. In this community, assume we have 36 houses. We use previous data in Fig.4.4 to presents the cumulative power consumption of these houses. Note that the power load on weekdays is different from weekends. We'll also use similar CTMC model the EV fleet behaviour.

By observing the three-state base Markov chains (red) on Fig.4.23, we can find the corresponding transition rate matrix for the one port FCS, it should be identical to equation (4.6). The multi-port-charger example is built on the blocks of the first three-state one. For example the four-port-charger is described as chains red, pink, light blue and blue as a whole in Fig.4.23. In this 15 states topology, the Q Matrix will be similar to equation (4.13), but with a Matrix with 15 by 15 scale. Shown in equation (4.23) below,

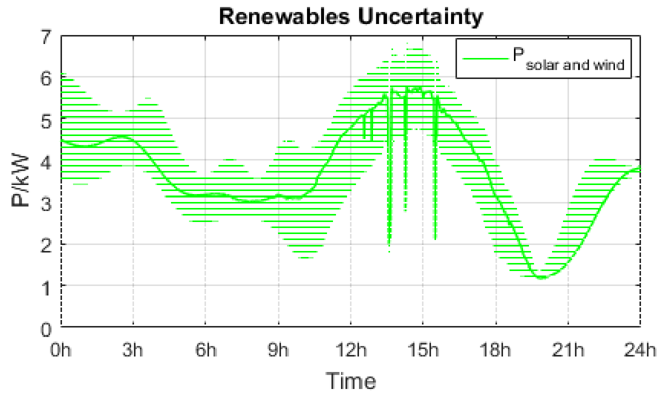

Figure 4.22: Solar and wind generation uncertainty in one home according to historical data. Uncertainty output region is around its mean value±30%

$$Q = \begin{bmatrix} -\lambda & (1-p_{ch})\,\lambda & p_{ch}\lambda & 0 & 0 & 0 & \cdots & 0 \\ \mu_{\mathrm{T}} & -\lambda-\mu_{\mathrm{T}} & 0 & (1-p_{ch})\,\lambda & 0 & p_{ch}\lambda & \cdots & 0 \\ \mu_{\mathrm{c}} & 0 & -\lambda-\mu_{\mathrm{c}} & 0 & p_{ch}\lambda & (1-p_{ch})\,\lambda & \cdots & 0 \\ 0 & \mu_{\mathrm{T}} & 0 & -\lambda-\mu_{\mathrm{T}} & 0 & 0 & \cdots & 0 \\ 0 & 0 & \mu_{\mathrm{c}} & 0 & -\lambda-\mu_{\mathrm{c}} & 0 & \cdots & 0 \\ 0 & \mu_{\mathrm{c}} & \mu_{\mathrm{T}} & 0 & 0 & -\lambda-\mu_{\mathrm{c}}-\mu_{\mathrm{T}} & \cdots & 0 \\ \vdots & \vdots & \vdots & \vdots & \vdots & \vdots & \ddots & \vdots \\ 0 & 0 & 0 & 0 & 0 & 0 & \cdots & -\mu_{\mathrm{c}} \end{bmatrix} \tag{4.23}$$

As from Fig.4.23 the state 1 to state 15 are: (0, 0), (T, 0), (C, 0), (T, T), ... , (C, C, C, C). After the steady-state probabilities of all states $\vec{p}$ are achieved, the average available battery capacity from fleet can be computed by:

$$\begin{aligned} N = \ \overrightarrow{p} \cdot States = \ & 0 \cdot p_1 + Tesla_{kWh} \cdot p_2 + \\ & Chevy_{kWh} \cdot p_3 + ... + 4 \cdot \ Chevy_{kWh} \cdot p_{15} \end{aligned} \tag{4.24}$$

The 15-state CTMC has the downward compatibility to explain 3-state, 6-state or 10-state model. So they can be universally represented by a 15-state CTMC model. For example, The state 6 or state (T,C) is a common state shared by 3-port-FCS and 4-port-FCS model, so it can be visualized in Fig.4.24 that contains two different topologies.

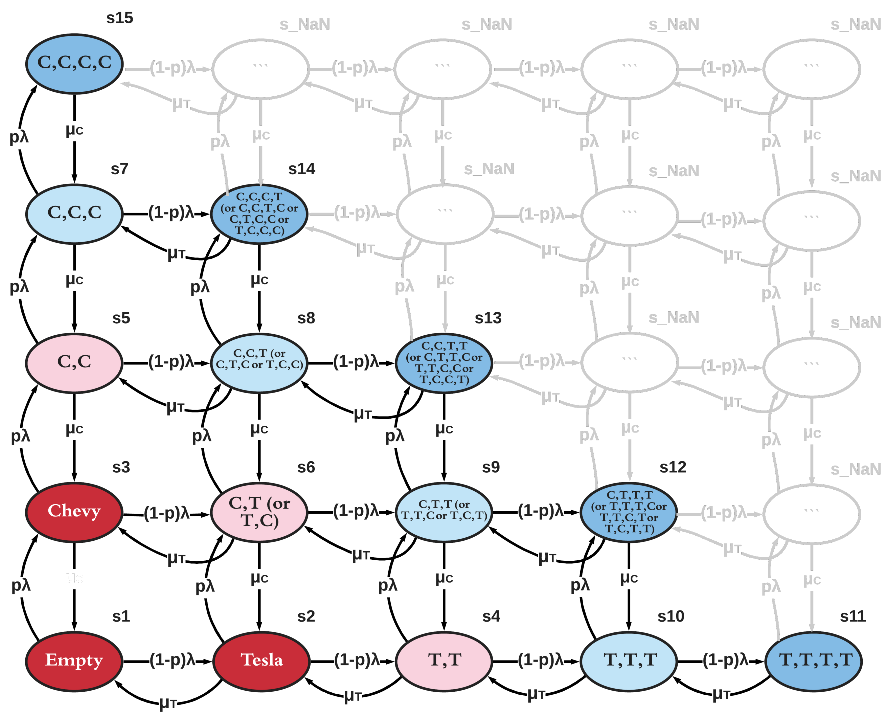

Figure 4.23: The Markov chain for a 1-CS-4-Ports system with fifteen basic states. It can serve 4 vehicles at the same time. The red three states only can represent a 1-CS-1-Port system. Red plus pink can represent a 1-CS-2-Port system. Red plus pink plus light blue can represent a 1-CS-3-Port system. Red plus pink plus light blue plus blue can represent a 1-CS-4-Port system. The greyed states s_{NaN} are the future extendable states

B. Battery Capacity Requirement Reduction

We first assume the whole girds are equipped with the 1-port type of FCS. In the second round, all grids are adopting the 2-charging port type station. There are totally 4 sub case studies as we have 4 types of stations. After the battery planning results are obtained under the same type FCS assumption, we can summarize the data and combine the results. Under these 4 pure FCS type assumptions, considering weekdays/weekend difference and upper/lower renewable generation limits we can calculate 16 battery reduction results, shown in Fig.4.25.

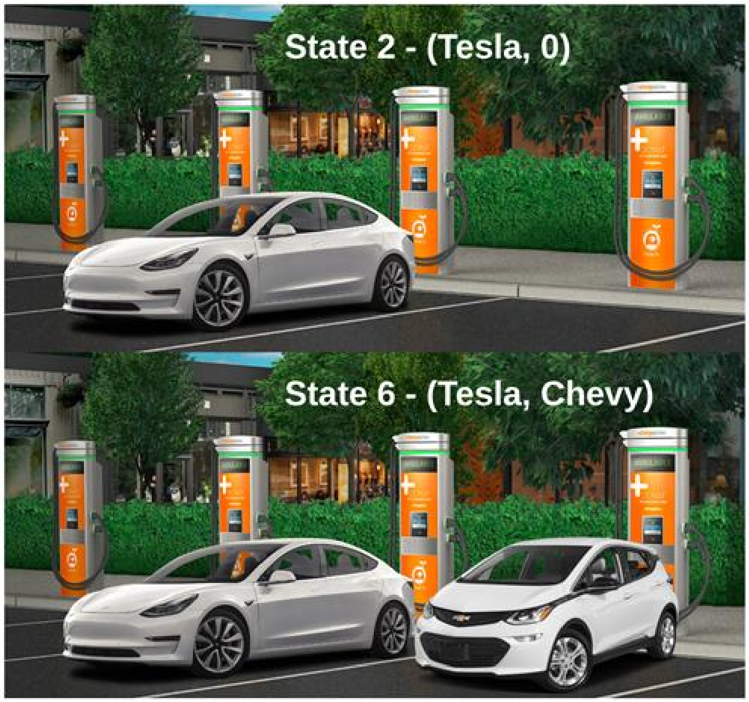

Figure 4.24: States explained for 4 port FCS system. State 2 refers to one Tesla charging, State 6 is one Tesla and one Chevy charging together

Similar to Case 1, in Case 2, a sub-graph, the graph of Fig.4.26 illustrates how the reduced battery capacity is measured. There are three lines $E1, E2$ and $E1 - E2$ in the figure. It is the graph of Fig.4.23 on +30% renewables situation using FCS with 15 states on weekdays. The $E1$ is the fixed battery capacity needed, to store excess renewable generation if EV as battery strategy is not considered. The green line, $E2$ is the dynamic capacity potential for the fleet. For G2V purpose $E2$ is the SOC provided by the fleet. In addition, blue curve $E1 - E2$ is the net dynamic battery capacity needed. Its max value suggests the fixed battery capacity needed after the current strategy is considered. Before the strategy, it could be as high as $max\, E1$.

C. Results

The results in Table 4.6 conclude more details of Fig.4.23. We now compare the results in table first two rows and the last two rows. The first two rows are weekdays profile, the

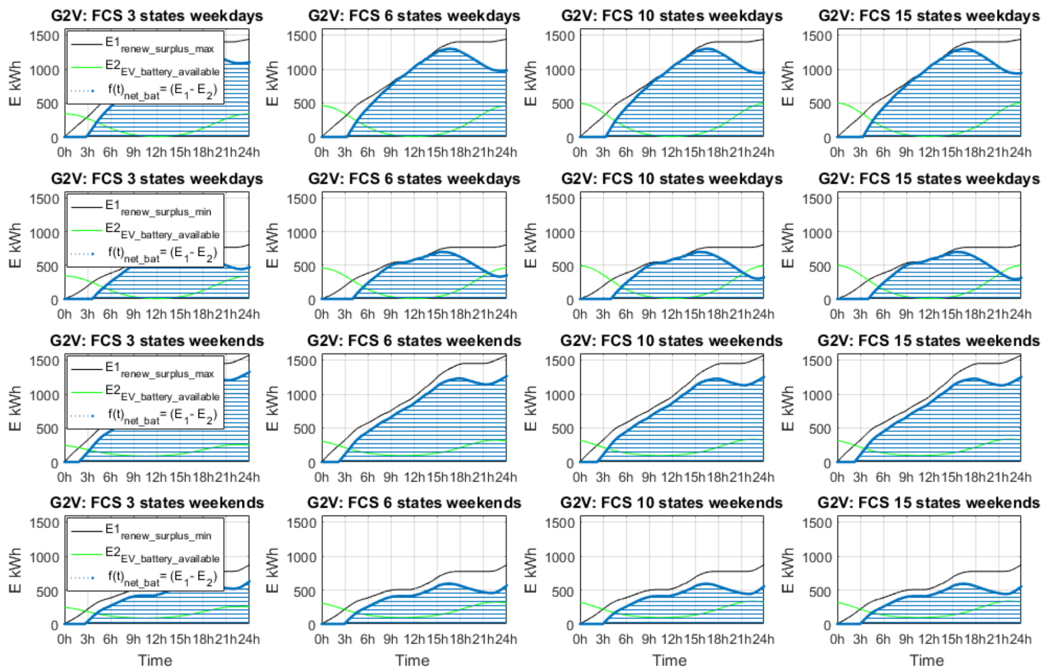

Figure 4.25: Battery capacity requirement after each G2V strategy is applied. It is a batched G2V figures under weekdays and weekends plus and minus 30% renewables situations. If Fast charging station (FCS) has 1 port, then it can be represented by a 3 state Q matrix. If 2 charging port, then 6 states. The 3-port FCS has 10 states, 4-port has 15 states. For detailed explanation on each figure please refer to the next figure, Fig.4.26

average reduction ratio is around 10.0%. The last two rows are weekends profile, as the renewable generation stays the same but the EV load is more significant during afternoons, the reduction ratio is higher, around 20.0% to 30.0%.

Compare results from rows 1 to 2 we know that, under the maximum renewable generation situation, the battery requirement is higher but the reduction ratio will be lower. Compare results from the left end column (1-port FCS) to the right end column (4-port FCS), the reduction ratio is generally growing. In a word, the multiport charging station has more battery storage potential than single-port FCS. This is the advantage of the EV as storage strategy.

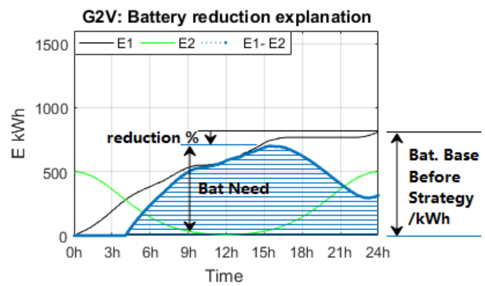

Figure 4.26: Battery capacity needed after "EV as battery" applied. For instance the system saw a 47.8% capacity saving after EV as battery strategy

Base	RE output	FCS 1 port (↓ %)	FCS 2 port (↓ %)	FCS 3 port (↓ %)	FCS 4 port (↓ %)
weekdays	plus 30%	1304.3 kWh (9.4%)	1298.8 kWh (9.8%)	1298.5 kWh (9.8%)	1298.5 kWh (9.8%)
	lose 30%	701.0 kWh (13.6%)	699.2 kWh (13.8%)	699.2 kWh (13.8%)	699.2 kWh (13.8%)
weekends	plus 30%	1326.5 kWh (15.6%)	1266.2 kWh (19.4%)	1255.0 kWh (20.1%)	1253.2 kWh (20.2%)
	lose 30%	628.1 kWh (28.0%)	593.8 kWh (31.9%)	591.8 kWh (32.2%)	591.6 kWh (32.2%)

* RE - Renewable energy. The bases for G2V on weekdays and weekends with +30% RE, G2V on weekdays and weekends with -30% RE are 1440 kWh, 811.3 kWh, 1571 kWh and 872.7 kWh. These four bases are obtained from Fig.4.25.

Table 4.6: BATTERY CAPACITY REQUIREMENT AFTER EACH STRATEGY APPLIED

However, compare the group of maximum renewable generation situation row (1,3) to the minimum renewable generation row (2,4), we can see a shortcoming of this strategy is the EV capacity may not be sufficient when a renewable generation has +30% more generation than the mean value.

4.3.3 Case 3 - TOU-price Enabled Case with Unified Charging Topology

Additional to Case 1 and 2, this case study takes into consideration the behavioral characteristics of EV users in terms of their reaction to the time-of-use (TOU) electricity pricing. A logistic function-based discount factor has been introduced to distinguish between price-sensitive and price-insensitive users. The experimental results show that the adoption of the EV fleet as DER can help reduce line overload during emergencies. Although TOU reduces the number of EVs connected to the grid during peak hours, the EVs at the fast-charging station (FCS) could still provide necessary load support.

A. Charging System Configuration

Stationary batteries have a certain life expectancy, typically ten to fifteen years [2, 6, 51]. They are still expensive and need maintenance. But the EV fleets will not stop renewing themselves and they will keep a healthy and dynamic DER battery resource as a whole. Thus, the microgrid system operator can expect EV fleets as available DERs in the power grids.

In this research, we assume EV fleet batteries in the microgrid to be dynamic, and their behavior is also affected by time-of-use (TOU) electricity pricing. The reason to consider TOU is that such price control is now widely used as a method of controlling electricity demand in the short term. Research shows there is a causal relationship between load and electricity price in different time periods [61, 62].

The microgrid considered here is assumed to contain photo-voltaic (PV) farm and EV charging equipment. We also assume that the microgrid serves a remote factory. It has critical industrial loads consuming reactive power (VAR) and active power (kW). The factory has more than one hundred people, and the EV penetration level is 100% so that the staff needs at least ten fast-charging stations (FCS), to charge their EVs.

The local utility grid and FCS both allow V2G functions. Their EVs can backup their microgrid using FCS [63] under emergency grid conditions.

TOU period	Hours	Price
Off-peak	Weekdays from 7 p.m. to 7 a.m. and all holidays	8.5¢/ kWh
Mid-peak	Weekdays from 11 a.m. to 5 p.m.	11.9¢/ kWh
On-peak	Weekdays from 7 a.m. to 11 a.m. and 5 p.m. to 7 p.m.	17.6¢/ kWh

*The table displays prices [64] which take effects from Feb.23, 2021. Price average under TOU is 11.625¢/ kWh

Table 4.7: TIME-OF-USE (TOU) RATES TORONTO HYDRO

B. EV Incoming Rate and TOU

In practice, EVs arrive at the charging port in a stochastic process. The incoming rate of EVs depends on the EV-to-charging port ratio. If the vehicle number doubles, the ratio doubles, and as a result the EV incoming rate will also double.

From paper [38], the EVs are more frequently charged in the mornings and afternoons compared to noon times. Thus, the vehicle incoming rate graph will result in a double peak shape, as shown in the upper subplot in Fig.4.28. If we also allow employees' guest EVs to visit the local FCS, the incoming rate will be linearly increased. The guest population is set to 10% of the company's workforce.

The time of use electricity price will also affect vehicle charging desire, thus affecting EV arrival rate.

According to [61], for every 1% increase in electricity price, the peak load will be reduced by 4.4517%. The intermediate load will be reduced by 2.4193%; the electricity load in the flat period is positively correlated with the electricity price. For every 1% increase in electricity price, the electricity load will increase by 0.2699%. However, the linear relationship between load increase with a price drop (or vice versa) has a zone of validity. Outside the zone, the price change can no longer boost electricity use or decrease it. Based on this fact, we introduce a logistic function type price-sensitive discount factor to demonstrate such effect. The EV load change equations are shown below.

TOU period	load change r_1 For every 1% increase in electricity price [61]	EV demand[†]
Off-peak	load will increase by + 0.2699%	+ 3.76%
Mid-peak	load will reduce by - 2.4193%	- 2.78%
On-peak	load will reduce by - 4.4517%	- 21.08%

*Data from this 2019 paper [61]. It studied the electricity load and price relationships in different time periods
[†] column three results come from price sensitivity equation.

Table 4.8: EMPIRICAL RELATIONSHIP BETWEEN LOAD AND TOU

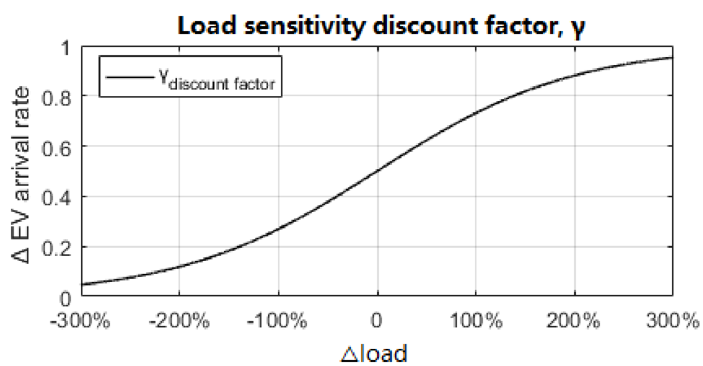

Figure 4.27: Price sensitivity model using the standard logistic function

$$\Delta_{load} = r_1 \cdot \left[\left(\frac{c - c_{avg}}{c_{avg}} \right) \cdot 100 \right] \tag{4.25}$$

$$\Delta_{EVarrival} = \Delta_{load} \cdot \gamma \left(\Delta_{load} \right) \tag{4.26}$$

where,

$$\gamma = \frac{1}{1 + e^{-\Delta load}} \tag{4.27}$$

As the discount factor γ implies, when the TOU price reaches its peak, there will still be a certain number of EVs coming to the charging station, as their charging needs are not price-sensitive. If the γ is not introduced, as peak TOU price is twice as much as TOU price off-peak, the EV arrival rate could be reduced to zero, which is not realistic.

The base TOU scheme we refer to is from Toronto Hydro, see Table 4.7. Combining Table 4.7 's data into Eq.(4.25) (relationship plot in Figure 4.27) we obtain the result in Table 4.8, column three.

Similar to previous Section 4.3.1 and 4.3.2, We use the continuous-time Markov Chain (CTMC) Queue Model to analyze the status of ports in the CS.

The arrival of EVs occurs at the rate λ, that is, every minute, an average λ cars are visiting the charging port. The λ variable is assumed to follow a Poisson process. An arrival event will move the state from i to $(i+1)$ after one arrival.

$$\lambda\,(\mathrm{t}) = \mathrm{ratio}\,(\mathrm{t}) \cdot [\lambda_0 \cdot (1 + 10\%)] \tag{4.28}$$

As shown in equation (4.28), which is similar to equation (4.2), consider a nominal arrival rate λ_0 of 1/1440 per min (one car per day), then the contents in $[\cdot]$ of Eq.(4.28) is going to be a constant. λ (t) will be varying according to ratio(t) over the day. The ratio(t) over time is referring to [24, 28, 50]. So the bell curve is employed to reflect the probability density function of battery charging start time. The EV arrival rate ratio(t) over time also depends on price sensitivity, so it will result in the stepped bell type plot in the lower figure in Fig.4.28.

C. PowerWorld Simulation Settings

Item	Value
Series Resistance (R)	0.010
Series Reactance (X)	0.030
Shunt Charging (B)	0.020
Shunt Conductance (G)	0.000
MVA Rating	20 MVA

*The per unit impedance parameters are default PowerWorld [65] settings.

Table 4.9: PARAMETERS OF POWER LINES

Same for the EV fleet constitution, we assume that some are Chevrolet Bolts and the most are Tesla Model 3s. According to the EV sales status in Canada [58], the p_{ch} in the

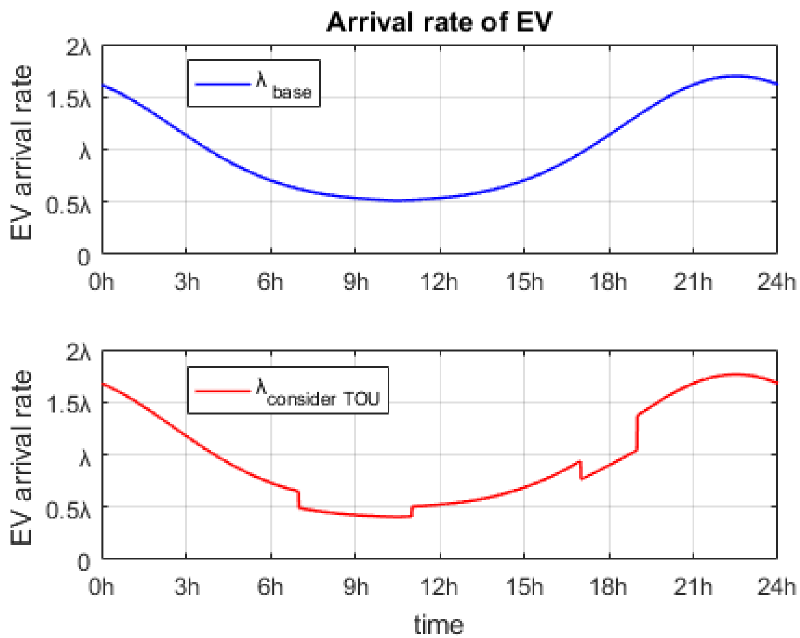

Figure 4.28: Arrival rate of EVs. The average number of cars visiting per minute before and after consider TOU price influence on EV behaviour

community is set to 20%, and p_{ch} denotes the probability for an EV to be a Chevy Bolt.

Same as Section 4.3.1 case study 1, in this case study 3, the battery capacity of the Chevy and Tesla are also 60 kWh and 75 kWh respectively. The on-board charging rates are assumed to be 19.2 kW and 50 kW, respectively. As the initial SOC is assumed to be 33.3% for the charging EVs, similarly the service rates μ_c for Chevy and μ_T for Tesla per minute are also $\mu_c = 1/125min^{-1}$ and $\mu_T = 1/60min^{-1}$.

D. Microgrid Topology

In this microgrid, we assume that the factory serves two critical loads, each has 1 MW and 1 MVar power need, shown in Fig.4.32. There are six transmission lines with settings described in Table 4.9. The grid can work in standalone mode, in this case, it has a PV farm as a distributed generation resource. The normal operation of a PV farm has 2 MW output, however, in the case study, we assume an extreme condition in which that PV farm has a 4 MW output for half an hour, see Fig.4.32.

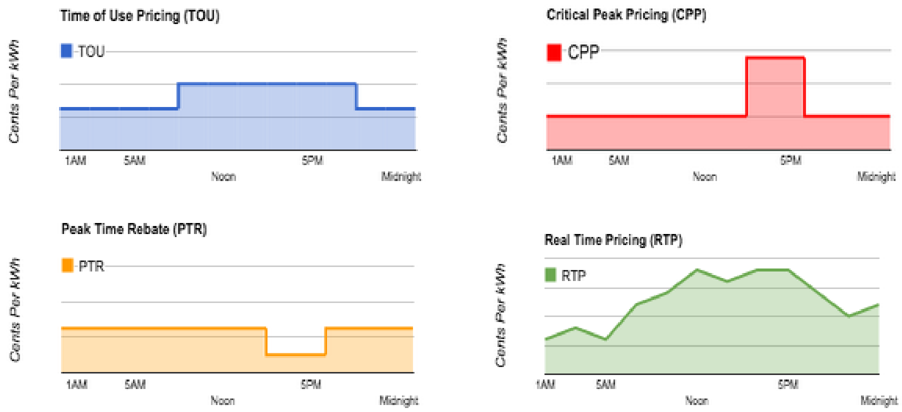

Figure 4.29: Time varying rates (TVR) come in four general categories [4]: Time-of-Use (TOU), Critical Peak Pricing (CPP), Peak Time Rebate (PTR) and Real Time Pricing (RTP). TOU is adopted in the research as it is the most basic pricing scheme which consists of pre-defined peak and off-peak time periods

Assume we have 140 people and there are 14 charging stations. Each FCS has four ports, a topology as described in Figure 4.23. As we are adopting 4-port CS in the system, the steady-state probability vector will have 15 elements. The result is shown in Fig.4.30.

E. Results

The Fig.4.30 shows that the probability at state 1 (station empty state) is always the highest, before and after TOU pricing. The second-highest spike is the state 2, or (T, 0, 0, 0), which represents one Tesla connected to the grid. The probability is around 0.16 included TOU for state 2, and 0.17 without TOU.

In this case study, we have taken TOU into account, so as Fig.4.30 shows, all probabilities from state 1 to state 3 will decrease, and state 4 to state 15 will increase. State 1 to state 3 are almost "empty" states, but the rest of all are similar to the "full" state, there are two vehicles or more at the FCS. Because full state probabilities are increasing, the TOU has added extra fleet energy into the system. This positive effect is shown in Fig.4.31.

As Fig.4.31 first yellow bar illustrates, with TOU price influence, the EV SOC available at maximum vehicle arrival rate (3.5 λ) at one FCS is going to be 45 kWh. According to

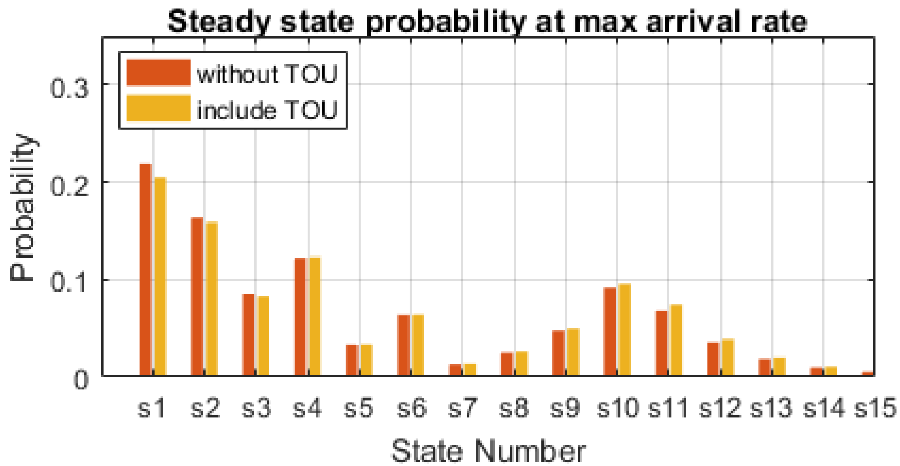

Figure 4.30: Comparison of states probabilities at maximum EV arrival rate, without and with time-of-use price influence

the second subfigure in Fig.4.28, at 12 pm when solar has the maximum output, the arrival rate is around half the base λ rate (0.5 λ). So that the available SOC energy at one FCS is $0.5/3.5 \cdot 45 = 6.43$ kWh per minute.

If four port-connected EV's energy is transferred back to the grid, at one FCS, the 6.43 kWh per minute represents 385 kilo-Watt power. Note that in 2021, recent level-2 vehicles only have 19.2 kilo-Watt power AC bidirectional V2G system [66]. So the Maximum out put per four-port-FCS should be restricted to $19.2 \cdot 4 = 76.8$ kilo-Watt power.

for 14 FCS, it should multiply 14 and the product is 1.0752 MW. To keep things simple, we round it to 1 MW in simulation. This 1MW power injection from storage can be found at the left side of lower graph at Fig.4.32.

The results for the case study are shown in Fig.4.32 and Fig.4.33. Figure 4.32 shows that, when solar farm to the second-load transmission line is congested (85% line rating), 14 FCS could inject 1 MW back into the system and the line congestion will be reduced to 84% of its rating which is less risky for the system. Figure 4.33 shows that, when EV fleet power was not injected, the overloaded line was conveying 1.88 MW power. After the "EV as distributed energy resource" strategy was applied the power line has lower load burden, carrying only 1.75 MW power.

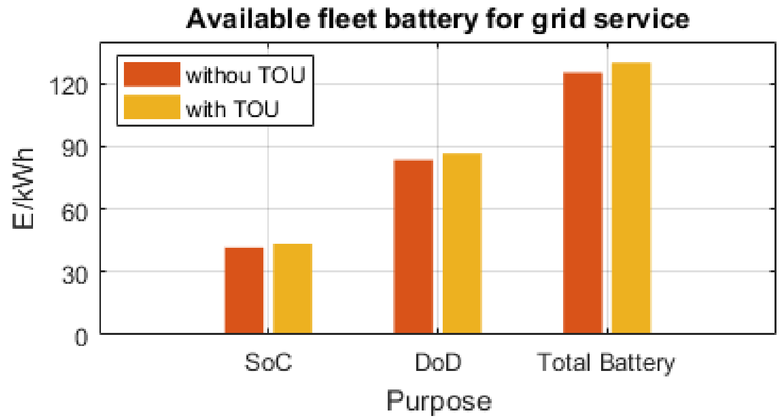

Figure 4.31: Comparison of battery capacity provided at maximum EV arrival rate, without and with time-of-use price influences

4.4 Chapter Summary

In Section 4.3.1, we introduced EV fleet batteries as an important sector in Community Energy Storage (CES). Unlike a stationary CES system, the EV batteries operate in dynamic states. To determine the potential energy capacity of this virtual resource, we addressed the problem using continuous time Markov chain EV queueing model. One of the main contributions of our work is to break down EV based CES planning into different aspects (G2V/V2G, single charging port/multiport, weekdays/weekends) and to propose means to solve it using an area-based divide-and-conquer method. A discussion on the performance of 12 strategies has been provided. In particular, we show that a multiport charging station with a parking spot has more dynamic EV battery reserve than a single port non-queueing station.

In 4.3.2, we present a framework to analyze the impact of using electric vehicle batteries as energy storage. We have shown that the EV fleet batteries and CES fixed storage can complement each other. The EV fleet batteries will cut down the total fixed battery needs and may also bring in more competition in the battery market as a whole. The renewable generation has uncertainties, redundancy design is needed to ensure the maximum generation situation is covered in every ”EV as battery” project, such as encouraging EVs to charge more during afternoons when solar generation is high.

In Section 4.3.3, we used EV fleet batteries as emergency DER to deal with the line

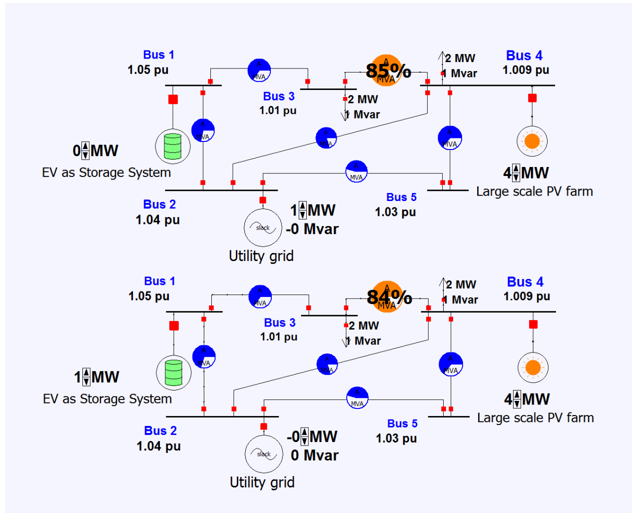

Figure 4.32: Comparison of microgrid line overload profile, using PowerWorld Simulation. After 1MW fleet power (green icon on the left) back transferred to the grid, the overload transmission line drop from 85% to 84% in loading ratio

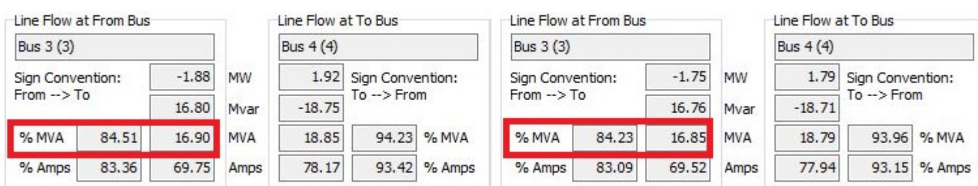

Figure 4.33: The overload transmission line parameter details, before and after EV transfer power to the grid, using PowerWorld Simulation

overload issue in a microgrid. The dynamic electricity pricing (TOU) is considered so that the arrival rate of EVs in the microgrid is affected. Introducing TOU reflects the practical utility environment so that the fleet battery result is more reasonable. The estimation of available EV batteries in the grid is based on the continuous-time Markov chain vehicle queuing model. It is shown that the EV batteries can offer power back to the grid, relieve grid congestion, and help integrate a higher share of solar power.

Chapter 5

Conclusion

5.1 Summary

Along this thesis, we studied the problem of scheduling EVs and planning EV fleet as a distributed energy resource (DER) in the community microgrid.

Conventional approaches focus on the adverse effect of massive EV plugging into the grids, such as power shortage and power quality issues. In this thesis, we showed that with reasonable scheduling strategies, the fleet will gladly work and interact with the existing energy storage system (ESS) via a unified management interface. Connecting EV fleet into the grid makes it possible to store the surplus electricity generated from intermittent renewable solar and wind sources in their batteries during non-peak periods, and feed power back to the grid when needed. It will enhance grid reliability and cut down initial investment for grid planners to set up a community energy storage (CES) system.

We also developed a new scheduling algorithm for the fleet coordinator to achieve superior automation than the available approaches. The main contributions and corresponding results are summarized as follows.

In Chapter 2, we developed an EV fleet load modeling method based on load features observed from meter side data. We conclude the two key features of charging are start-of-charging time and the duration of charging time. The distribution of these two parameters is concluded in bi-modal distribution expressions. The case study showed that the proposed approach can reflect the stochastic nature of EV charging and can predict the peak power of EVCL in a given period. The Chapter picks the bus voltage as a power quality indicator and introduced a load management strategy to reduce the voltage dip via load shifting and backed it up with a reactive power injection scheme. The result shows even without static var compensator activated, the loads reschedule strategy proposed is effective to ensure grids safe operation.

Chapter 3 proposes the method to solve the multi-dimensional EV charging scheduling problem. The time-of-use pricing TOU, the V2G capability of vehicles, and the flexibility of charging are taken into account. This chapter solves the scheduling problem by using the Q-learning algorithm. Research pointed out the importance of adaptability in EV scheduling algorithms, in terms of providing more degree of freedom for EV to take action. An improved algorithm for solving multi-EVs congestion at fast-charging stations is also established. The research proved that the congestion can still happen when the serving rate of FCS is higher than the vehicle arriving rate, thus the reward table must be updated to avoid the charging (or discharging) conflicts. The surplus for the FCS coordinator has been considered, and the penetration level is also taken into account.

In Chapter 4, we introduced EV fleet batteries into the community energy storage (CES) system. Unlike a stationary CES system, the EV batteries operate in dynamic states. To determine the potential energy capacity of this virtual resource, we addressed the problem using a continuous time Markov chain EV queueing model. One of the main contributions of our work is to break down EV-based CES planning into different aspects (G2V/V2G, single charging port/multiport, weekdays/weekends) and to propose means to solve it using an area-based divide-and-conquer method. We have shown that the EV fleet batteries and CES fixed storage can complement each other. The EV fleet batteries will cut down the total fixed battery needs. The renewable generation has uncertainties, redundancy design is needed to ensure the maximum generation situation is covered in every project.

It is shown that the EV batteries can offer power back to the grid, relieve grid congestion, and help integrate a higher share of renewable power.

5.2 Potential Future Research

Although several issues regarding EV fleet modeling, impacts and management in distribution grid system have been addressed in this thesis, many interesting related problems remain to be answered and hence, deserve further attention. The proposed future work is given as follows:

When developing the Q table for the EV scheduling problem in Chapter 3, it should be noted that the model developed will be compute-intensive if the size of table for the problem is huge. It is expected the developed Q learning model will benefit EV users and automakers to optimally dispatch the battery power of EV, if the dispatch interval is in hour-level and not in minute-level.

Also when dealing with charging station congestion, in the future, the research is going to consider the priority of the charging queue of EVs according to the rest of SOC in the battery. For instance, the 20% SOC vehicle will have privilege to charge against a 60% SOC vehicle.

In Chapter 4, some limitations should be noted. In the case study one, first, the fleet battery capacity is only accessible through a charging station, either at home when parked on the driveway or a dedicated FCS. Second, the Operation and Maintenance (O&M) cost of battery component is ignored throughout its life expectancy. In case study two, future work will focus on the deep learning-based time sequence forecasting method to reduce the uncertainty envelope of renewable load generation. In case study three, besides TOU, other dynamic pricing schemes such as progressive utility rate is not fully analyzed. And new price schemes will end up with new user behaviors to be further studied.

Bibliography

[1] L. Luo, W. Gu, Y. Wang, and C. Chen, "An affine arithmetic-based power flow algorithm considering the regional control of unscheduled power fluctuation," *Energies*, vol. 10, no. 11, p. 1794, 2017.

[2] Q. Dang, D. Wu, and B. Boulet, "Community microgrid energy storage sizing considering ev fleet batteries as supplemental resource," in *2020 IEEE Electric Power and Energy Conference (EPEC)*, pp. 1–5, IEEE, 2020.

[3] "Home solar battery storage system prices for jan 2018 - solar choice." `https://www.solarchoice.net.au/blog/home-solar-battery-storage-prices-january-2018`.

[4] C. Girouard, "Time varying rates: An idea whose time has come." `https://blog.aee.net/time-varying-rates-an-idea-whose-time-has-come`.

[5] C. Acosta, M. Ortega, T. Bunsen, B. P. Koirala, and A. Ghorbani, "Facilitating energy transition through energy commons: An application of socio-ecological systems framework for integrated community energy systems," *Sustainability*, vol. 10, no. 2, p. 366, 2018.

[6] D. Wu, H. Zeng, C. Lu, and B. Boulet, "Two-stage energy management for office buildings with workplace ev charging and renewable energy," *IEEE Transactions on Transportation Electrification*, vol. 3, no. 1, 2017.

[7] D. Wu, *Machine Learning Algorithms and Applications for Sustainable Smart Grid*. McGill University (Canada), 2018.

[8] B. P. Koirala, J. P. Chaves Ávila, T. Gómez, R. A. Hakvoort, and P. M. Herder, "Local alternative for energy supply: Performance assessment of integrated community energy systems," *Energies*, vol. 9, no. 12, p. 981, 2016.

[9] E. Wood, "Commonwealth edison makes move into community energy storage." `https://microgridknowledge.com/community-energy-storage-comed/`, 2017.

[10] Hydro-Québec, "Hydro-québec launches evlo, a subsidiary specializing in energy storage systems." `http://news.hydroquebec.com/en/press-releases/1668/`, 2020.

[11] Q. Dang, D. Wu, and B. Boulet, "Ev charging management with ann-based electricity price forecasting," in *2020 IEEE Transportation Electrification Conference & Expo (ITEC)*, pp. 626–630, IEEE, 2020.

[12] R. G. Di Wu, F. lavet Vincent, P. Doina, and B. Benoit, "Optimizing home energy management and electric vehicle charging with reinforcement learning," *Proceedings of the 16th Adaptive Learning Agents*, 2018.

[13] Q. Dang, D. Wu, and B. Boulet, "An advanced framework for electric vehicles interaction with distribution grids based on q-learning," in *2019 IEEE Energy Conversion Congress and Exposition (ECCE)*, pp. 3491–3495, IEEE.

[14] A. Cohen, "Tesla's new lithium-ion patent brings company closer to promised 1 million-mile battery." `https://medium.datadriveninvestor.com/will-the-ultimate-battery-finally-overcome-tesla-range-anxiety`, accessed on Jan. 12, 2021.

[15] S. Li, H. He, Y. Chen, M. Huang, and C. Hu, "Optimization between the pv and the retired ev battery for the residential microgrid application," *Energy Procedia*, vol. 75, pp. 1138–1146, 2015.

[16] Y. Deng, Y. Zhang, F. Luo, and Y. Mu, "Operational planning of centralized charging stations utilizing second-life battery energy storage systems," *IEEE Transactions on Sustainable Energy*, vol. 12, no. 1, pp. 387–399, 2020.

[17] N. B. Arias, S. Hashemi, P. B. Andersen, C. Træholt, and R. Romero, "V2g enabled evs providing frequency containment reserves: Field results," in *2018 IEEE International Conference on Industrial Technology (ICIT)*, pp. 1814–1819, Ieee, 2018.

[18] J. Zhong, L. He, C. Li, Y. Cao, J. Wang, B. Fang, L. Zeng, and G. Xiao, "Coordinated control for large-scale ev charging facilities and energy storage devices participating in frequency regulation," *Applied Energy*, vol. 123, pp. 253–262, 2014.

[19] Q. Yan, B. Zhang, and M. Kezunovic, "Optimized operational cost reduction for an ev charging station integrated with battery energy storage and pv generation," *IEEE Transactions on Smart Grid*, vol. 10, no. 2, pp. 2096–2106, 2018.

[20] K. Mahmud, M. J. Hossain, and G. E. Town, "Peak-load reduction by coordinated response of photovoltaics, battery storage, and electric vehicles," *IEEE Access*, vol. 6, pp. 29353–29365, 2018.

[21] K. Mahmud, S. Morsalin, Y. Kafle, and G. Town, "Improved peak shaving in grid-connected domestic power systems combining photovoltaic generation, battery storage, and v2g-capable electric vehicle," in *2016 IEEE International Conference on Power System Technology (POWERCON)*, pp. 1–4, IEEE, 2016.

[22] L. Masotti, A. Dolara, and S. Leva, "Vehicle-to-grid for peak shaving in a medium voltage grid with pv plants," in *2019 International Conference on Clean Electrical Power (ICCEP)*, pp. 482–489, IEEE, 2019.

[23] Y. Wang, B. Wang, C.-C. Chu, H. Pota, and R. Gadh, "Energy management for a commercial building microgrid with stationary and mobile battery storage," *Energy and Buildings*, vol. 116, pp. 141–150, 2016.

[24] Q. Dang and Y. Huo, "Modeling ev fleet load in distribution grids: a data-driven approach," in *2018 IEEE Transportation Electrification Conference and Expo (ITEC)*, pp. 720–724, IEEE, 2018.

[25] Q. Dang, "Electric vehicle (ev) charging management and relieve impacts in grids," in *2018 9th IEEE International Symposium on Power Electronics for Distributed Generation Systems (PEDG)*, pp. 1–5, IEEE, 2018.

[26] A. Arif, Z. Wang, J. Wang, B. Mather, H. Bashualdo, and D. Zhao, “Load modeling—a review,” *IEEE Transactions on Smart Grid*, vol. 9, no. 6, pp. 5986–5999, 2017.

[27] L. Gao, S. Liu, and R. A. Dougal, “Dynamic lithium-ion battery model for system simulation,” *IEEE transactions on components and packaging technologies*, vol. 25, no. 3, pp. 495–505, 2002.

[28] K. Qian, C. Zhou, M. Allan, and Y. Yuan, “Modeling of load demand due to ev battery charging in distribution systems,” *IEEE transactions on power systems*, vol. 26, no. 2, pp. 802–810, 2010.

[29] P. Zhang, K. Qian, C. Zhou, B. G. Stewart, and D. M. Hepburn, “A methodology for optimization of power systems demand due to electric vehicle charging load,” *IEEE Transactions on Power Systems*, vol. 27, no. 3, pp. 1628–1636, 2012.

[30] G. Li and X.-P. Zhang, “Modeling of plug-in hybrid electric vehicle charging demand in probabilistic power flow calculations,” *IEEE Transactions on Smart Grid*, vol. 3, no. 1, pp. 492–499, 2012.

[31] J. Brady and M. O’Mahony, “Modelling charging profiles of electric vehicles based on real-world electric vehicle charging data,” *Sustainable Cities and Society*, vol. 26, pp. 203–216, 2016.

[32] N. Liu, J. Chen, L. Zhu, J. Zhang, and Y. He, “A key management scheme for secure communications of advanced metering infrastructure in smart grid,” *IEEE Transactions on Industrial electronics*, vol. 60, no. 10, pp. 4746–4756, 2012.

[33] O. Sundstrom and C. Binding, “Flexible charging optimization for electric vehicles considering distribution grid constraints,” *IEEE Transactions on Smart grid*, vol. 3, no. 1, pp. 26–37, 2011.

[34] R. C. Green II, L. Wang, and M. Alam, “The impact of plug-in hybrid electric vehicles on distribution networks: A review and outlook,” *Renewable and sustainable energy reviews*, vol. 15, no. 1, pp. 544–553, 2011.

[35] R. D. Zimmerman, C. E. Murillo-Sánchez, and R. J. Thomas, "Matpower: Steady-state operations, planning, and analysis tools for power systems research and education," *IEEE Transactions on power systems*, vol. 26, no. 1, pp. 12–19, 2010.

[36] B. Adornato, R. Patil, Z. Filipi, Z. Baraket, and T. Gordon, "Characterizing naturalistic driving patterns for plug-in hybrid electric vehicle analysis," in *2009 IEEE Vehicle Power and Propulsion Conference*, pp. 655–660, IEEE, 2009.

[37] N. Mohan, T. M. Undeland, and W. P. Robbins, *Power electronics: converters, applications, and design*. John wiley & sons, 2003.

[38] Q. Dang, D. Wu, and B. Boulet, "A q-learning based charging scheduling scheme for electric vehicles," in *2019 IEEE Transportation Electrification Conference and Expo (ITEC)*, pp. 1–5, IEEE, 2019.

[39] Q. Dang, Y. Huo, and C. Sun, "Privacy preservation needed for smart meter system: A methodology to recognize electric vehicle (ev) models," in *2018 IEEE Innovative Smart Grid Technologies-Asia (ISGT Asia)*, pp. 1016–1020, IEEE, 2018.

[40] S. Ahmed and F. Bouffard, "Building load management clusters using reinforcement learning," in *2017 8th IEEE Annual Information Technology, Electronics and Mobile Communication Conference (IEMCON)*, pp. 372–377, IEEE, 2017.

[41] C. J. Watkins and P. Dayan, "Q-learning," *Machine learning*, vol. 8, no. 3-4, pp. 279–292, 1992.

[42] M. A. Ortega-Vazquez, F. Bouffard, and V. Silva, "Electric vehicle aggregator/system operator coordination for charging scheduling and services procurement," *IEEE Transactions on Power Systems*, vol. 28, no. 2, pp. 1806–1815, 2012.

[43] Q. Dang, D. Wu, and B. Boulet, "Ev fleet as virtual battery resource for community microgrid energy storage planning le parc de véhicules électriques comme ressource de batterie virtuelle pour la planification du stockage d'énergie des micro-réseaux communautaires," *IEEE Canadian Journal of Electrical and Computer Engineering*, 2021.

[44] Q. Dang, D. Wu, and B. Boulet, “Electric vehicle battery as energy storage unit consider renewable power uncertainty,” in *2021 IEEE Energy Conversion Congress and Exposition (ECCE)*, pp. 668–673, IEEE, 2021.

[45] Q. Dang, D. Wu, and B. Boulet, “Ev fleet batteries as distributed energy resources considering dynamic electricity pricing,” in *2021 IEEE 12th International Symposium on Power Electronics for Distributed Generation Systems (PEDG)*, pp. 1–6, IEEE, 2021.

[46] “Dataport — login — signup.” `https://dataport.pecanstreet.org/`.

[47] T. Tony, P. Sivraj, and K. Sasi, “Net energy meter with appliance control and bi-directional communication capability,” in *2016 International Conference on Advances in Computing, Communications and Informatics (ICACCI)*, pp. 2650–2653, IEEE, 2016.

[48] “Average electricity consumption in quebec 2020.” `https://www.hydroquebec.com/residential/customer-space/electricity-use/tools/electricity-use.html/`.

[49] A. B. Nassif, H. Yazdanpanahi, M. Wright, and M. Dong, “Planning and optimization of a small-scale hybrid microgrid in a northern community,” in *2020 47th IEEE Photovoltaic Specialists Conference (PVSC)*, pp. 2554–2556, IEEE, 2020.

[50] Z.-Y. Hou, P.-Y. Lou, and C.-C. Wang, “State of charge, state of health, and state of function monitoring for ev bms,” in *2017 IEEE International Conference on Consumer Electronics (ICCE)*, pp. 310–311, IEEE, 2017.

[51] Q. Dang and Y. Huo, “Flexibility scheduling for microgrids with electric vehicle (ev) penetration,” in *2018 IEEE Energy Conversion Congress and Exposition (ECCE)*, pp. 1078–1083, IEEE, 2018.

[52] M. S. Islam, N. Mithulananthan, and D. Q. Hung, “A day-ahead forecasting model for probabilistic ev charging loads at business premises,” *IEEE Transactions on Sustainable Energy*, vol. 9, no. 2, pp. 741–753, 2017.

[53] J. H. Christensen, G. D. Rudebusch, and P. J. Shultz, “Accounting for low long-term interest rates: Evidence from canada,” Federal Reserve Bank of San Francisco, 2020.

[54] R. H. Parker, "Discounted cash flow in historical perspective," *Journal of Accounting Research*, vol. 6, no. 1, pp. 58–71, 1968.

[55] M. Merten, C. Olk, I. Schoeneberger, and D. U. Sauer, "Bidding strategy for battery storage systems in the secondary control reserve market," *Applied Energy*, vol. 268, p. 114951, 2020.

[56] T. Kerdphol, K. Fuji, Y. Mitani, M. Watanabe, and Y. Qudaih, "Optimization of a battery energy storage system using particle swarm optimization for stand-alone microgrids," *International Journal of Electrical Power & Energy Systems*, vol. 81, pp. 32–39, 2016.

[57] R. Urban, "Electricity prices in canada 2020." `https://www.energyhub.org/electricity-prices/`, accessed on Feb. 11, 2021.

[58] "Electric vehicle sales in canada – q1 2020." `https://emc-mec.ca/wp-content/uploads/EMC-Sales-Report-2020-Q1.pdf`.

[59] H. Ambrose, A. Kendall, M. Lozano, S. Wachche, and L. Fulton, "Trends in life cycle greenhouse gas emissions of future light duty electric vehicles," *Transportation Research Part D: Transport and Environment*, vol. 81, p. 102287, 2020.

[60] A. Meintz, B. Rowden, and T. Bohn, "Charging infrastructure technologies: Development of a multiport,¿ 1 mw charging system for medium-and heavy-duty electric vehicles," tech. rep., National Renewable Energy Lab.(NREL), Golden, CO (United States), 2020.

[61] M. Wen, Y. Chen, F. Chen, L. An, Q. He, and C. Fu, "The relationship between load and electricity price in different time periods based on granger causality test," in *E3S Web of Conferences*, vol. 118, p. 02045, EDP Sciences, 2019.

[62] S. Kwon, S.-H. Cho, R. K. Roberts, T. Kim, and T. E. Yu, "Effects of changes in electricity price on electricity demand and resulting effects on manufacturing output," tech. rep., 2015.

[63] X. Huang, D. Wu, and B. Boulet, "Ensemble learning for charging load forecasting of electric vehicle charging stations," in *2020 IEEE Electric Power and Energy Conference (EPEC)*, pp. 1–5, IEEE, 2020.

[64] torontohydro, "Time varying rates: An idea whose time has come." `https://www.torontohydro.com/for-home/rates`, 2021.

[65] powerworld, "Powerworld simulator – version 22." `https://www.powerworld.com/download-purchase/demo-software`, 2021.

[66] E. Myers, "The 2021 lucid air warrantied for 19.2 kw ac bidirectional v2g.." `https://sepapower.org/knowledge/hope-or-only-hype-for-residential-v2g/`, Sept. 2020.